OPTICAL PULSE PROPAGATION

IN DISPERSIVE SYSTEMS

by

Michael J. Ware

A dissertation submitted to the faculty of

Brigham Young University

in partial fulfillment of the requirements for the degree of

Doctor of Philosophy

Department of Physics and Astronomy

Brigham Young University

December 2001

BRIGHAM YOUNG UNIVERSITY

GRADUATE COMMITTEE APPROVAL

of a dissertation submitted by

Michael J. Ware

This thesis has been read by each member of the following graduate committee and by majority vote has been found to be satisfactory.

Date	Justin Peatross, Chair
Date	William Dibble
Date	William Evenson
Date	Scott Glasgow
Date	Bret Hess

BRIGHAM YOUNG UNIVERSITY

As chair of the candidate's graduate committee, I have read the dissertation of Michael J. Ware in its final form and have found that (1) its format, citations, and bibliographical style are consistent and acceptable and fulfill university and department style requirements; (2) its illustrative materials including figures, tables, and charts are in place; and (3) the final manuscript is satisfactory to the graduate committee and is ready for submission to the university library.

Date

Justin Peatross
Chair, Graduate Committee

Accepted for the Department

R. Steven Turley, Chair
Department of Physics and Astronomy

Accepted for the College

G. Rex Bryce, Associate Dean
College of Mathematics and Physical Sciences

ABSTRACT

OPTICAL PULSE PROPAGATION

IN DISPERSIVE SYSTEMS

Michael J. Ware

Department of Physics and Astronomy

Doctor of Philosophy

A new context for the group delay function is presented describing electromagnetic pulse propagation in a uniform linear dielectric medium. In contrast to the traditional formulation, this new context retains validity for pulses of any bandwidth, propagating in media with arbitrarily complicated resonance structures. The new context defines the arrival time of a light pulse at a point in space (using a time expectation integral over the Poynting vector) and considers the delay between pulse arrival times at two distinct points. This delay consists of two parts: a spectral superposition of group delays and a delay due to spectral reshaping via absorption or amplification. The traditional formulation of group velocity is recovered by taking a narrowband limit of this generalized context. The use of the new context is illustrated for pulses propagating both superluminally and subluminally in amplifying and absorbing media. The inevitable transition to subluminal behavior for any initially superluminal pulse is also demonstrated.

The energy exchanged between an electromagnetic pulse and a linear dielectric medium in which it propagates is also considered. It is this exchange of energy which allows for the superluminal behavior of the centroid of field energy. While group velocity indicates the presence of field energy (the locus of which can move with arbitrary speed), the velocity of energy transport maintains strict luminality. This indicates that the medium exchanges energy differently with the leading and trailing portions of the pulse. The reason for this asymmetric treatment is clearly demonstrated by rewriting the exchange energy in terms of the instantaneous spectrum (i.e., the spectrum of the pulse truncated at each new instant as a given locale in the medium experiences the pulse). This description for the exchange energy directly emphasizes the role of the principle of causality and gives insight into the phenomenon of superluminal pulse propagation.

ACKNOWLEDGMENTS

Many people deserve thanks for helping me to a successful completion of this degree. My advisor Justin Peatross initially came up with the idea for the new group delay context (reportedly on a napkin in McDonalds), and it has been a pleasure working with him to fully develop the theory. Beyond simply helping me understand the physics we have studied, he has helped me see the satisfaction that can come from studying the natural world. Scott Glasgow has also been very involved in this study, especially with regard to the material on pulse/medium interactions. My father, Gene Ware, set the example for me to follow when he returned to school with five children to get his own doctorate degree, and my mother, Janis Ware, showed me the importance of education by returning to school after raising a family to get her teaching certificate. Both parents have been unfailing in their support of my efforts.

Contents

List of Figures

Chapter 1

Introduction

The speed at which light travels has captured the interest of people throughout history. In the 1600's Galileo Galilei attempted to determine the speed of light by measuring the time required for an assistant located about a mile away to return a light signal produced by uncovering a lantern. In his report of the experiment, Galileo records that "I was unable to make sure whether the facing light appeared instantaneously. But if not instantaneous, light is very swift."[2] In subsequent years, as scientific understanding and technology have progressed, researchers have greatly improved upon this preliminary observation. Today we are able to measure the vacuum speed of light (c) with such precision that in 1983 the meter was redefined in terms of c.

Propagation in a dispersive system is somewhat more complicated than the vacuum case. Nevertheless, the methods used to solve Maxwell's equations in these systems are well developed, and the behavior of the solutions has been described in great detail. Researchers also routinely measure the velocity of propagation through these systems in the laboratory. The generic experiment used to determine propagation velocity consists of measuring the time delay between when the peak (or some other feature) of a pulse enters and exits a system. Since the spatial dimensions of the system are known, the

average velocity of the pulse in the system can then be inferred. For the vast majority of dispersive systems this type of experiment yields the pedestrian result that the pulse traverses the system at a velocity somewhat slower than c. However, by carefully selecting the pulse and system it is possible to create situations where the delay times correspond to velocities greater than c, or are even negative (i.e., the exiting pulse peak leaves the system before the entering pulse peak arrives at the entrance). These observations have led to a revived interest in studying the theoretical explanation of how pulses propagate.

In this work, we consider the propagation of electromagnetic pulses in dispersive systems. We present a new context which gives a natural explanation for the apparently anomalous 'superluminal' results mentioned above. We begin by briefly sketching the history of the study of propagation velocity in dispersive systems. Although this history is in no way comprehensive, it is included to give context and motivation for the work presented in subsequent chapters. We then give an overview of the concepts that will be addressed in this work, and point out how they relate to previous work done in this area.

1.1 Historical Background

The study of wave propagation is among the oldest and most well explored branches of physics. One of the fundamental issues that arises in this study is the velocity at which a disturbance propagates from point to point in a dispersive medium. In 1839, Hamilton introduced the concept of group velocity to describe the speed at which mechanical disturbances propagate from regions that are fully excited to regions that are at rest in a system. The idea of group velocity was later re-introduced by Stokes in 1876 and further developed and generalized by Lord Rayleigh, again in connection with mechanical waves. (For a summary of the history of group velocity see Ref. [3].) This early work demonstrated that if absorption is small, the group velocity gives the speed at which a mechanical pulse

propagates through a system. As the wave nature of light was fully appreciated, this result was also applied to optical pulses in dispersive systems.

In the early 1900's, as the principles of relativity unfolded, there was a resurgence of interest in the concept of group velocity. This renewed interest stemmed from the fact that it is possible to have group velocities larger than c in an absorption band of a dielectric medium. If group velocity represents the speed at which a signal can be sent, this situation presents a problem for the theory of relativity, which predicts that causality can only be preserved if communication at speeds greater than c is prohibited. This led Sommerfeld and Brillouin[4] to study whether it is possible to send information faster than the speed of light. They analyzed the behavior of a signal produced when a harmonic electric field is abruptly turned on and then allowed to propagate in a medium. In this analysis, they proved that the velocity at which an abrupt signal edge travels in a causal medium (i.e., a medium that cannot anticipate the form of a pulse before experiencing it) is always strictly bounded by c, thus confirming the prediction of relativity. Additionally, they introduced the concept of energy velocity, which is defined as the rate of energy flow (i.e., the Poynting vector) divided by the energy density at a point.

In 1970 Garrett and McCumber revisited the problem of pulse propagation in absorption regions where group velocity exceeds c. In their paper[5] they analyzed the propagation of a Gaussian light pulse whose spectrum is centered on-resonance. They demonstrated that if a pulse has sufficiently narrow bandwidth, it remains almost Gaussian as it propagates and the pulse peak can move at velocities faster than c (as predicted by group velocity). In 1971, Crisp commented on this paper and pointed out that the superluminal velocity of the peak is simply a result of the leading edge of the pulse experiencing less absorption than the trailing portion, causing the pulse's "center of gravity to move forward at a velocity greater than the phase velocity of light."[6] In 1982, Chu and Wong[7] observed the Garrett and McCumber effect (i.e., a superluminal delay time for an

on-resonance pulse in an absorbing media) in the laboratory.

Because the Garrett and McCumber effect occurs in an absorbing medium, the leading edge of the propagating pulse is always within the envelope of the initial pulse propagated forward at c. Thus, this situation presents no problems for causality. An analogous 'superluminal' situation could be constructed by sending the pulse through vacuum and setting a first detector to click at the peak amplitude of the incoming pulse, and a second detector to click at a lower amplitude. The second detector is then triggered before the arrival of the pulse peak, and the delay between the clicks is 'superluminal' while obviously nothing has gone faster than the speed of light.

Perhaps more intriguing than the Garrett and McCumber effect is an experiment proposed by Raymond Chiao[8] in 1993. In this experiment, a narrowband pulse is tuned to the spectral region just outside of an amplifying resonance. As the pulse passes through the medium, the peak of the transmitted pulse travels faster than c. However, unlike the absorbing case the exiting pulse is not contained within the envelope of the original pulse propagated forward at c. Thus, the simple argument presented in the previous paragraph about causality in the absorbing case is not obviously applied here. In 2000 Wang[9] experimentally demonstrated the Chiao effect using Caesium gas as the propagation medium.

1.2 Motivation

While the solutions to Maxwell's equations accurately model each of the pulse propagation situations mentioned in section 1.1 (as they must), there has been considerable discussion about validity of several of the methods used to describe the behavior of these solutions. In order to get a flavor for this discussion and give motivation for this work, we include several quotes from various participants in the discussion. This presentation

simplifies the issues involved, but introduces many of the key questions to be addressed in this work.

One of the principle concepts that has come under scrutiny in this discussion is group velocity. The analysis of Sommerfeld and Brillouin revealed some of the shortcomings of group velocity in describing the velocity of a signal front. The energy velocity description introduced by Sommerfeld and Brillouin does not suffer from the same shortcomings (although it has some of its own), possibly making it more appealing than the group velocity description. This prompted Chu and Wong to make the following comment in the report detailing their observation of the Garrett and McCumber effect:

> Physicists may be tempted to analyze pulse propagation experiments in terms of energy velocities and not group velocities. Nevertheless, Garrett and McCumber have shown under certain easily satisfied approximations ... that the pulse will propagate with a velocity equal to the group velocity, even when [superluminal or negative]. ... The work reported here ... clearly demonstrates that [energy velocity] is not the measured quantity in this type of pulse propagation experiment.[7]

Oughstun took issue with this statement of Chu and Wong. He stated that the experimental results published by Chu and Wong, which "were purported to disprove the energy velocity description while verifying the group velocity description,"[10] rather showed that the the two descriptions had different regions of validity. Oughstun summarized this result as follows:

> As a pulse propagates away from its input plane, its dynamical evolution is initially characterized by the group velocity description, but as the propagation distance increases and the pulse dispersion becomes mature, its dynamical evolution becomes characterized by the asymptotic description

> and its resultant energy velocity description.[11]

Oughstun also pointed out[12] that the Taylor series expansion techniques used to derive the group velocity description fail when broadband pulses are considered. Because of these failures, he champions the energy velocity description as the more useful description:

> Whereas the group-velocity description decreases monotonically in accuracy as the propagation distance increases above an absorption depth, the asymptotic description and its derivative energy velocity description increase in accuracy as the propagation distance increases. . . . Although the asymptotic description is somewhat more complicated than the group-velocity description, that is a small price to pay for a correct description of this important problem.[12]

In chapter 6 we consider the group-velocity versus energy-velocity issue in more detail. For now, we simply point out that there has not been a uniform opinion on the usefulness of the concept of group velocity.

The quotes presented above relate primarily to propagation in an absorbing medium. There have also been discussions about the proper way to describe propagation in amplifying media. For instance, Chiao initially explained how superluminal propagation occurs in an amplifying medium as follows:

> The inverted medium can temporarily loan part of its stored energy to the forward tail of the wave packet, in a pulse-reshaping process which moves the peak of the wave packet forward in time. One can think of this pulse-reshaping process as the virtual amplification of the forward tail of the wave packet, followed by the virtual absorption of the peak, resulting in an advancement of the wave packet.[13]

However, Wang specifically denies that the reshaping process described by Chiao could have caused the effect. In his article reporting the observation of the Chiao effect Wang states:

> The probe pulse ... contains essentially no spectral components that are resonant with the Raman gain lines to be amplified. Therefore, the argument that the probe pulse is advanced by amplification of its front edge does not apply. The superluminal light propagation observed here is the result only of the anomalous dispersion region... It can be understood by the classical theory of wave propagation in an anomalous dispersion region where interference between different frequency components produces this rather counterintuitive effect.[9]

Again, the above statements indicate that there is not a general consensus on which descriptive technique is the 'best' for explaining the superluminal phenomena.

In light of the above excerpts, it is interesting to recall a statement made by Galileo after detailing his attempt to measure propagation velocity.

> But in what seas are we inadvertently engulfing ourselves, bit by bit? Among voids, infinities, indivisibles, and instantaneous movements, shall we ever be able to reach harbor even after a thousand discussions?[2]

When reading this statement, one might almost believe that Galileo foresaw the recent proliferation of discussions addressing the theoretical description of pulse propagation. Even with the many carefully thought-out discussions on the subject, there are still issues related to the topic of pulse propagation where our understanding is not what it needs to be. While the present work will certainly not be the last word in this discussion, hopefully it is a step towards the final harbor mentioned by Galileo.

1.3 Overview

We address two main issues related to pulse propagation in this work. First, we introduce a new context for the group delay function (group delay is inversely proportional to group velocity). In chapter 2 we review the solutions to Maxwell's equations and how the concept of group delay is traditionally obtained from these solutions. We show why traditional group velocity often fails, and then derive the new context for group delay. This new context does not rely on expansion techniques, so it retains validity for a pulse of any bandwidth propagating in a medium with arbitrarily complicated resonance structures. In addition, this new context retains validity for any propagation distance.

In chapter 3 we illustrate how our new context for group delay may be applied to gain insight into the behavior of the solutions of Maxwell's equations. We explain the effect of pulse bandwidth on the delay time between pulse arrival at one point versus another. We describe how delay times depend on propagation distance, and also point out that superluminal behavior inevitably becomes subluminal as propagation distance is increased. We also discuss how the new context may be applied to determine delay times in angularly dispersive systems and in precursor fields.

The second major issue addressed in this work is the flow of energy as a pulse propagates in a dielectric medium. In chapter 4 we review how Poynting's theorem is obtained and how the concept of energy transport velocity is defined. We show how the velocity of the centroid of total energy (i.e., the average spatial position of total energy) is strictly bounded by c. We then demonstrate that the centroid of *field* energy can move with any velocity, even though the rate at which field energy is transported from one point to another is strictly bounded by c. To explain this seeming paradox, we derive an expression for the energy exchanged between the pulse field and the medium. This new expression shows how the medium treats the leading and trailing portions of the pulse

differently. The asymmetric exchange of energy between the field and the medium during various parts of a pulse is a key to understanding how the locus of field energy can move superluminally while no energy is transported faster than c.

Chapter 5 discusses energy exchange and transport for several specific examples and illustrates the concepts introduced in chapter 4. We discuss energy exchange for superluminal propagation in single resonance absorbing and amplifying media. We also discuss media composed of more complicated resonance structures. In addition, we address situations in which pulses are observed to propagate at highly subluminal speeds. In chapter 6 we summarize the results presented in the preceding chapters. We then use these results to discuss the implausibility of using superluminal effects mentioned in this work for a practical purpose.

Chapter 2

Group Delay

In this chapter we discuss the meaning of group velocity. We begin with a review of the solutions to the Maxwell equations, and show how the traditional concept of group delay (inverse of group velocity) is obtained using these solutions. This traditional context of group velocity fails when the bandwidth of the pulse encompasses a resonance structure. We replace the old context with a new one wherein the group delay function always retains meaning for electromagnetic pulses propagating in linear homogeneous media. This includes broadband pulses with arbitrarily complicated temporal structure and with spectra in regions of anomalous dispersion. The new context reduces to the result obtained in traditional pedagogy[4,14,15] in the narrowband limit.

2.1 Maxwell's Equations

The basic laws governing electromagnetic phenomena are contained in the Maxwell equations. In this work we consider only neutral, nonconducting, nonmagnetic media. In this situation, the Maxwell equations can be written as

$$\nabla \cdot [\epsilon_0 \mathbf{E}(\mathbf{r}, t) + \mathbf{P}(\mathbf{r}, t)] = 0 \tag{2.1}$$

$$\nabla \cdot \mathbf{B}(\mathbf{r}, t) = 0 \tag{2.2}$$

$$\nabla \times \mathbf{E}(\mathbf{r}, t) = -\frac{\partial \mathbf{B}(\mathbf{r}, t)}{\partial t} \tag{2.3}$$

$$\frac{1}{\mu_0} \nabla \times \mathbf{B}(\mathbf{r}, t) = \frac{\partial}{\partial t} \left[\epsilon_0 \mathbf{E}(\mathbf{r}, t) + \mathbf{P}(\mathbf{r}, t) \right], \tag{2.4}$$

where **E** is the electric field, **P** is the electric polarization of the medium, and **B** is the magnetic induction (**r** denotes the spatial coordinate and t denotes time). In order to solve Maxwell's equations for the fields within a medium, it is necessary to specify the relationship between **E** and **P** (i.e. the constitutive relation which defines the material response to the electric field). In the time domain, this relationship is usually complicated. However, in the frequency domain it is often possible to write a simple linear relation between the electric field and polarization. In an isotropic, homogeneous medium, this constitutive relation is given by

$$\mathbf{P}(\mathbf{r}, \omega) = \epsilon_0 \chi(\omega) \mathbf{E}(\mathbf{r}, \omega), \tag{2.5}$$

where $\chi(\omega)$ is the susceptibility.

Because the constitutive relation (2.5) can be written in this simple form in the frequency domain, the solutions to Maxwell's equations are usually found in a frequency context. The frequency domain representation of the electric field **E** at a point **r** is related to the time domain representation by the Fourier transform

$$\mathbf{E}(\mathbf{r}, \omega) = \frac{1}{\sqrt{2\pi}} \int_{-\infty}^{\infty} e^{i\omega t} \mathbf{E}(\mathbf{r}, t) \, \mathrm{d}t. \tag{2.6}$$

The time domain representation of the field may be recovered via the inverse Fourier transform

$$\mathbf{E}(\mathbf{r}, t) = \frac{1}{\sqrt{2\pi}} \int_{-\infty}^{\infty} e^{-i\omega t} \mathbf{E}(\mathbf{r}, \omega) \, \mathrm{d}\omega. \tag{2.7}$$

The time/frequency connections for the electric polarization and magnetic field are

similarly defined by

$$\mathbf{P}(\mathbf{r},\omega) = \frac{1}{\sqrt{2\pi}} \int_{-\infty}^{\infty} e^{i\omega t} \mathbf{P}(\mathbf{r},t)\ \mathrm{d}t \ \Leftrightarrow\ \mathbf{P}(\mathbf{r},t) = \frac{1}{\sqrt{2\pi}} \int_{-\infty}^{\infty} e^{-i\omega t} \mathbf{P}(\mathbf{r},\omega)\ \mathrm{d}\omega \tag{2.8}$$

and

$$\mathbf{B}(\mathbf{r},\omega) = \frac{1}{\sqrt{2\pi}} \int_{-\infty}^{\infty} e^{i\omega t} \mathbf{B}(\mathbf{r},t)\ \mathrm{d}t \Leftrightarrow \mathbf{B}(\mathbf{r},t) = \frac{1}{\sqrt{2\pi}} \int_{-\infty}^{\infty} e^{-i\omega t} \mathbf{B}(\mathbf{r},\omega)\ \mathrm{d}\omega. \tag{2.9}$$

By convention, we take all fields to be real in the time domain. This produces the following symmetries in the frequency domain:

$$\mathbf{E}(\mathbf{r},-\omega) = \mathbf{E}^*(\mathbf{r},\omega), \tag{2.10}$$

$$\mathbf{P}(\mathbf{r},-\omega) = \mathbf{P}^*(\mathbf{r},\omega), \tag{2.11}$$

$$\mathbf{B}(\mathbf{r},-\omega) = \mathbf{B}^*(\mathbf{r},\omega), \tag{2.12}$$

$$\chi(-\omega) = \chi^*(\omega). \tag{2.13}$$

In the frequency domain, Maxwell's equations have as a solution

$$\mathbf{E}(\mathbf{r}_0 + \Delta\mathbf{r},\omega) = \mathbf{E}(\mathbf{r}_0,\omega)\, e^{i\mathbf{k}\cdot\Delta\mathbf{r}}, \tag{2.14}$$

where the initial pulse form $\mathbf{E}(\mathbf{r}_0,\omega)$ is chosen at a point $\mathbf{r}_0$. The solution (2.14) renders the pulse form $\mathbf{E}(\mathbf{r}_0+\Delta\mathbf{r},\omega)$ (in terms of the initial pulse form) at any other point shifted by the displacement $\Delta\mathbf{r}$. Linear superpositions of solutions of the form (2.14) are also solutions to Maxwell's equations. The properties of the medium enter this solution through the wave vector $\mathbf{k}(\omega)$. Maxwell's equations combined with the constitutive relation (2.5) require that the magnitude of the wave vector is given by

$$k^2(\omega) = \frac{\omega^2}{c^2}\left[1+\chi(\omega)\right]. \tag{2.15}$$

The direction of $\mathbf{k}(\omega)$ specifies the direction of propagation for each frequency. In writing the solution (2.14) we have made the implicit assumption that each frequency is associated with a single wave vector, although the wave vectors need not be all in the same

direction. Thus, diffraction effects associated with narrow beams[16] are ignored, but this approximation is reasonable for many optical systems.

The susceptibility $\chi(\omega)$ is allowed to take on complex values in order to describe absorption or amplification. Here we take the traditional vantage point of considering the frequency ω to be real, whereas the wave vector $\mathbf{k}(\omega)$ can be complex when the susceptibility $\chi(\omega)$ is complex. The magnetic field is obtained through

$$\mathbf{B}(\mathbf{r},\omega) = \mathbf{k}(\omega) \times \mathbf{E}(\mathbf{r},\omega)/\omega \,. \tag{2.16}$$

The time representation of the fields at the new point are obtained by transforming (2.5), (2.14), and (2.16) to the time domain via (2.7), (2.8), and (2.9).

2.2 Traditional Group Delay

In the time domain, the solution for the electric field at $\mathbf{r} \equiv \mathbf{r}_0 + \Delta\mathbf{r}$ can be written as

$$\mathbf{E}(\mathbf{r},t) = \frac{1}{\sqrt{2\pi}} \int_{-\infty}^{\infty} \mathbf{E}(\mathbf{r}_0,\omega)\, e^{i(\mathbf{k}(\omega)\cdot\Delta\mathbf{r}-\omega t)}\, \mathrm{d}\omega. \tag{2.17}$$

The traditional concept of group velocity is obtained by expanding the frequency-dependent phase delay as

$$\mathbf{k}(\omega)\cdot\Delta\mathbf{r} \approx [\mathbf{k}|_{\bar\omega}\cdot\Delta\mathbf{r}] + \left[\left.\frac{\partial\mathbf{k}}{\partial\omega}\right|_{\bar\omega}\cdot\Delta\mathbf{r}\right](\omega-\bar\omega) + \cdots. \tag{2.18}$$

If we retain only the first two terms in this expansion then (2.17) becomes

$$\mathbf{E}(\mathbf{r},t) = e^{i\left[\mathbf{k}(\bar\omega)-\bar\omega\left.\frac{\partial\mathbf{k}}{\partial\omega}\right|_{\bar\omega}\right]\cdot\Delta\mathbf{r}} \frac{1}{\sqrt{2\pi}} \int_{-\infty}^{\infty} \mathbf{E}(\mathbf{r}_0,\omega)\, e^{-i\omega\left(t-\left.\frac{\partial\mathbf{k}}{\partial\omega}\right|_{\bar\omega}\cdot\Delta\mathbf{r}\right)}\, \mathrm{d}\omega. \tag{2.19}$$

We now make the approximation that the imaginary part of $\mathbf{k}$ is roughly constant over the range of frequencies present in the original pulse, so that $\partial\mathbf{k}/\partial\omega \approx \partial\,\mathrm{Re}\,\mathbf{k}/\partial\omega$. The integral in (2.19) is then seen to be the inverse Fourier transform of the original pulse with a modified time argument, so that we may write:

$$\mathbf{E}(\mathbf{r},t) = \mathbf{E}\left(\mathbf{r}_0, t-t'\right) e^{i\left[\mathbf{k}(\bar\omega)\cdot\Delta\mathbf{r}-\bar\omega t'\right]}, \tag{2.20}$$

where

$$t' \equiv \left.\frac{\partial \mathrm{Re}\,\mathbf{k}}{\partial \omega}\right|_{\bar{\omega}} \cdot \Delta\mathbf{r}. \tag{2.21}$$

Finally, we compute the square magnitude of (2.20) to compare the intensity profile of the pulse at $\mathbf{r}$ with the profile at $\mathbf{r}_0$

$$|\mathbf{E}(\mathbf{r}, t)|^2 = \left|\mathbf{E}\left(\mathbf{r}_0, t - t'\right)\right|^2 e^{-2\,\mathrm{Im}\,\mathbf{k}(\bar{\omega})\cdot\Delta\mathbf{r}}. \tag{2.22}$$

In (2.22) we see that (to first order) the delay t' given in (2.21) is the time required for the pulse to traverse the displacement $\Delta\mathbf{r}$. The exponential in (2.22) describes the amplitude of the pulse at the new point, which may have changed during propagation due to amplification or absorption. The function $\partial\,\mathrm{Re}\,\mathbf{k}/\partial\omega \cdot \Delta\mathbf{r}$ is known as the *group delay function*, and in this traditional context is evaluated at a single 'carrier' frequency $\bar{\omega}$. The traditional group velocity is obtained by dividing the displacement $\Delta\mathbf{r}$ by the group delay function evaluated at $\bar{\omega}$. (With more detailed analysis, expansion techniques can be used to show that higher order terms in the expansion (2.18) describe pulse reshaping and also influence delay time.)

2.2.1 Failure of Traditional Group Delay

The failings of the expansion (2.18) are well documented.[11,12] In particular, if the bandwidth of an electromagnetic pulse encompasses a substantial portion of a resonance structure, it becomes necessary to retain many terms in the expansion (2.18) to accurately describe the phase delay. Moreover, if the bandwidth of the pulse becomes too broad, the series fails to converge regardless of how many terms are used. To see why this expansion fails for broadband pulses, consider the index of refraction in a single resonance absorbing Lorentz medium:

$$[n(\omega)]^2 = 1 + \frac{f{\omega_p}^2}{\left({\omega_0}^2 - \omega^2 - i\gamma\omega\right)}, \tag{2.23}$$

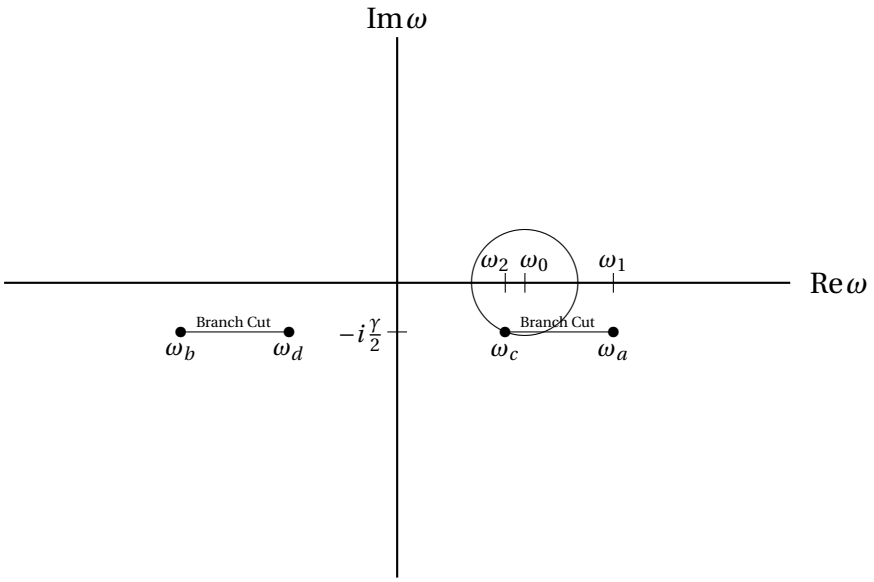

Figure 2.1: Singularities and branch cuts for $k(\omega)$ obtained using a single resonance Lorentz medium. The circle shows the radius of convergence for a Taylor series centered on the resonance frequency, ω_0.

where f, ω_p, and γ are positive constants. We construct the wave number using the standard relation $k(\omega) = \omega n(\omega)/c$, and write the result in the following form which makes the singularity structure of $k(\omega)$ apparent:

$$k(\omega) = \frac{\omega}{c}\left[\frac{(\omega-\omega_a)(\omega-\omega_b)}{(\omega-\omega_c)(\omega-\omega_d)}\right]^{1/2}. \tag{2.24}$$

The zeros of $k(\omega)$ occur at $\omega = 0$ and at the following frequencies in the complex ω plane

$$\omega_a = \omega_1 - \frac{i\gamma}{2}, \quad \omega_b = -\omega_1 - \frac{i\gamma}{2}, \quad \text{where } \omega_1^2 = \omega_0^2 + f\omega_p^2 - \frac{\gamma^2}{4}, \tag{2.25}$$

and the poles are located at

$$\omega_c = \omega_2 - \frac{i\gamma}{2}, \quad \omega_d = -\omega_2 - \frac{i\gamma}{2}, \quad \text{where } \omega_2^2 = \omega_0^2 - \frac{\gamma^2}{4}. \tag{2.26}$$

Figure 2.1 shows the singularity structure in the complex plane for $k(\omega)$.

We now recall a property of the Taylor series expansion which arises from the standard analysis of functions of complex variables.[17] Suppose that we expand a function $f(z)$

about some point z_0, and that the point z_1 represents the nearest singular point of $f(z)$ in the complex z plane. Our Taylor series expansion of $f(z)$ will then converge only for z contained in a circle of radius $|z_1 - z_0|$ centered at z_0.

To see how this applies in our case, suppose that we expand the expression (2.24) around the resonance frequency, ω_0. The nearest singular point occurs at ω_c. Thus, the expansion will only converge for frequencies within the circle shown in Fig. 2.1. Since we consider only real frequencies in (2.24), this means that the expansion (2.18) will converge for frequencies located between the two intersection points of the circle with the real ω-axis. If our pulse has spectrum which extends outside of this radius of convergence, the expansion technique leading to traditional group delay cannot accurately describe its propagation. More realistic models for the index of refraction produce a more complicated singularity structure in the complex ω-plane (all singularities remain in the lower half plane for a causal medium). Nevertheless, the singularity structures always result in the same convergence problem when expanding $k(\omega)$ near a resonance.

In addition to the convergence problem detailed above, broadband pulses also pose another problem for the traditional concept of group delay. Near a resonance the group delay function varies rapidly. Thus, the traditional group delay can be highly dependent on which frequency one chooses to expand around. For a broadband pulse there is a range of frequencies present which could be considered appropriate 'carrier' frequencies around which to expand, and the delay predicted by (2.21) can vary widely depending on which $\bar{\omega}$ is chosen. Because of these difficulties, textbooks on the subject state that the traditional concept of group velocity "has no longer any appreciable physical significance"[14] or "may even lack precise meaning"[15] for broadband pulses near resonance. In the remainder of this chapter we endeavor to supply this precise meaning that has been absent in the broadband context.

We note that the fact that group velocity can become superluminal and/or negative

in the vicinity of a resonance structure does not indicate a failure of the expansion (2.18).[1,5,8,13] This type of exotic behavior (well verified experimentally[7,9]) occurs in a narrowband limit where the expansion is valid. In chapter 3 we illustrate several cases where superluminal behavior occurs, and in chapters 4 and 5 we discuss the energy exchanged between the field and the medium which makes this behavior possible.

2.3 A New Context for Group Delay

The traditional context of group velocity introduced in the previous section relies on the assumption that the pulse has a similar shape at the initial and final points (aside from overall attenuation or amplification), as shown in (2.22). In the general case, this need not be true. Thus, in order to concretely discuss the time required for a pulse to traverse a given displacement, we must first define the arrival time of a pulse to a point (say where a detector is located). This definition need only involve the Poynting vector, since it alone transports energy. To deal with arbitrary broadband pulses, the arrival time should avoid presupposing a specific pulse shape, since the pulse may evolve in complicated ways during propagation. For example, the peak or the midpoint on the rising edge of a pulse is a poor indicator of arrival time if the pulse contains multiple peaks or has a long and non-uniform rise time.

For the reasons given, we use a time expectation integral (proposed by Smith[18] in 1970) to specify the arrival of the pulse:

$$\langle t \rangle_{\mathbf{r}} \equiv \int_{-\infty}^{\infty} t \rho(\mathbf{r}, t)\ \mathrm{d}t, \tag{2.27}$$

where $\rho(\mathbf{r}, t)$ is a normalized temporal distribution of the Poynting flux at $\mathbf{r}$:

$$\rho(\mathbf{r}, t) \equiv \hat{\eta} \cdot \mathbf{S}(\mathbf{r}, t) \Big/ \hat{\eta} \cdot \int_{-\infty}^{\infty} \mathbf{S}(\mathbf{r}, t)\ \mathrm{d}t\,. \tag{2.28}$$

The Poynting vector is defined as usual:

$$\mathbf{S}(\mathbf{r},t) \equiv \mathbf{E}(\mathbf{r},t) \times \frac{\mathbf{B}(\mathbf{r},t)}{\mu_0}. \tag{2.29}$$

As Smith explained, this definition of arrival time "is not restricted to a quasi monochromatic pulse or to a situation which one has always only a single pulse. ... It yields a unique value regardless of the dispersion present." The unit vector $\hat{\eta}$ refers to the direction in which the energy flow is detected (normal to a detector surface). It has importance for angularly dispersive systems, such as grating pairs used for pulse compression, where the result of the integral in the numerator is not necessarily parallel to that in the denominator.

Before proceeding, we make a note of caution. It may be tempting to equate the arrival time of the *temporal* center of mass to a point, given by (2.27), with the time at which the *spatial* center of mass arrives at the point. Although in many cases these two arrival times happen to give the same value (e.g., if there is no attenuation or amplification), they do not measure the same thing. For example, consider a pulse which is chirped such that the leading portion arrives at the observation point with little attenuation, while the trailing portion is composed of spectral components that are completely absorbed before they can be detected. The temporal center of mass arrives some time during the leading portion of the pulse. However, when the spatial center of mass arrives at the observation point, the energy in the trailing portion (which will be absorbed before reaching the detector) may still be affecting its location. This makes the arrival time of the spatial center of mass later than the arrival time of the temporal center of mass. The temporal center of mass used in (2.27) is the more relevant arrival time, since it is what a detector would measure.

With the definition (2.27) of arrival time in hand, we are prepared to discuss the time required for a pulse to traverse a given distance within the medium. Mathematically, the

delay between the time when a pulse arrives at a point $\mathbf{r}_0$ and when it arrives at a point $\mathbf{r} \equiv \mathbf{r}_0 + \Delta\mathbf{r}$ is defined by

$$\Delta t \equiv \langle t \rangle_{\mathbf{r}} - \langle t \rangle_{\mathbf{r}_0}. \tag{2.30}$$

In section 2.4 we recast the delay time (2.30) into a form that makes clear the connection between Δt and the group delay function $\partial \mathrm{Re}\,\mathbf{k}/\partial\omega \cdot \Delta\mathbf{r}$. Section 2.5 begins with the result of this derivation, so that section 2.4 may be skipped without a loss of continuity.

2.4 Derivation of the New Context

Motivated by a desire to make connection with the traditional group velocity, we rewrite the arrival time (2.27) of the pulse in terms of the frequency representations of the fields involved. The denominator of (2.28) may be transformed immediately via Parseval's theorem:

$$\int_{-\infty}^{\infty} \mathbf{S}(\mathbf{r}, t)\ \mathrm{d}t = \int_{-\infty}^{\infty} \mathbf{S}(\mathbf{r}, \omega)\ \mathrm{d}\omega, \tag{2.31}$$

where the frequency representation of the Poynting vector is given by

$$\mathbf{S}(\mathbf{r}, \omega) \equiv \mathbf{E}(\mathbf{r}, \omega) \times \frac{\mathbf{B}^*(\mathbf{r}, \omega)}{\mu_0}. \tag{2.32}$$

Employing the Fourier relation (2.7) in the numerator of (2.27) (with (2.28) inserted), we find

$$\begin{aligned} \int_{-\infty}^{\infty} t\mathbf{S}(\mathbf{r}, t)\ \mathrm{d}t \quad &= \quad \int_{-\infty}^{\infty} t \left[\frac{1}{\sqrt{2\pi}} \int_{-\infty}^{\infty} \mathbf{E}(\mathbf{r}, \omega)\, e^{-i\omega t}\, \mathrm{d}\omega \right] \\ &\quad \times \left[\frac{1}{\sqrt{2\pi}} \int_{-\infty}^{\infty} \mathbf{B}\left(\mathbf{r}, \omega'\right) e^{-i\omega' t}\, \mathrm{d}\omega' \right] \mathrm{d}t. \end{aligned} \tag{2.33}$$

By introducing a frequency derivative to account for the factor t, the expression (2.33) can be recast as

$$\int_{-\infty}^{\infty} t\mathbf{S}(\mathbf{r}, t)\ \mathrm{d}t = i \int_{-\infty}^{\infty} \mathrm{d}\omega \mathbf{E}(\mathbf{r}, \omega) \times \frac{\partial}{\partial\omega} \left[\int_{-\infty}^{\infty} \mathrm{d}\omega' \frac{\mathbf{B}\left(\mathbf{r}, \omega'\right)}{\mu_0} \frac{1}{2\pi} \int_{-\infty}^{\infty} e^{-i(\omega+\omega')t}\, \mathrm{d}t \right]. \tag{2.34}$$

The final integral is recognized as a delta function, which permits the integration over ω' to be performed:

$$\begin{aligned}\int_{-\infty}^{\infty} t\mathbf{S}(\mathbf{r},t)\ \mathrm{d}t &= i\int_{-\infty}^{\infty}\mathbf{E}(\mathbf{r},\omega)\times\frac{\partial}{\partial\omega}\frac{\mathbf{B}(\mathbf{r},-\omega)}{\mu_0}\,\mathrm{d}\omega \\ &= -i\int_{-\infty}^{\infty}\frac{\partial\mathbf{E}(\mathbf{r},\omega)}{\partial\omega}\times\frac{\mathbf{B}^*(\mathbf{r},\omega)}{\mu_0}\,\mathrm{d}\omega. \end{aligned} \tag{2.35}$$

Here we have invoked the symmetry relation (2.10). We have also integrated by parts in order to place (by preference) the derivative on the electric field rather than on the magnetic field. In doing this, we have assumed a pulse of a finite duration. Equations (2.31) and (2.35) lead to the frequency domain representation of the arrival time:

$$\langle t\rangle_{\mathbf{r}} = T\left[\mathbf{E}(\mathbf{r},\omega)\right], \tag{2.36}$$

where

$$T\left[\mathbf{E}(\mathbf{r},\omega)\right] \equiv -i\frac{\hat{\eta}\cdot\int_{-\infty}^{\infty}\frac{\partial\mathbf{E}(\mathbf{r},\omega)}{\partial\omega}\times\frac{\mathbf{B}^*(\mathbf{r},\omega)}{\mu_0}\,\mathrm{d}\omega}{\hat{\eta}\cdot\int_{-\infty}^{\infty}\mathbf{S}(\mathbf{r},\omega)\ \mathrm{d}\omega}. \tag{2.37}$$

In (2.37) we have indicated that the function T depends only on the electric field since the magnetic field can be written in terms of the electric field through (2.16).

The arrival time of the pulse as expressed in (2.37) is not very useful in itself. Its usefulness is revealed when applied to the difference in arrival times of a pulse to two different locations, say $\mathbf{r}_0$ and $\mathbf{r} = \mathbf{r}_0 + \Delta\mathbf{r}$. As defined in (2.30), the difference in the arrival times of the two points is

$$\Delta t \equiv \langle t\rangle_{\mathbf{r}} - \langle t\rangle_{\mathbf{r}_0} = T\left[\mathbf{E}(\mathbf{r}_0+\Delta\mathbf{r},\omega)\right] - T\left[\mathbf{E}(\mathbf{r}_0,\omega)\right]. \tag{2.38}$$

Our goal is to recast (2.38) into a form that makes clear the connection between Δt and the group delay function $\partial\,\mathrm{Re}\,\mathbf{k}/\partial\omega\cdot\Delta\mathbf{r}$.

To obtain the desired result, we first examine an explicit form for $T\left[\mathbf{E}(\mathbf{r}_0+\Delta\mathbf{r},\omega)\right]$. With the solution (2.14) we can evaluate the integrand of the numerator of (2.37) at $\mathbf{r}_0+\Delta\mathbf{r}$

as follows:

$$\begin{aligned}\frac{\partial \mathbf{E}(\mathbf{r}_0,\omega)\,e^{i\mathbf{k}\cdot\Delta\mathbf{r}}}{\partial\omega}\times\frac{\mathbf{B}^*(\mathbf{r}_0,\omega)\,e^{-i\mathbf{k}^*\cdot\Delta\mathbf{r}}}{\mu_0} &= \frac{\partial}{\partial\omega}\left(\left[\mathbf{E}(\mathbf{r}_0,\omega)\,e^{-\mathrm{Im}\mathbf{k}\cdot\Delta\mathbf{r}}\right]e^{i\,\mathrm{Re}\mathbf{k}\cdot\Delta\mathbf{r}}\right)\\ &\quad\times\frac{\mathbf{B}(\mathbf{r}_0,\omega)}{\mu_0}e^{-\mathrm{Im}\mathbf{k}\cdot\Delta\mathbf{r}}e^{-i\,\mathrm{Re}\mathbf{k}\cdot\Delta\mathbf{r}}\\ &= i\frac{\partial\,\mathrm{Re}\mathbf{k}\cdot\Delta\mathbf{r}}{\partial\omega}\mathbf{E}(\mathbf{r}_0,\omega)\times\mathbf{B}^*(\mathbf{r}_0,\omega)\,e^{-2\,\mathrm{Im}\mathbf{k}\cdot\Delta\mathbf{r}}\\ &\quad+\frac{\partial\mathbf{E}(\mathbf{r}_0,\omega)\,e^{-\mathrm{Im}\mathbf{k}\cdot\Delta\mathbf{r}}}{\partial\omega}\times\frac{\mathbf{B}^*(\mathbf{r}_0,\omega)\,e^{-\mathrm{Im}\mathbf{k}\cdot\Delta\mathbf{r}}}{\mu_0}.\end{aligned} \tag{2.39}$$

The integrand of the denominator in (2.37) is also evaluated at $\mathbf{r}_0+\Delta\mathbf{r}$, giving

$$\begin{aligned}\mathbf{S}(\mathbf{r}_0+\Delta\mathbf{r},\omega) &= \mathbf{E}(\mathbf{r}_0,\omega)\,e^{i\,\mathrm{Re}\mathbf{k}\cdot\Delta\mathbf{r}}e^{-\mathrm{Im}\mathbf{k}\cdot\Delta\mathbf{r}}\times\frac{\mathbf{B}^*(\mathbf{r}_0,\omega)\,e^{-i\,\mathrm{Re}\mathbf{k}\cdot\Delta\mathbf{r}}e^{-\mathrm{Im}\mathbf{k}\cdot\Delta\mathbf{r}}}{\mu_0}\\ &= \mathbf{E}(\mathbf{r}_0,\omega)\,e^{-\mathrm{Im}\mathbf{k}\cdot\Delta\mathbf{r}}\times\frac{\mathbf{B}^*(\mathbf{r}_0,\omega)\,e^{-\mathrm{Im}\mathbf{k}^*\cdot\Delta\mathbf{r}}}{\mu_0}\\ &= \mathbf{S}(\mathbf{r}_0,\omega)\,e^{-2\,\mathrm{Im}\mathbf{k}\cdot\Delta\mathbf{r}}.\end{aligned} \tag{2.40}$$

Upon using (2.39) and (2.40) with the arrival time (2.37) we obtain

$$\begin{aligned}T\left[\mathbf{E}(\mathbf{r}_0+\Delta\mathbf{r},\omega)\right] &= \frac{\hat{\eta}\cdot\int_{-\infty}^{\infty}\mathbf{S}(\mathbf{r},\omega)\left(\frac{\partial\,\mathrm{Re}\mathbf{k}}{\partial\omega}\cdot\Delta\mathbf{r}\right)\mathrm{d}\omega}{\hat{\eta}\cdot\int_{-\infty}^{\infty}\mathbf{S}(\mathbf{r},\omega)\;\mathrm{d}\omega}\\ &\quad-i\frac{\hat{\eta}\cdot\int_{-\infty}^{\infty}\frac{\partial\mathbf{E}(\mathbf{r}_0,\omega)e^{-\mathrm{Im}\mathbf{k}\cdot\Delta\mathbf{r}}}{\partial\omega}\times\frac{\mathbf{B}^*(\mathbf{r}_0,\omega)e^{-\mathrm{Im}\mathbf{k}^*\cdot\Delta\mathbf{r}}}{\mu_0}\,\mathrm{d}\omega}{\hat{\eta}\cdot\int_{-\infty}^{\infty}e^{-2\,\mathrm{Im}\mathbf{k}\cdot\Delta\mathbf{r}}\mathbf{S}(\mathbf{r}_0,\omega)\;\mathrm{d}\omega}.\end{aligned} \tag{2.41}$$

Using the expressions (2.37) and (2.41), we can now write the delay time (2.38) as

$$\Delta t=\frac{\hat{\eta}\cdot\int_{-\infty}^{\infty}\mathbf{S}(\mathbf{r},\omega)\left(\frac{\partial\,\mathrm{Re}\mathbf{k}}{\partial\omega}\cdot\Delta\mathbf{r}\right)\mathrm{d}\omega}{\hat{\eta}\cdot\int_{-\infty}^{\infty}\mathbf{S}(\mathbf{r},\omega)\;\mathrm{d}\omega}+T\left[e^{-\mathrm{Im}\mathbf{k}\cdot\Delta\mathbf{r}}\mathbf{E}(\mathbf{r}_0,\omega)\right]-T\left[\mathbf{E}(\mathbf{r}_0,\omega)\right], \tag{2.42}$$

which is our final result.

2.5 Discussion of the New Context

Using the result (2.42), we can write the delay time as the sum of two terms with intuitive interpretations:

$$\Delta t = \Delta t_G(\mathbf{r}) + \Delta t_R(\mathbf{r}_0). \tag{2.43}$$

The first term in (2.43), the *net group delay*, is a spectral average of the group delay function weighted by the spectral intensity that is experienced at the final point $\mathbf{r}$:

$$\Delta t_G(\mathbf{r}) = \int_{-\infty}^{\infty} \rho(\mathbf{r},\omega)\left(\frac{\partial \mathrm{Re}\,\mathbf{k}}{\partial\omega}\cdot\Delta\mathbf{r}\right)\mathrm{d}\omega, \tag{2.44}$$

where $\rho(\mathbf{r},\omega)$ is a normalized spectral distribution of field energy at the *final* point $\mathbf{r}$ after propagation:

$$\rho(\mathbf{r},\omega) \equiv \hat{\eta}\cdot\mathbf{S}(\mathbf{r},\omega) \Big/ \hat{\eta}\cdot\int_{-\infty}^{\infty}\mathbf{S}(\mathbf{r},\omega)\ \mathrm{d}\omega. \tag{2.45}$$

Note the close resemblance between (2.27) and (2.44). Both are expectation integrals, the former being executed as a 'center of mass' integral in time, the later being executed in the frequency domain on $\partial\,\mathrm{Re}\,\mathbf{k}/\partial\omega\cdot\Delta\mathbf{r}$. In contrast to the traditional group delay derived in section 2.2, the group delay function evaluated *at every frequency present in the final pulse* (rather than at a single carrier frequency) influences the delay time in this new context. The net group delay depends only on the spectral content of the pulse, independent of its temporal organization (i.e. the phases of $\mathbf{E}(\mathbf{r},\omega)$ and $\mathbf{B}(\mathbf{r},\omega)$ do not contribute). Only the real part of $\mathbf{k}$ plays a direct role in (2.44).

The second term in (2.43) represents a delay which arises solely from a reshaping of the spectrum through absorption (or amplification) and is given by

$$\Delta t_R(\mathbf{r}_0) \equiv T\left[e^{-\mathrm{Im}\,\mathbf{k}\cdot\Delta\mathbf{r}}\mathbf{E}(\mathbf{r}_0,\omega)\right] - T\left[\mathbf{E}(\mathbf{r}_0,\omega)\right], \tag{2.46}$$

where T is the arrival time given in (2.27), but written as a function of the pulse spectrum (see (2.37)). This reshaping delay is evaluated at $\mathbf{r}_0$, *before* propagation takes place. The

reshaping delay is the difference between the pulse arrival time at the initial point $\mathbf{r}_0$ evaluated *without* and *with* the spectral *amplitude* that will be lost (or with and without the spectral amplitude that will be gained) during propagation. Both terms in (2.46) utilize the phase of the fields at $\mathbf{r}_0$. Thus, in contrast to the net group delay, the reshaping delay is sensitive to how the pulse is organized.

The expression (2.43) gives the delay between the 'center of mass' arrival times for any two points in a medium regardless of how the pulse evolves during transit. Since the form is obtained without approximation, it is valid for pulses with arbitrary bandwidths. This formalism does not attempt to define a specific 'group velocity' as being representative of the overall pulse propagation, since propagation velocity need not be constant. Rather we have demonstrated that the delay between arrival times at two points is related to a linear superposition of group delays weighted by the pulse's spectral content, as in (2.44). (By taking the limit of small separation a local velocity can be defined at each point along the propagation.[18] However, we prefer to consider the difference in arrival times at two discretely separated points since this is more directly applicable to experiment.)

In chapter 3 we demonstrate how this result may be used to understand several properties of pulse propagation. Here we examine some of the general properties of this result.

2.5.1 Reshaping Delay is Often Small

The two terms in (2.43) generally do not make equal contributions to the total delay time. In particular, the reshaping delay is often negligible, so that the total delay time is given by Δt_G. This is the case if the spectral amplitude of the pulse is unaltered during propagation (i.e. if the imaginary part of $\mathbf{k}$ can be neglected). The reshaping delay is also relatively unimportant in the narrowband limit even if pulses experience strong absorption (or amplification). If the pulse is unchirped before propagation the reshaping delay is again

unimportant. In the specific case that a pulse is initially symmetric in time (indicating that it must not be chirped) and propagates in one dimension, we can show analytically that Δt_R vanishes completely.

To demonstrate this, we assume an initially symmetric pulse and choose the time origin such that $\mathbf{E}(\mathbf{r}_0, t) = \mathbf{E}(\mathbf{r}_0, -t)$. The arrival time of the original pulse at $\mathbf{r}_0$ is then

$$T[\mathbf{E}(\mathbf{r}_0, \omega)] \equiv \langle t \rangle_{\mathbf{r}_0} = 0. \tag{2.47}$$

Fourier transform pairs have the property that if either the time or frequency domain representation is real and even (in t or ω), the corresponding time/frequency representation will also have these properties. Thus, $\mathbf{E}(\mathbf{r}_0, \omega)$ is real and an even function of ω. We distinguish the spectrum of the modified pulse used in (2.46) from the original pulse with a tilde, as follows

$$\widetilde{\mathbf{E}}(\mathbf{r}_0, \omega) \equiv e^{-\operatorname{Im}\mathbf{k}\cdot\Delta\mathbf{r}}\mathbf{E}(\mathbf{r}_0, \omega). \tag{2.48}$$

Evidently, $\widetilde{\mathbf{E}}(\mathbf{r}, \omega)$ is real since $\mathbf{E}(\mathbf{r}_0, \omega)$ is real. For one dimensional propagation (in the $\hat{z}$ direction) exponential term in (2.48) may be written as $-\omega \operatorname{Im} n(\omega) \Delta z/c$, where $n(\omega)$ is the complex index of refraction. It is fairly elementary to show that $\operatorname{Re}[n(\omega)]$ is even while $\operatorname{Im}[n(\omega)]$ is odd. Using this fact, we see that the product $\omega \operatorname{Im} n(\omega)$ must be even. Thus $\widetilde{\mathbf{E}}(\mathbf{r}_0, \omega)$ is real and even, indicating that $\widetilde{\mathbf{E}}(\mathbf{r}_0, t)$ will also be real and even. The magnetic field of the modified pulse is found using (2.16):

$$\widetilde{\mathbf{B}}(\mathbf{r}_0, \omega) = \hat{z} \times \widetilde{\mathbf{E}}(\mathbf{r}_0, \omega) [\operatorname{Re} n(\omega) + i \operatorname{Im} n(\omega)]/c. \tag{2.49}$$

Because of the even/odd nature of the real and imaginary parts of $n(\omega)$, when the inverse Fourier transform is carried out only the real part of $\widetilde{\mathbf{B}}(\mathbf{r}_0, \omega)$ (which is even) contributes, resulting in an even $\widetilde{\mathbf{B}}(\mathbf{r}_0, t)$. The even $\widetilde{\mathbf{E}}(\mathbf{r}_0, t)$ and $\widetilde{\mathbf{B}}(\mathbf{r}_0, t)$ combine to make an even $\widetilde{\mathbf{S}}(\mathbf{r}_0, t)$, so that the expression (2.27) for arrival time shows that

$$T\left[e^{-\operatorname{Im}\mathbf{k}\cdot\Delta\mathbf{r}}\mathbf{E}(\mathbf{r}_0, \omega)\right] = 0. \tag{2.50}$$

Hence, the reshaping delay is identically zero for any initially symmetric pulse.

2.5.2 Narrowband Limit of the New Context

In the narrowband limit the delay time (2.43) reduces to the traditional result presented in section 2.2. In this limit the reshaping delay tends to zero, as discussed above, so that the total delay is given by the net group delay. The normalized spectral distribution in this case becomes a delta function

$$\rho(\mathbf{r},\omega) \to \delta(\omega-\bar{\omega}), \tag{2.51}$$

where $\bar{\omega}$ is the central frequency of the pulse. The total delay is then calculated from (2.44) as

$$\Delta t = \int_{-\infty}^{\infty} \delta(\omega-\bar{\omega}) \left(\frac{\partial \mathrm{Re}\,\mathbf{k}}{\partial\omega}\cdot\Delta\mathbf{r}\right) \mathrm{d}\omega \tag{2.52}$$

$$= \left.\frac{\partial \mathrm{Re}\,\mathbf{k}}{\partial\omega}\right|_{\bar{\omega}} \cdot \Delta\mathbf{r}. \tag{2.53}$$

This is in agreement with the well verified observation[1,5,7,8,13] that a pulse travels at the group velocity evaluated at $\bar{\omega}$ in the narrowband limit.

2.5.3 Group and Reshaping Delays can be Reversed

Finally, it is interesting to note that in (2.43) the ordering for the evaluation of the net group delay and reshaping delay can be reversed. In other words, the arguments $\mathbf{r}$ and $\mathbf{r}_0$ in (2.43) can be interchanged which gives

$$\Delta t_G(\mathbf{r}) + \Delta t_R(\mathbf{r}_0) = \Delta t_G(\mathbf{r}_0) + \Delta t_R(\mathbf{r}). \tag{2.54}$$

This commutative property can dramatically alter the group and reshaping delays taken individually. Nevertheless, their sum Δt is unaffected by the ordering. The group delay computed over the initial spectrum is

$$\Delta t_G(\mathbf{r}_0) = \int_{-\infty}^{\infty} \rho(\mathbf{r}_0,\omega) \left(\frac{\partial \mathrm{Re}\,\mathbf{k}}{\partial\omega}\cdot\Delta\mathbf{r}\right) \mathrm{d}\omega. \tag{2.55}$$

When the group delay is computed using the initial spectrum before the propagation, the reshaping delay is evaluated at the end of propagation without and with the lost spectral amplitude (speaking as though the medium is absorptive):

$$\Delta t_R(\mathbf{r}) = T[\mathbf{E}(\mathbf{r}_0+\Delta\mathbf{r},\omega)] - T\left[e^{\mathrm{Im}\,\mathbf{k}\cdot\Delta\mathbf{r}}\mathbf{E}(\mathbf{r}_0+\Delta\mathbf{r},\omega)\right]. \tag{2.56}$$

In this expression, the initial spectral amplitude is restored to the second term. The proof of (2.54) is straightforward. Directly by substitution into (2.41) we have

$$\begin{aligned} T\left[e^{\mathrm{Im}\,\mathbf{k}\cdot\mathbf{r}}\mathbf{E}(\mathbf{r}_0+\Delta\mathbf{r},\omega)\right] &= \frac{\hat{\eta}\cdot\int_{-\infty}^{\infty}\mathbf{S}(\mathbf{r}_0,\omega)\left(\frac{\partial\,\mathrm{Re}\,\mathbf{k}}{\partial\omega}\cdot\Delta\mathbf{r}\right)\mathrm{d}\omega}{\hat{\eta}\cdot\int_{-\infty}^{\infty}\mathbf{S}(\mathbf{r}_0,\omega)\,\mathrm{d}\omega} \\ &\quad -i\frac{\hat{\eta}\cdot\int_{-\infty}^{\infty}\frac{\partial\mathbf{E}(\mathbf{r}_0,\omega)}{\partial\omega}\times\frac{\mathbf{B}^*(\mathbf{r}_0,\omega)}{\mu_0}\,\mathrm{d}\omega}{\hat{\eta}\cdot\int_{-\infty}^{\infty}\mathbf{S}(\mathbf{r}_0,\omega)\,\mathrm{d}\omega} \end{aligned} \tag{2.57}$$

When this and (2.41) are used in (2.56), the commutative relationship (2.54) is immediately verified. Although the two orderings stand on equal footing in a mathematical sense, we prefer the ordering presented in (2.43) because it has a more obvious interpretation than the reversed ordering in (2.54).

2.6 Net Group Delay

One of the appealing aspects of the new group delay context developed in this chapter is the intuitive interpretation that can be given to the expressions. In this section, we discuss the interpretation of the net group delay, Δt_G. In order to appreciate this interpretation, we first discuss some of the qualitative aspects of pulse propagation.

We begin with the spectral representation of the Poynting vector. $\mathbf{S}(\mathbf{r},\omega)$ can be viewed as a 'flux per frequency' density function which indicates how much of the electromagnetic energy flowing from the point $\mathbf{r}$ can be associated with a given spectral range. For

example, the flux associated with the frequency range dω centered at a frequency ω is given by $\mathbf{S}(\mathbf{r},\omega)\,\mathrm{d}\omega$. When discussing a pulse in the frequency context, it is tempting to ask how long it will take the energy associated with a given spectral range at one point to propagate to a distant point. (In asking this question a definition of arrival time somewhat akin to (2.27) is implied since the flux associated with a spectral range does not simply 'arrive' at an instant, but must be experienced over a length of time.) However, in a dielectric medium this is a complicated question because of the fact that the medium can exchange energy with the pulse.

As an example, consider a near-resonance, narrowband pulse as it propagates in an absorbing medium. A point in the medium must experience a portion of the leading edge of the pulse before it 'realizes' the amount of on-resonance spectrum in the pulse, whereupon it begins absorbing these components from the subsequent portions of the pulse. (For a more rigorous discussion of this principle, see section 4.5.) This asymmetric (in time) absorption of the pulse can lead to the appearance of extremely fast or even negative propagation velocity when arrival time is reckoned in the center of mass description. This does not indicate that anything was actually transported at the propagation velocity; the flux that arrives at the second point corresponds only to the early portion of the flux leaving the original point.

This example illustrates why we must be cautious in associating a velocity with the rate at which energy in a given spectral range is transported from one point to another. It is generally not very important to know the speed at which the energy associated with a certain spectral range is *transported* from one point to another. In the frequency context, the more useful question is: If the flux for a given spectral range is observed at some time at a given point, at what time will the flux for that same spectral range be observed at a distant point (without necessarily requiring that it be transported from one point to the other). The answer to this question is that *the flux associated with a narrow spectral range*

will be delayed according to its group delay function, $\partial \operatorname{Re}\mathbf{k}/\partial\omega \cdot \Delta\mathbf{r}$. This is seen explicitly in the net group delay as given in (2.44):

$$\Delta t_G(\mathbf{r}) = \int_{-\infty}^{\infty} \rho(\mathbf{r},\omega)\left(\frac{\partial \operatorname{Re}\mathbf{k}}{\partial\omega}\cdot\Delta\mathbf{r}\right) \mathrm{d}\omega.$$

The distribution $\rho(\mathbf{r},\omega)$ is a spectral density function (i.e., it has units of $1/\omega$) which describes what fraction of the pulse's flux may be associated with a given frequency range. The total delay of the pulse is the average of the group delay function at each frequency, weighted by the fraction of the final pulse that can be associated with that frequency (i.e., $\rho(\mathbf{r},\omega)\ \mathrm{d}\omega$). The distribution $\rho(\mathbf{r},\omega)$ is evaluated at the end of propagation so that only the spectral components that actually arrive at $\mathbf{r}$ contribute to the delay.

2.7 Reshaping Delay

The need for the reshaping delay Δt_R can be illustrated by a simple physical analogy. Consider two runners as they travel at different (but constant) speeds down a street. The runners each lose weight as they run (but at different rates) so that their masses, $m_1(x)$ and $m_2(x)$, are functions of position. We define the arrival time of the two-runner system to a point x on the street by analogy to (2.27) as

$$\langle t\rangle_x \equiv \frac{m_1(x)}{m_1(x)+m_2(x)}t_1 + \frac{m_2(x)}{m_1(x)+m_2(x)}t_2, \tag{2.58}$$

where t_1 and t_2 give the individual arrival times of the two runners at the point x. The delay function for a runner to traverse a displacement Δx is given by $\Delta x/v$, where v is the runner's velocity. In this analogy, the runners correspond to different spectral components in a pulse, their normalized masses correspond to $\rho(\mathbf{r},\omega)$, and the time it takes them to run between two points on the street corresponds to the group delay function. (The runners in this analogy are actually transported according to their delay time. Recall, however, that the group delay function does not describe energy transport

but simply the difference in arrival times.) The initial positions of the two runners at $t = 0$ are given by x_1 and x_2. We now seek the overall delay between the arrival time of the two-runner system at point x_a and $x_b = x_a + \Delta x$. This is directly found to be

$$\begin{aligned} \Delta t &\equiv \langle t \rangle_{x_b} - \langle t \rangle_{x_a} \\ &= \frac{m_1(x_b)\frac{x_b - x_1}{v_1} + m_2(x_b)\frac{x_b - x_2}{v_2}}{m_1(x_b) + m_2(x_b)} - \frac{m_1(x_a)\frac{x_a - x_1}{v_1} + m_2(x_a)\frac{x_a - x_2}{v_2}}{m_1(x_a) + m_2(x_a)}. \end{aligned} \tag{2.59}$$

We can recast (2.59) in an expression analogous to (2.43) as follows:

$$\Delta t = \Delta t_G + \Delta t_R, \tag{2.60}$$

where the first term is given by

$$\Delta t_G \equiv \frac{m_1(x_b)}{m_1(x_b) + m_2(x_b)} \frac{\Delta x}{v_1} + \frac{m_2(x_b)}{m_1(x_b) + m_2(x_b)} \frac{\Delta x}{v_2}. \tag{2.61}$$

This expression for Δt_G is simply the weighted average (using final weights) of the runner's individual delay times, and corresponds to (2.44). The second term in (2.60) is given by

$$\Delta t_R \equiv \frac{m_1(x_b)\frac{x_a - x_1}{v_1} + m_2(x_b)\frac{x_a - x_2}{v_2}}{m_1(x_b) + m_2(x_b)} - \frac{m_1(x_a)\frac{x_a - x_1}{v_1} + m_2(x_a)\frac{x_a - x_2}{v_2}}{m_1(x_a) + m_2(x_a)}. \tag{2.62}$$

It gives the difference between the arrival time at the point x_a calculated with the original and with the final masses. With a little algebra, we can cast (2.62) in a more illuminating form:

$$\Delta t_R = \left(\frac{x_a - x_1}{v_1} - \frac{x_a - x_2}{v_2} \right) \left(\frac{m_1(x_b)\, m_2(x_a) - m_1(x_a)\, m_2(x_b)}{[m_1(x_a) + m_2(x_a)]\,[m_1(x_b) + m_2(x_b)]} \right). \tag{2.63}$$

Once we have specified the mass functions for the two runners (in the case of a pulse, this corresponds to specifying the initial spectral profile and the absorptive properties of the medium), the second factor in (2.63) is a constant. The reshaping delay is then seen to depend only on the initial positions of the two runners, as found in the first factor. In a physical sense, the first factor in (2.63) measures how much of a head start one runner

has over the other at the time when the two-runner system arrives at x_a. If both runners start the race at x_a at the same time, the reshaping delay is identically zero.

If the runners maintain a constant mass as they run, the center of mass in this system has the same delay time between two points along the street regardless of whether or not one of the runners was initially given a head start. (In this case the second factor in (2.63) is zero.) In contrast, imagine that one of the runners loses mass as he runs and completely disappears before reaching x_b. The arrival time at x_a will be between the individual arrival times of the two runners, while the arrival time at x_b will coincide exactly with the arrival of the non-disappearing runner. In this case, the delay time is highly dependent on the head start that one runner has over the other at the time when the system arrives at x_a.

From the analogy, we can see that the reshaping delay is required to compensate for the affect of absorption when a pulse is *initially* chirped at $\mathbf{r}_0$. Note the correspondence between (2.62) and the reshaping delay (2.46) for an optical pulse:

$$\Delta t_R(\mathbf{r}_0) \equiv T\left[e^{-\mathrm{Im}\mathbf{k}\cdot\Delta\mathbf{r}}\mathbf{E}(\mathbf{r}_0,\omega)\right] - T\left[\mathbf{E}(\mathbf{r}_0,\omega)\right].$$

In a chirped pulse, the various spectral components of the flux do not pass the initial point $\mathbf{r}_0$ at the same time (i.e., some spectral components have a 'head start' on others). If there is no amplification or absorption, this presents no problems since the center of mass is delayed by the same amount regardless of when the different spectral components occur in the pulse. However, if the spectral amplitudes are modified during propagation, the delay time of the center of mass will be affected. The reshaping delay measures the magnitude of this effect.

Chapter 3

Application of the New Group Delay Context

This chapter illustrates several situations in which the new context for group delay derived in chapter 2 may be used to study pulse propagation. We begin by discussing the effect of bandwidth on delay time. Next we discuss the effects of propagation distance on delay time. We then discuss the effects that angular dispersion can have on delay times. The angular dispersive case illustrates the effect of sensor orientation when detecting the incoming pulse. Finally, we illustrate how the new group delay context can be applied to describe precursors. The material presented in this chapter closely reflects the examples used in Refs. [19], [20], and [21].

3.1 Pulse Bandwidth and Delay Time

In this section we study how the bandwidth of a pulse affects the delay time as it propagates through a medium. In order to simplify the discussion, we consider an initially symmetric pulse propagating in one dimension, so that the reshaping delay vanishes.

Equation (2.43) then reduces to:

$$\Delta t = \int_{-\infty}^{\infty} \rho(\mathbf{r},\omega)\left(\frac{\partial \operatorname{Re}\mathbf{k}}{\partial\omega}\cdot\Delta\mathbf{r}\right)\mathrm{d}\omega, \tag{3.1}$$

where $\rho(\mathbf{r},\omega)$ is the spectral distribution of field energy at the *final point* $\mathbf{r}$:

$$\rho(\mathbf{r},\omega) \equiv \hat{\eta}\cdot\mathbf{S}(\mathbf{r},\omega) \Big/ \hat{\eta}\cdot\int_{-\infty}^{\infty}\mathbf{S}(\mathbf{r},\omega)\ \mathrm{d}\omega. \tag{3.2}$$

We will first examine the group delay function $\partial \operatorname{Re}\mathbf{k}/\partial\omega\cdot\Delta\mathbf{r}$ (which is a property of the medium only, once $\Delta\mathbf{r}$ is chosen) and then look at the pulse and its interaction with the medium (which enters (3.1) via the distribution $\rho(\mathbf{r},\omega)$).

The new context derived in chapter 2 is independent of the model used to describe the medium. However, for illustration purposes we now employ the Lorentz model with a single resonance at ω_0 and a damping frequency γ. As mentioned in section 2.2, the complex index of refraction in this model is given by

$$[n(\omega)]^2 = 1 + \frac{f{\omega_p}^2}{{\omega_0}^2 - \omega^2 - i\gamma\omega}, \tag{3.3}$$

where ω_p is the plasma frequency and f is the oscillator strength. The oscillator strength f is positive for an absorbing media and negative for an amplifying medium.[1] We consider a pulse with a Gaussian electric field at $\mathbf{r}_0$, given by

$$\mathbf{E}(\mathbf{r}_0,t) = \mathbf{E}_0\exp\left(-t^2/\tau^2\right)\cos(\bar{\omega}t) \tag{3.4}$$

as it propagates through this medium. Notice that this pulse is symmetric about $t=0$ as is required in order to write the delay time as in (3.1).

3.1.1 Absorbing Medium Example

For our first example we choose the model parameters to be $\omega_0 = 100\gamma$ and $f{\omega_p}^2 = 100\gamma^2$ (an absorbing medium), and consider propagation through a displacement $\Delta\mathbf{r} =$

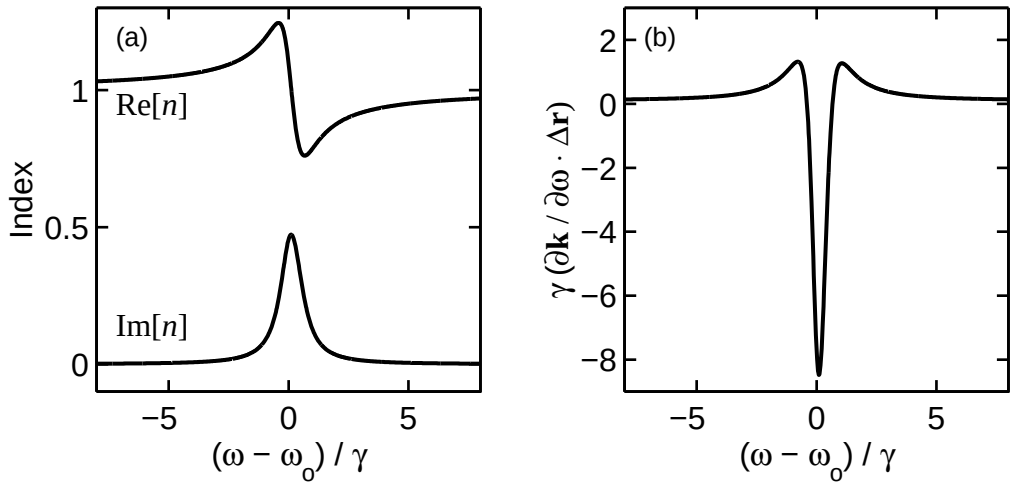

Figure 3.1: (a) Index of refraction for an absorbing medium. (b) Group delay function for a displacement of $\Delta\mathbf{r} = 0.1\left(c/\gamma\right)\hat{z}$.

$0.1\left(c/\gamma\right)\hat{z}$. Figure 3.1(a) plots the real and imaginary parts of the index of refraction for a medium with these parameters. For simplicity, we consider propagation in only one dimension (the $\hat{z}$ direction). The wavevector is obtained from the index of refraction through $\mathbf{k}(\omega) = \hat{z}\omega n(\omega)/c$, allowing calculation of the group delay function $\partial\mathbf{k}/\partial\omega \cdot \Delta\mathbf{r}$. Figure 3.1(b) shows the group delay function corresponding to the index plotted in Fig. 3.1(a). Notice that for the parameters we have chosen, the spectral region near the resonance frequency ω_0 exhibits negative group delay values. While not all group delay functions exhibit negative values, the general shape of the functions in Fig. 3.1(b) (i.e., the delays are shortest near resonance and increase away from resonance) is typical for single resonance absorbing media.

We first look at a relatively narrowband pulse with initial duration $\tau = 10/\gamma$, and the spectrum centered on resonance (i.e. $\bar{\omega} = \omega_0$). Figure 3.2(a) depicts the normalized spectral distribution function (3.2) for this pulse at $\mathbf{r}_0$ before propagation and Fig. 3.2(b) shows the distribution after propagating through the displacement $\Delta\mathbf{r}$. Because the initial pulse spectrum is narrow compared to the resonance, the absorption is roughly constant

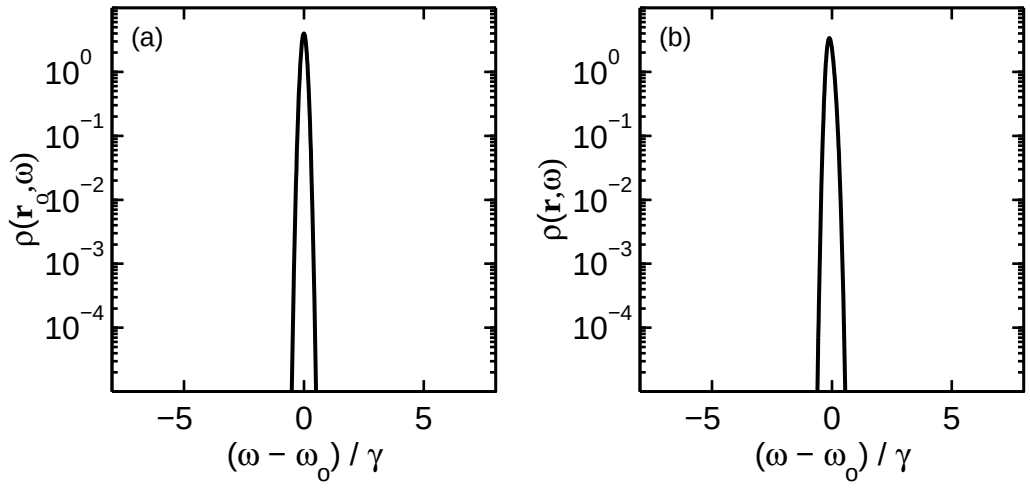

Figure 3.2: (a) $\rho(\mathbf{r}_0,\omega)$, the normalized spectral profile for a narrowband pulse at $\mathbf{r}_0$. (b) $\rho(\mathbf{r},\omega)$, the normalized spectral profile for the same pulse at $\mathbf{r} \equiv \mathbf{r}_0 + \Delta\mathbf{r}$.

over the pulse's spectrum. Thus the distribution $\rho(\omega)$ changes little during propagation, even though the amplitude of $\mathbf{S}(\omega)$ decreases significantly due to absorption. The total delay time is given by the expectation of the group delay function (shown in Fig. 3.1(b)) weighted by the final spectral distribution at $\mathbf{r}$ (shown in Fig. 3.2(b)) as prescribed by (3.1).

As the carrier frequency $\bar{\omega}$ is varied, the distribution $\rho(\mathbf{r},\omega)$ effectively scans through the group delay function. Figure 3.3(a) plots the delay time as the pulse's central frequency $\bar{\omega}$ is varied relative to the resonance frequency ω_0. Since $\rho(\mathbf{r},\omega)$ is narrow compared to the width of the resonance, the total delay closely resembles the group delay function in Fig. 3.1(b). Notice that for frequencies near resonance, the total delay time is negative. This indicates that the pulse center of mass at $\mathbf{r}$ arrives before the center of mass at $\mathbf{r}_0$ arrives. Figure 3.3(b) plots the ratio of total pulse energy after propagation to that before propagation as the pulse's central frequency is varied. Notice that the pulses with negative delay times also experience strong absorption. The negative delay times are closely associated with this absorption.

To help visualize how absorption causes negative delay times for the pulse above, we

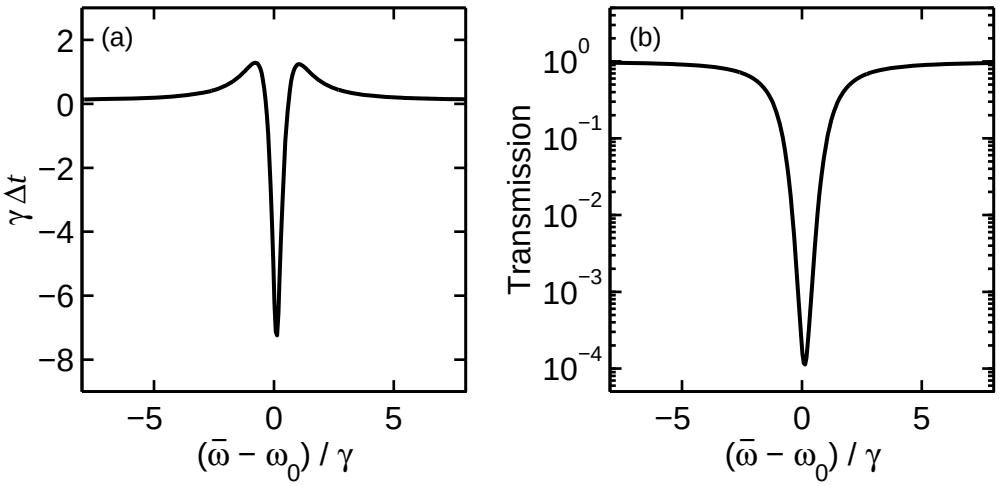

Figure 3.3: (a) Total delay Δt for the narrowband pulse in an absorbing medium as the carrier frequency $\bar{\omega}$ is varied. (b) Overall transmission as the carrier frequency $\bar{\omega}$ is varied.

construct the spatial profile of the pulse at various times using the techniques discussed in section 2.1. For this illustration we again center the pulse spectrum on the resonance frequency (i.e. $\bar{\omega} = \omega_0$). Figure 3.4 shows a sequence of spatial profiles for the pulse at different times. The vertical line at $z = 0$ represents an absorbing medium (the parameters are as above, and the thickness is $\Delta\mathbf{r} = 0.1\left(c/\gamma\right)\hat{z}$) with vacuum on either side. The dotted lines represent the original pulse as it would have propagated in vacuum (i.e., as if the absorbing medium were not there), and the solid line represents the pulse as it propagates through the absorber. Reflections from the boundaries have been ignored. (In Fig. 3.4 we plot only the envelope of the pulse while ignoring the rapid oscillations which occur beneath the envelope. Unless otherwise noted, this is the case for all temporal and spatial profiles plotted in this work.) In this time sequence it is apparent that the medium absorbs more field energy from the trailing portion of the pulse than from the leading portion (the frame at $\gamma t = 0$ illustrates this particularly well). This shifts the center of mass forward in time, resulting in the negative delay time predicted in Fig. 3.3.

We now examine the behavior of a relatively broadband pulse as it propagates through

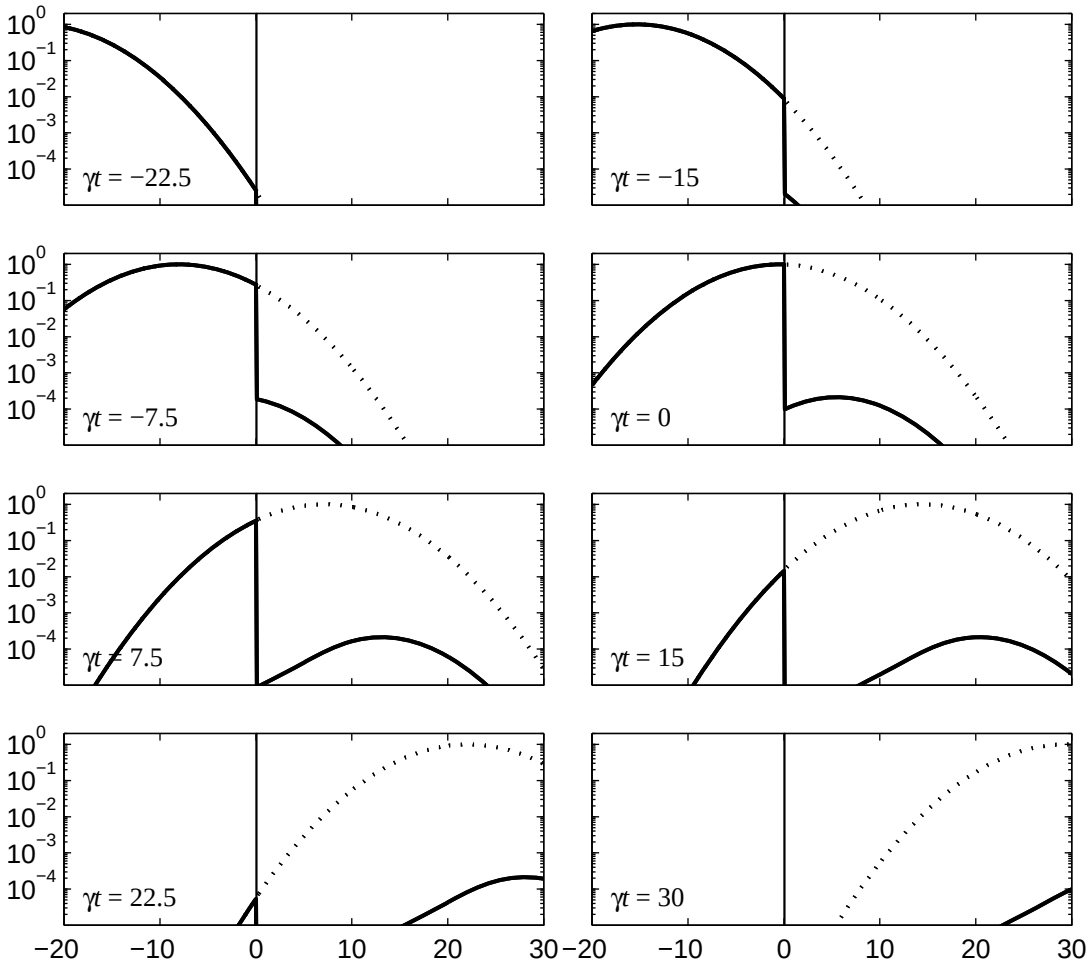

Figure 3.4: Time sequence of the spatial profile of the pulse in Fig. 3.3 with the pulse centered on resonance ($\bar{\omega} = \omega_0$). Distances are measured in units of c/γ.

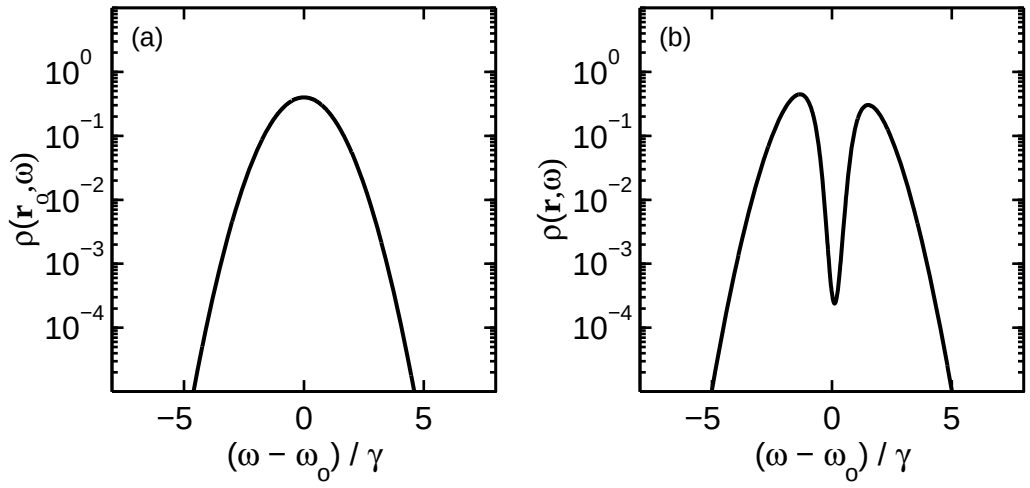

Figure 3.5: (a) $\rho(\mathbf{r}_0,\omega)$, the normalized spectral profile for a broadband pulse at $\mathbf{r}_0$. (b) $\rho(\mathbf{r},\omega)$, the normalized spectral profile for the same pulse at $\mathbf{r} \equiv \mathbf{r}_0 + \Delta\mathbf{r}$.

the absorbing medium described in relation to Fig. 3.1. The pulse is again Gaussian as given by (3.4), but the width is now chosen as $\tau = 1/\gamma$. Fig. 3.5 shows the initial and final spectral distributions for this pulse with its spectrum centered on-resonance ($\bar{\omega} = \omega_0$). In this case, the absorption is not uniform over the spectral components present in the pulse, and $\rho(\omega)$ changes significantly during propagation. Note that it is the near-resonance spectral components with the short delay times that are removed from the final distribution. Again, the total delay time is given by the expectation of the group delay function (Fig. 3.1(b)) weighted by the final spectral distribution at $\mathbf{r}$ (Fig. 3.5(b)) as prescribed by (3.1).

Figure 3.6(a) plots the total delay time as the central frequency $\bar{\omega}$ is varied. Note that in the broadband case, the negative delay times seen in Fig. 3.3(a) disappear since the spectral components with short delay times were removed from $\rho(\mathbf{r},\omega)$. This illustrates the general principle that superluminal effects are a narrowband phenomenon which disappears as bandwidth is increased. Figure 3.6(b) plots the ratio of the total initial pulse energy to the final energy. Because the spectrum is broad compared to the resonance,

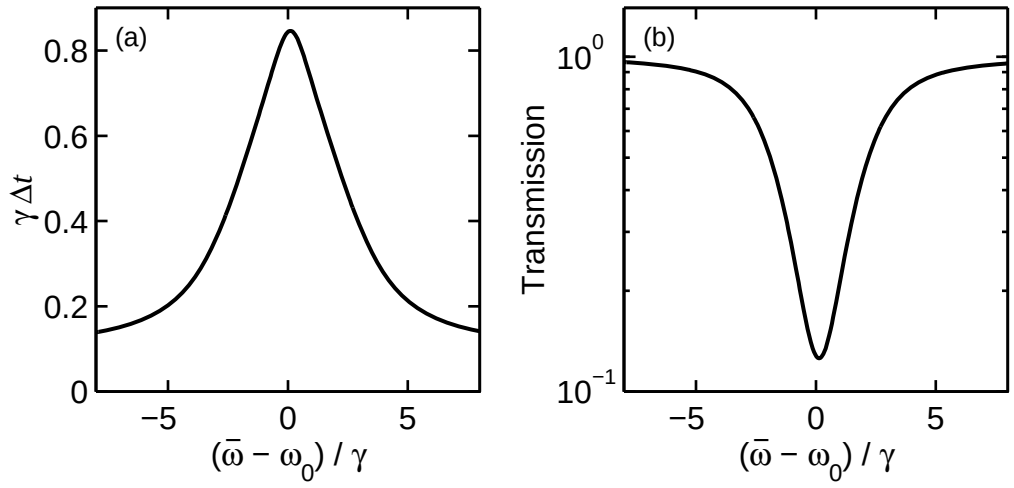

Figure 3.6: (a) Total delay Δt for the broadband pulse in an absorbing medium as the carrier frequency $\bar{\omega}$ is varied. (b) Overall transmission as the carrier frequency $\bar{\omega}$ is varied.

the fraction of the pulse energy that is absorbed by the medium is much smaller than in the narrowband case.

To illustrate the difference between the narrowband and broadband cases, in Fig. 3.7 we again construct a time sequence of spatial profiles for the narrowband case (with the pulse spectrum centered at $\bar{\omega} = \omega_0$). This example illustrates the commonplace situation in which the exiting pulse is delayed with respect to the entering pulse. Note that the medium absorbs more field energy from the leading portion of the pulse than from the trailing portion of the pulse, resulting in the overall delay. (In fact, the figure shows that during the trailing portion of the pulse the medium actually gives energy to the pulse. To see this, note that during the trailing portion the transmitted pulse rises above the vacuum pulse. Thus, while the overall effect of the medium is absorptive, there are times during the trailing portion when the medium amplifies the pulse by returning some of the energy taken from the leading portion. We discuss this effect further in the chapters 4 and 5.)

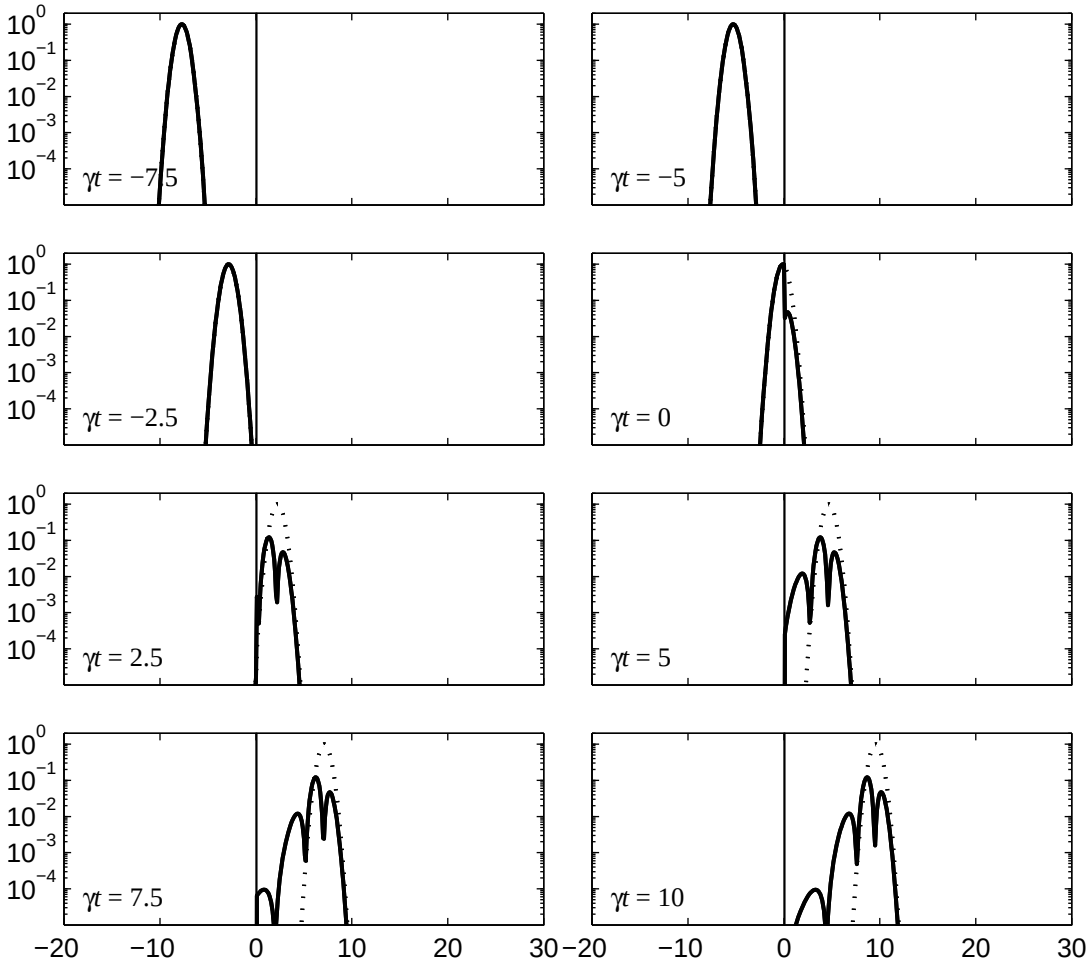

Figure 3.7: A time sequence of the spatial profile of the pulse in Fig. 3.6 with the pulse centered on resonance ($\bar{\omega} = \omega_0$). Distances are measured in units of c/γ.

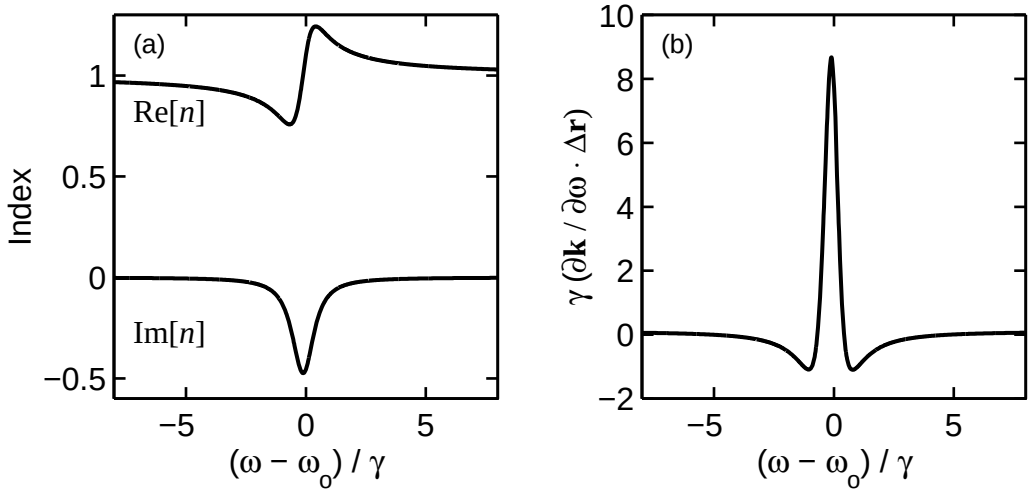

Figure 3.8: (a) Index of refraction for an amplifying medium. (b) Group delay function for a displacement of $\Delta\mathbf{r} = 0.1\left(c/\gamma\right)\hat{z}$.

3.1.2 Amplifying Medium Example

The description of delay time for an amplifying medium is very similar to the absorbing case. To illustrate, we choose the model parameters to be $\omega_0 = 100\gamma$ and $f{\omega_p}^2 = -100\gamma^2$ (i.e., the same parameters as for the absorbing medium just discussed except f is negative), and consider propagation through a displacement $\Delta\mathbf{r} = 0.1\left(c/\gamma\right)\hat{z}$. Figure 3.8(a) plots the real and imaginary parts of the index of refraction for a medium with these parameters. Figure 3.8(b) plots the group delay function corresponding to this index of refraction. In the amplifying case we observe that the shortest delay times occur at frequencies just away from the resonance frequency and the longest delay times occur right on resonance. For the parameters chosen here, the group delay function takes on negative values at its minima, although this need not be the case in general.

To observe the difference between broadband and narrowband pulses in an amplifying medium, we consider the same two initial pulses discussed in relation to the absorbing medium as they propagate through this amplifying medium. Figure 3.9(a)

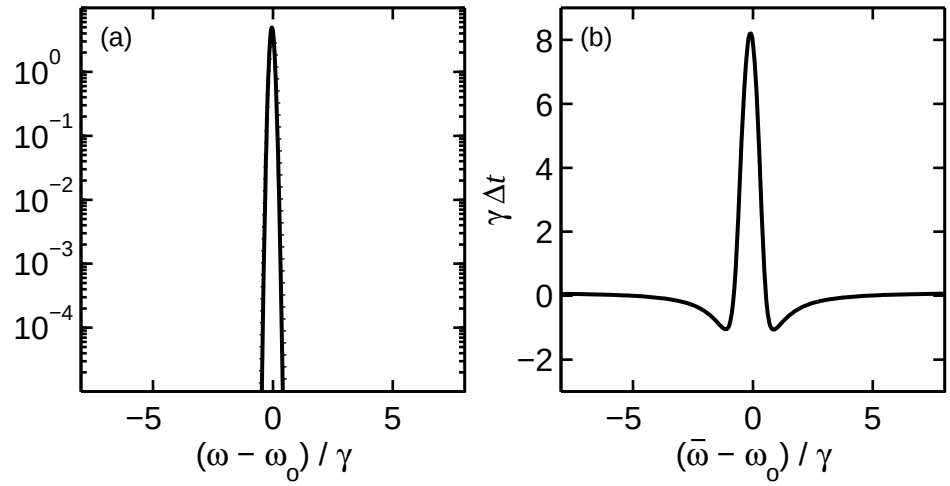

Figure 3.9: (a) Normalized spectral profile for a narrowband pulse at $\mathbf{r}_0$ (dotted line) and $\mathbf{r} \equiv \mathbf{r}_0 + \Delta\mathbf{r}$ (solid line). (b) Total delay Δt for this pulse in an amplifying medium as the carrier frequency $\bar{\omega}$ is varied.

plots the initial and final spectral distributions for the narrowband pulse ($\tau = 10/\gamma$) in the case where its spectrum is centered on-resonance. As with the narrowband pulse in the absorbing medium, the initial and final distributions are very similar since amplification is roughly constant over the pulse's spectrum. Figure 3.9(b) plots the total delay of the pulse as its central frequency $\bar{\omega}$ is varied relative to the resonance frequency. In this amplifying case we see that negative delay times are possible for a pulse whose spectrum is located just off-resonance.

As with the absorbing case, it is informative to view the spatial profile of the pulse as it propagates through the amplifying medium. For this illustration we center the spectrum just above resonance at $\bar{\omega} = \omega_0 + \gamma$, where the pulse exhibits the largest negative delay time in Fig. 3.9(b). Figure 3.10 shows the spatial profile of this narrowband pulse as it traverses the medium. Notice that the leading edge is amplified to a greater extent than the trailing edge. This asymmetric amplification shifts the center of the pulse forward in time, leading to the negative delay time.

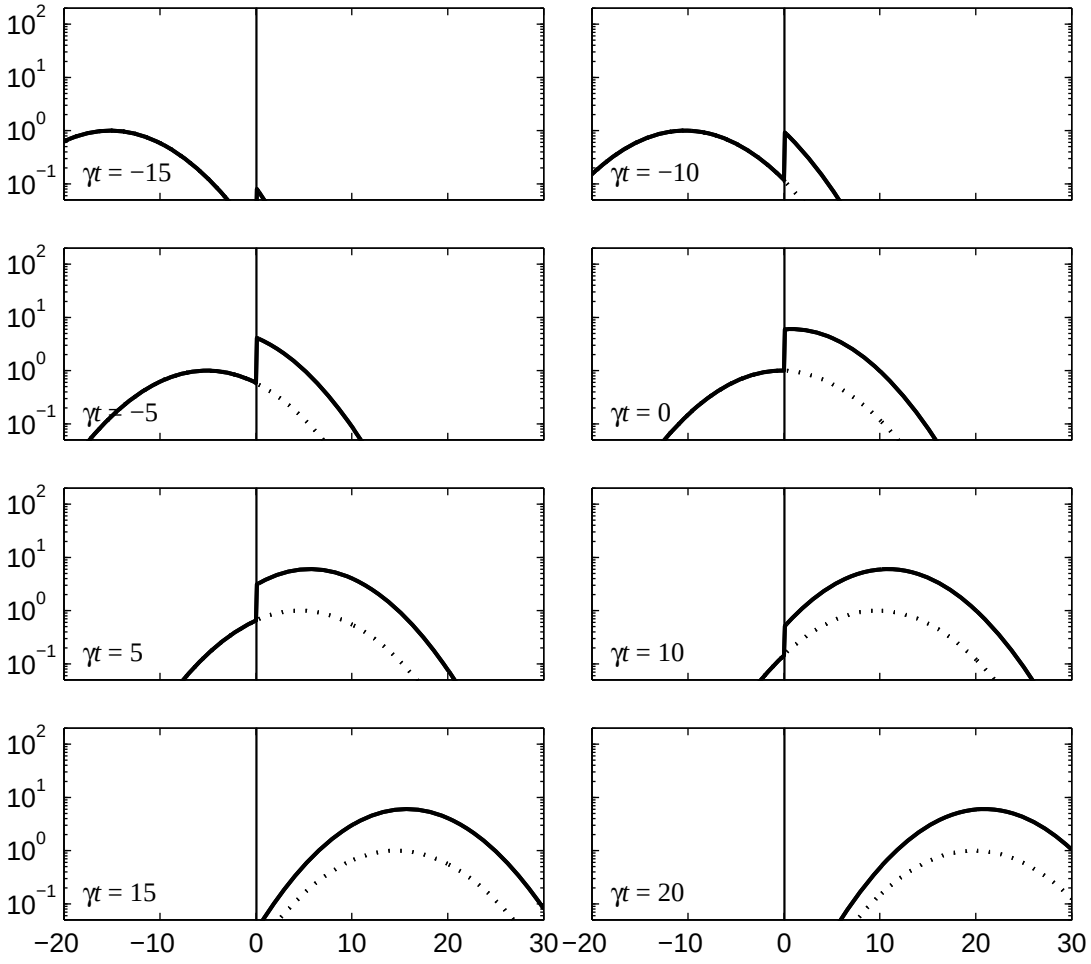

Figure 3.10: Time sequence of the spatial profile of the pulse in Fig. 3.9 with the pulse centered above resonance at $\bar{\omega} = \omega_0 + \gamma$. Distances are measured in units of c/γ.

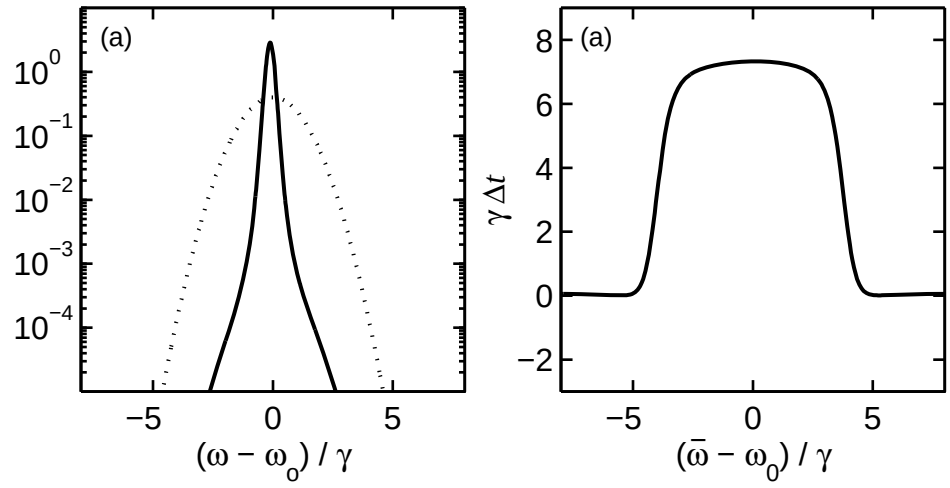

Figure 3.11: (a) Normalized spectral profile for a broadband pulse at $\mathbf{r}_0$ (dotted line) and $\mathbf{r} \equiv \mathbf{r}_0 + \Delta\mathbf{r}$ (solid line). (b) Total delay Δt for this pulse in an amplifying medium as the carrier frequency $\bar{\omega}$ is varied.

Figure 3.11(a) plots the initial and final spectral distributions for the broadband pulse ($\tau = 1/\gamma$) centered on-resonance. Here we see that the distribution becomes much more sharply peaked around the resonance frequency after propagation. This places more weight on the slow on-resonance delay times when the expectation (3.1) is taken. Figure 3.11(b) plots the total delay of the broadband pulse as its central frequency is varied relative to the resonance. Because the longer delay times receive more weight in the expectation integral, the negative delay times disappear.

Figure 3.12 shows a time sequence for the broadband pulse as it propagates in the amplifying medium (with $\bar{\omega} = \omega_0 + \gamma$). In this case the trailing edge is amplified more than the leading edge, and the outgoing pulse is significantly delayed with respect to the incoming pulse. This is the more common situation for pulses propagating in an amplifying medium.

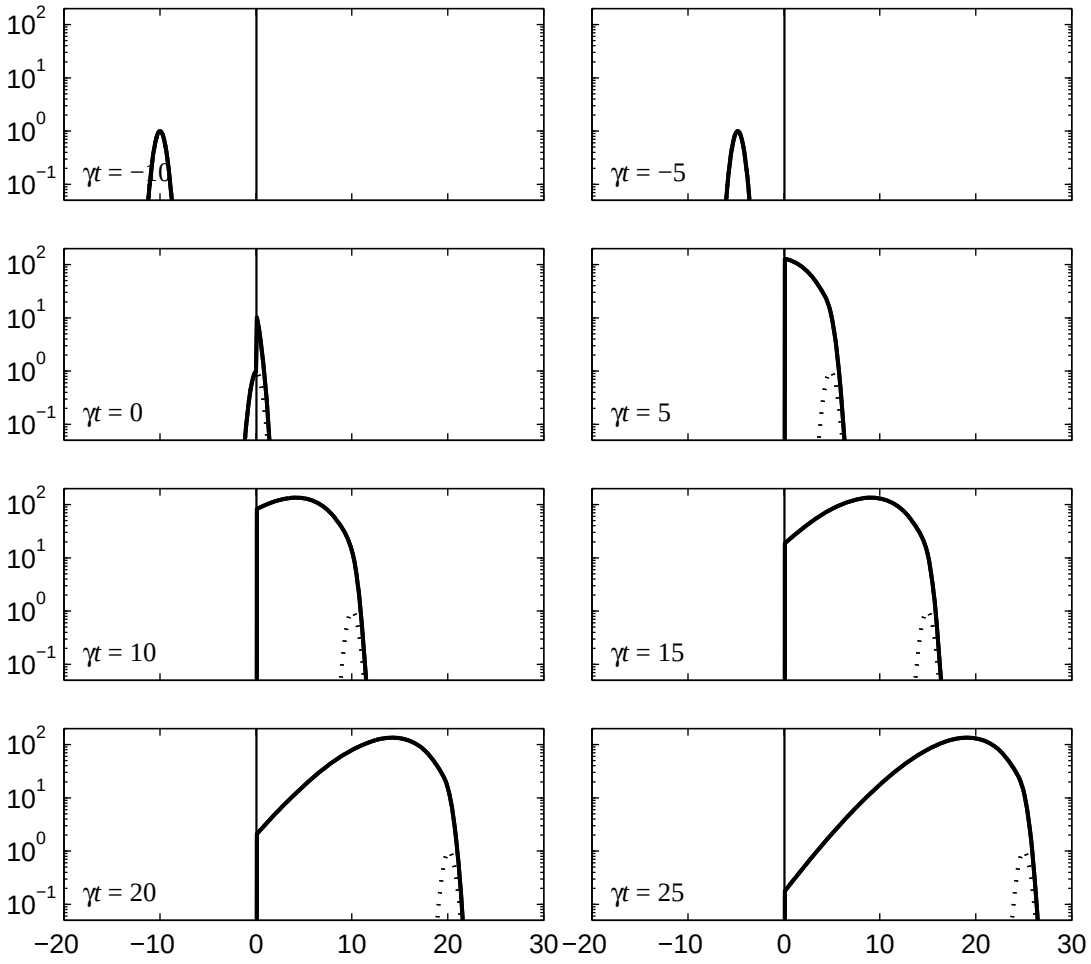

Figure 3.12: Time sequence of the spatial profile of the pulse in Fig. 3.10 with the pulse centered above resonance at $\bar{\omega} = \omega_0 + \gamma$. Distances are measured in units of c/γ.

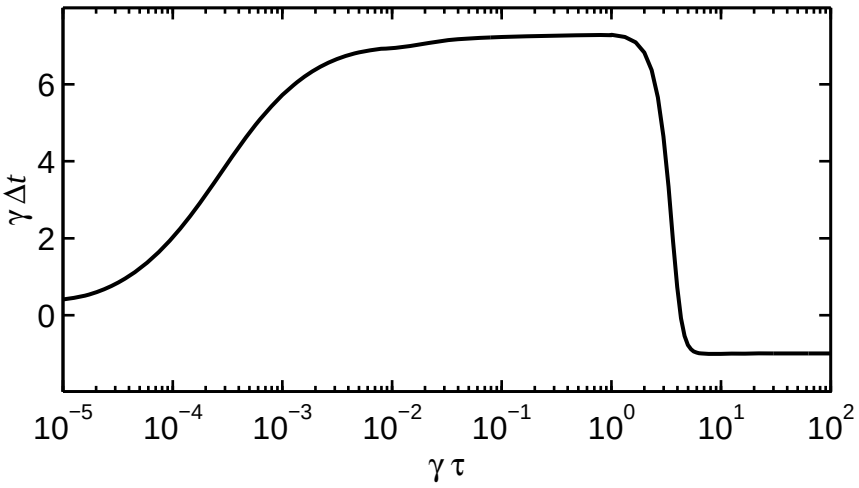

Figure 3.13: Delay time as a function of pulse duration (bandwidth) for a pulse with carrier frequency $\bar{\omega} = \omega_0 + \gamma$ propagating in an amplifying medium.

3.1.3 Continuous Variation of Bandwidth Example

The two preceding examples illustrate how the delay times change when two discrete pulses with different bandwidths are considered. It is also interesting to examine how the delay time changes as we vary the pulse bandwidth continuously. For this example we use the amplifying medium described in subsection 3.1.2 and center the bandwidth of the pulse at $\bar{\omega} = \omega_0 + \gamma$ (i.e. where the narrowband pulse exibited the most negative delay time). Figure 3.13 plots the delay time as the pulse duration τ (and hence the bandwidth) is varied. As expected, the pulses with narrow bandwidths (large τ) exhibit superluminal effects. The behavior becomes subluminal as the bandwidth increases (τ decreases). This is easily understood in terms of (3.1). As the bandwidth increases, $\rho(\mathbf{r},\omega)$ includes more and more of the 'slow' spectral components near ω_0. When the expectation (2.44) is taken, these 'slow' spectral components outweigh the effect of the frequencies with a negative group delay function resulting in a subluminal delay time.

As the pulse duration goes to zero in Fig. 3.13, the total delay time decreases and

approaches an exactly luminal delay time. This is a general phenomenon which can be clearly understood in terms of the broadband context developed in chapter 2. In the limit where the duration of the pulse goes to zero, becoming a delta function in time, the spectral content of the pulse extends uniformly over all frequencies. By comparison, any resonance structure encompasses a finite bandwidth, and the reshaping delay tends to zero. For simplicity, we consider all wave vectors to be parallel, with $\mathbf{k}(\omega) = k(\omega)\,\hat{k}$. Then we have from (2.44) that $\Delta t \to \Delta t_G \approx \mathrm{Re}\,\mathbf{k}/\omega|_\infty \cdot \Delta\mathbf{r} = \hat{k} \cdot \Delta\mathbf{r}\,/\,c$, assuming a refractive index which approaches unity at high frequency. This demonstrates (without lengthy analyses or numerical simulations) the well-known fact that the velocity for a sharply defined signal is exactly c. Thus, the Sommerfeld-Brillouin result[4] of luminality for pulses of definite support is consistent with and even implied by the new group delay context.

3.2 Propagation Distance and Delay Time

Although we have demonstrated that superluminal behavior is most pronounced for narrowband pulses, if $\Delta\mathbf{r}$ is small enough it is possible to observe superluminal effects for broadband pulses also. This was demonstrated recently by Talukder and coworkers[22] when they performed a superluminal propagation experiment in an absorbing medium under relatively broadband conditions (where the traditional narrowband expansion of group velocity fails). Although their on-resonance femtosecond laser pulses initially propagated superluminally through a dye cell, as the effective length of the propagation medium was increased, they observed a transition to subluminal behavior. The formalism developed in chapter 2 may be used to explain why this transition inevitably occurs as an initially superluminal pulse is allowed to propagate longer distances in an absorbing medium.

If a pulse is initially unchirped, the reshaping delay is negligable, and the total delay is

given by $\Delta t_G(\mathbf{r})$. When the pulse spectrum is centered on-resonance, the initial spectral profile $\rho(\mathbf{r}_0,\omega)$ will primarily include the 'fast' spectral components near ω_0. (Remember that in an absorbing medium, frequencies near ω_0 have the shortest group delay function.) However, as it propagates the fast spectral components near ω_0 are absorbed from the pulse spectrum. Eventually only spectral components away from the resonance (i.e. frequencies where the group delay function gives a luminal delay) are left in the spectrum. Since it is the final distribution $\rho(\mathbf{r},\omega)$ that is used to calculate the net group delay (2.44), the delay time inevitably becomes subluminal.

The situation in an amplifying medium is similar. In this case, it is the off-resonance frequency components that have the superluminal group delays. As the pulse propagates, the amplifying medium adds the slow near-resonance frequencies to the pulse spectrum. Thus, an initially superluminal pulse whose spectrum is centered off-resonance will eventually have a luminal delay time as $\rho(\mathbf{r},\omega)$ changes to include more and more near-resonance frequencies.

3.2.1 Superluminal Delays and Propagation Distance

The preceding arguments imply that any finite pulse that initially exhibits superluminal delay times will eventually have luminal delay times as $\Delta\mathbf{r}$ is increased. To illustrate this transition, Fig. 3.14(a) plots delay time as a function of displacement in an amplifying medium. The medium parameters are the same as in Fig. 3.8 except for the variable displacement. The initial pulse is chosen to be a narrowband gaussian as in Fig. 3.9, with $\tau = 10/\gamma$ and $\bar{\omega} = \omega_0 + \gamma$. The delay time is scaled by $c/\Delta\mathbf{r}$ so that propagation at the speed of light has a scaled delay time of 1. Figure 3.14(b) shows the group delay function, also scaled by $c/\Delta\mathbf{r}$ for comparison . For small displacements, the delay time matches the group delay function evaluated at $\bar{\omega}$. As the pulse propagates and acquires more on-resonance spectral intensity, the delay time shifts to the on-resonance value of the

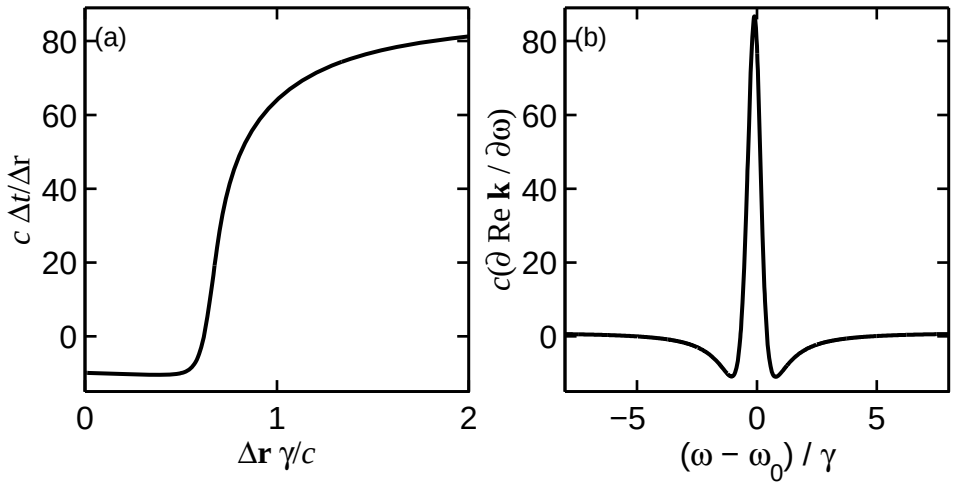

Figure 3.14: (a) Total delay, scaled by $c/\Delta r$, as a function of displacement. (b) Group delay function divided by displacement.

group delay function.

This example illustrates the principle that superluminal effects in amplifying media will be observed over the longest distances when the pulse's spectrum has little spectral content on the resonance. In absorbing media, as mentioned above, superluminal effects persist longest for pulses with the least spectral content away from resonance. (This is why narrowband pulses are generally used in both amplifying and absorbing experiments designed to observe these effects.)

3.2.2 Increasing Superluminal Propagation Distance

Bolda et. al.[1] proposed a technique to achieve the longest possible superluminal propagation distances in amplifying media. They proposed to initially send the pulse through an absorbing medium to remove the near-resonance components from the pulse spectrum. This modified pulse is then sent through an amplifier with the same resonance frequency as the absorber. Since the slow near-resonance spectral components were attenuated in

the absorber, a relatively large propagation distance is required before the on-resonance frequency components enter into the expectation (2.44). (Of course there is no free lunch here: the extra long delay time in the absorber counterbalances the short delay time in the amplifier.)

Figure 3.15 reproduces a time sequence of spatial the distribution of field energy which appeared in the article describing the experiment proposed by Bolda. Again, a dashed pulse is shown which propagates at exactly c (i.e. as if the absorber and amplifier were not there). The Lorentz model is used for the two media with $\omega_0 = 2\times10^7\gamma$, $\omega_p = 100\gamma$, and $\Delta r = 0.5c/\gamma$. The oscillator strength is $f = 1$ for the absorbing medium and $f = -1$ for the amplifier. The pulse is chosen to be gaussian as in (3.4) with $\tau = 0.264/\sqrt{2}\gamma$ and $\bar{\omega} = \omega_0 + \omega_p/3$.

Figure 3.16(a) plots the spectral distribution of the pulse at different points in the medium. Figure 3.16(b) shows the group delay function for the amplifying medium. As usual, the delay time is predicted by the expectation of the group delay function weighted by the spectral distribution. (In the amplifying medium the reshaping delay Δt_R also plays a role since the pulse was chirped in the absorber. The reshaping delay is still small, however, amounting to about a 5% correction to Δt_G.) Because the near-resonance spectral components were removed, the large values of the group delay function near resonance do not play a role in the expectation integral (2.44). Thus, the pulse passing through the amplifier can exhibit superluminal behavior over a relatively long distance. If the full Gaussian is sent through the amplifier without the preparation in the pre-absorber, superluminal behavior persists over a displacement of only $\Delta r = 7\times10^{-3}c/\gamma$ before becoming subluminal (and experiencing extreme amplification). This transition occurs when the amplitude of the on-resonance peak in $\rho(\mathbf{r},\omega)$ has roughly the same amplitude as the original peak at the carrier frequency $\bar{\omega}$.

In addition to providing an example of how superluminal behavior can be extended

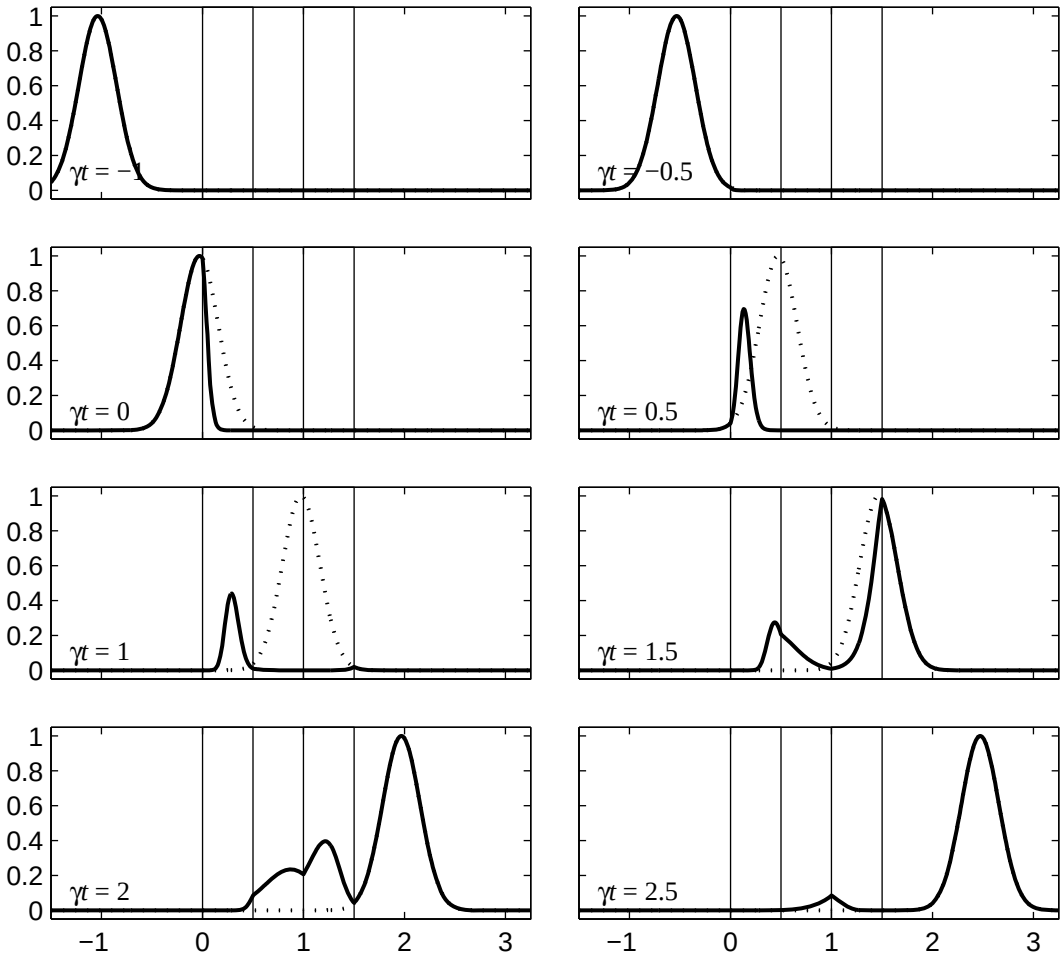

Figure 3.15: Time sequence of a Gaussian pulse traversing an absorbing medium followed by an amplifying medium as proposed by Bolda.[1]

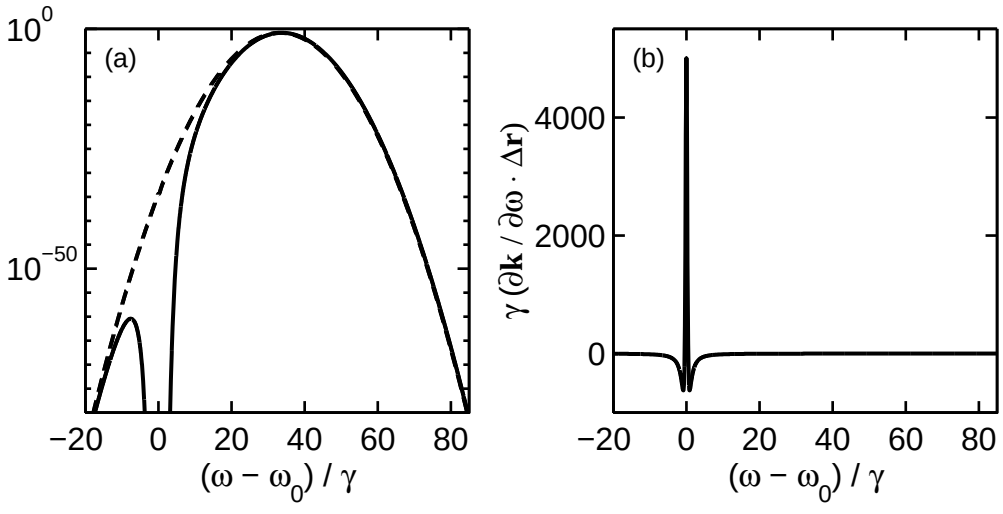

Figure 3.16: (a) Spectral distribution before (dashed) and after (solid) traversing the absorber. The distribution after the amplifier is the same as the initial distribution. (b) Group delay function for the amplifying medium.

over longer displacements, this example demonstrates the elegance and utility of our result (2.43). In Ref. [1] the prediction of a negative delay time is made using the traditional series expansion approach. The analytic motivation for introducing the absorber is simply that "frequencies very close to resonance are amplified by the gain medium to such an extent that the power-series expansion breaks down."[1] In contrast, our new context gives clear insight into the physical reasons why the power series approach cannot be used to describe the pulse in the amplifier without first sending it through the absorber. If the unabsorbed pulse were sent into the amplifier, as the near-resonance frequency components were added to the pulse its velocity would change rapidly from superluminal to highly subluminal (as in Fig. 3.14). Since the expansion terms evaluated at a single carrier frequency are useful to describe roughly constant velocity, they fail to describe the situation.

3.3 Angularly Dispersive Systems

In sections 3.1 and 3.2 we have discussed pulse propagation in only one dimension. It is also interesting to consider delay times in angularly dispersive optical systems where the direction of $\mathbf{k}(\omega)$ depends on frequency. Such systems include grating pairs, prism pairs, and material slabs which are angularly dispersive (within the material) under oblique incidence. These systems are routinely employed in short pulse lasers to control the temporal profile of pulses and to mitigate unwanted dispersion.[23–25] In an angularly dispersive system, the orientation of this energy sensor (specified by $\hat{\eta}$) influences arrival time for the pulse since different frequency components may illuminate the sensor closer to or farther away from normal incidence.

In many angularly dispersive systems the directional spread of $\mathbf{k}(\omega)$ is confined to a plane (say the x-y plane), so that the $\mathbf{k}(\omega)$ may be represented as

$$\mathbf{k}(\omega) = k(\omega)\left[\cos\theta(\omega)\,\hat{x} + \sin\theta(\omega)\,\hat{y}\right] \tag{3.5}$$

where $\theta(\omega)$ is the direction of travel for each frequency component referenced to the x-axis as depicted in Fig. 3.17(a). For a displacement $\Delta\mathbf{r} \equiv \hat{x}\Delta x + \hat{y}\Delta y$ as depicted in Fig. 3.17(b), the phase delay is then given by

$$\mathbf{k}(\omega)\cdot\Delta\mathbf{r} = \frac{\omega}{c}n(\omega)\left[\Delta x\cos\theta(\omega) + \Delta y\sin\theta(\omega)\right], \tag{3.6}$$

where we have incorporated the dispersion relation: $k(\omega) = \omega n(\omega)/c$. Once the direction of travel, given by $\theta(\omega)$, is specified we can compute $\mathbf{S}(\mathbf{r},\omega)$ at any point in the system in terms of a given input pulse using the methods described in section 2.1. In order to calculate delay times, we specify the detector angle (given by $\hat{\eta}$), then calculate the distribution $\rho(\mathbf{r},\omega)$, and finally determine Δt using (2.43). (For more details on angularly dispersive systems see Ref. [21])

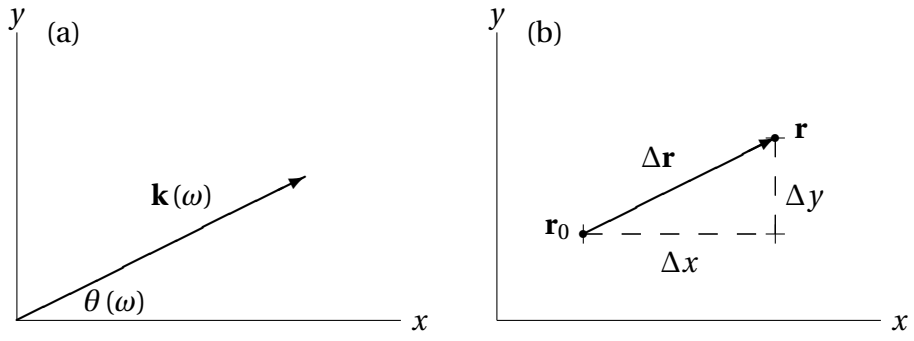

Figure 3.17: (a) Orientation of $\mathbf{k}(\omega)$ assumed to lie in the x-y plane. (b) Displacement $\Delta\mathbf{r}$ between points $\mathbf{r}_0$ and $\mathbf{r}$ where pulse forms will be examined.

3.3.1 Diffraction Grating Example

To illustrate the effect of angular dispersion on delay time, we consider the specific example of a pulse diffracting from a grating in vacuum. In this system the dispersion is due solely to the angular spread of $\mathbf{k}(\omega)$, with no contribution from a propagation medium (i.e., $n(\omega) = 1$ in (3.6)). Thus, the reshaping delay plays no part, and the total delay is given by (3.1). We orient the diffraction grating parallel to the y-axis and choose our initial reference point $\mathbf{r}_0$ on the diffraction grating surface as shown in Fig. 3.18. For first order diffraction $\theta(\omega)$ is readily obtained from the well-known diffraction grating law:

$$\theta(\omega) = \sin^{-1}\left[\frac{2\pi c}{\omega d} - \sin\theta_i\right], \tag{3.7}$$

where θ_i is the incident angle and d is the grating line spacing. We assume that all frequencies associated with the initial pulse travel in a single direction before diffracting from the grating, so that θ_i is a constant. Once the system parameters have been defined, we may use (3.7) together with (3.6) to calculate the group delay function $\partial\,\mathrm{Re}\,\mathbf{k}/\partial\omega \cdot \Delta\mathbf{r}$.

The spectral components of the electric field in this system can be written in terms of

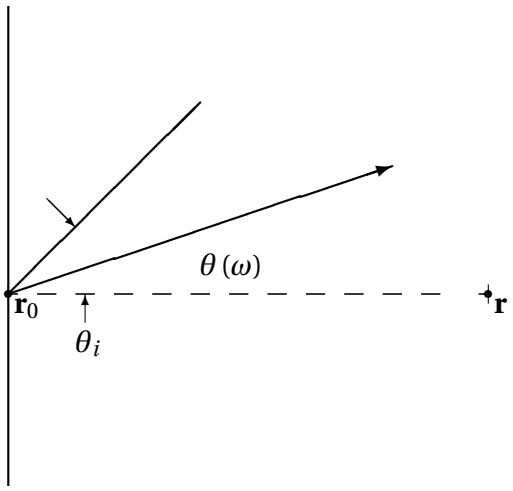

Figure 3.18: Geometry for the diffraction grating.

the field amplitude at $\mathbf{r}_0$ (after reflection) using the solution (2.14):

$$\mathbf{E}(\mathbf{r},\omega) = E(\mathbf{r}_0,\omega)\left[-\sin\theta(\omega)\,\hat{x} + \cos\theta(\omega)\,\hat{y}\right] e^{i\mathbf{k}(\omega)\cdot\Delta\mathbf{r}} \tag{3.8}$$

with the magnetic field given by

$$\mathbf{B}(\mathbf{r},\omega) = \frac{1}{c}\mathbf{E}(\mathbf{r},\omega)\,\hat{z}. \tag{3.9}$$

Here we have assumed p-polarized light propagating in the x-y plane. The spectral representation of the Poynting vector from (3.8) and (3.9) becomes

$$\begin{aligned}\mathbf{S}(\mathbf{r},\omega) &\equiv \mathbf{E}(\mathbf{r},\omega) \times \frac{\mathbf{B}^*(\omega,\mathbf{r})}{\mu_0} \\ &= \epsilon_0 c\,|\mathbf{E}(\mathbf{r}_0,\omega)|^2\left[\cos\theta(\omega)\,\hat{x} + \sin\theta(\omega)\,\hat{y}\right].\end{aligned} \tag{3.10}$$

Note that $\mathbf{S}(\mathbf{r},\omega)$ is independent of the observation point $\mathbf{r}$ since there is no attenuation or amplification in this system. Thus, the spectral distribution function $\rho(\mathbf{r},\omega)$ will not vary with position, but *will* vary with the choice of $\hat{\eta}$.

We consider a Gaussian pulse defined by (3.4) as it diffracts from a grating surface. The incoming pulse strikes the grating surface at an angle of $\theta_i = 20^\circ$ and the line spacing

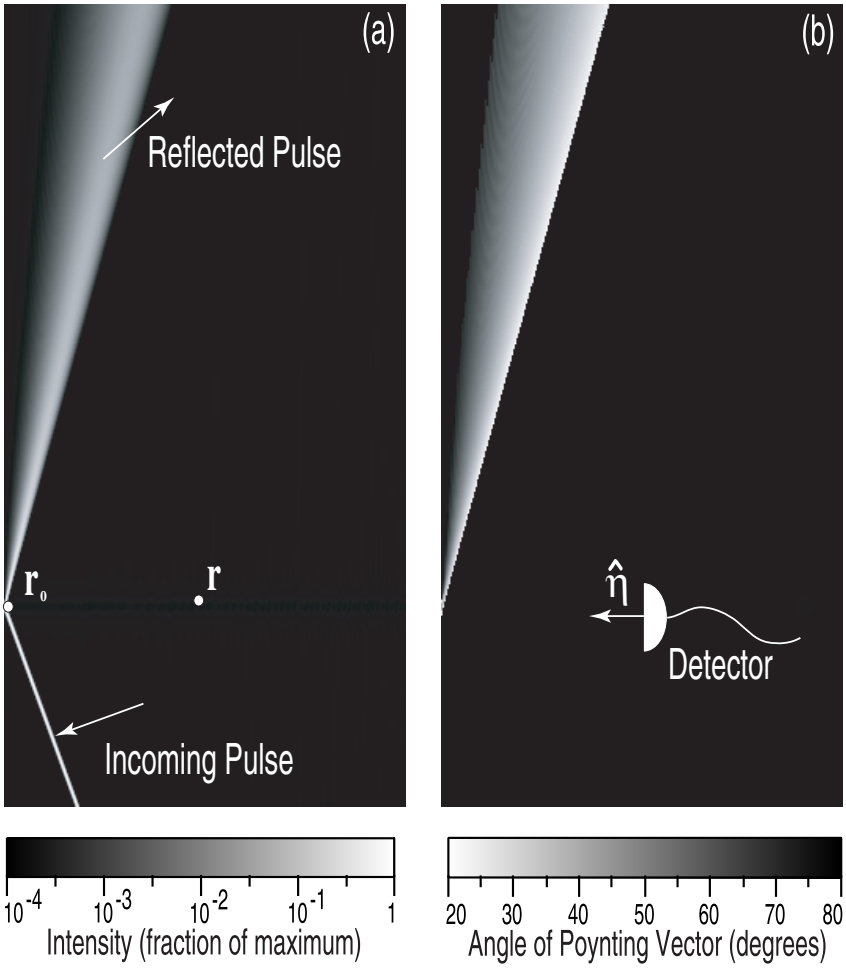

Figure 3.19: (a) Snapshot of the intensity distribution of a Gaussian pulse diffracting from a grating surface. (b) Angle of the Poynting vector, measured from the horizontal x-axis, for the pulse illustrated in (a).

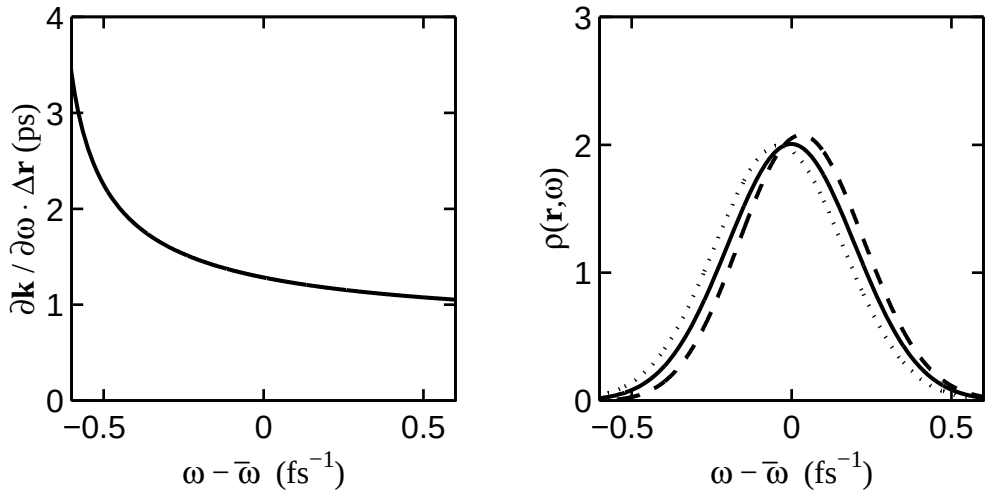

Figure 3.20: (a) Group delay function for a grating. (b) The normalized spectral distributions $\rho(\mathbf{r},\omega)$ when the detector angle is set to 160 (dashed), 220 (solid), and 280 (dotted) degrees.

is chosen to be $d = 1/1200$ mm. Figure 3.19(a) shows a two dimensional plot of the intensity at $t = 0$ for a pulse with width $\tau = 5$ fs, and $\bar{\omega}$ chosen to correspond with a vacuum wavelength of 800 nm. The spatial dimensions of the figure are 0.5 mm wide and 1 mm tall. For reference, the incoming pulse is also shown. Arrows show the direction of the wavevector associated with the center frequency $\bar{\omega}$. Figure 3.19(b) shows the direction of the Poynting vector at each point of the intensity distribution (points with an intensity less than 10^{-4} in Fig. 3.20(a) are set to black inFig. 3.19(b)). As time proceeds, both the intensity and direction patterns slide vertically downward along the grating surface while maintaining their forms. Thus, as a given point in the system experiences the pulse, the direction of the Poynting vector changes in time as the pulse passes. This change in direction is a general feature of a chirped pulse in an angularly dispersive system and influences the efficiency of detecting the pulse.

Figure 3.20(a) plots the group delay function for this system at a point displaced by $\Delta\mathbf{r} = 0.25$ mm $\hat{x}$ from $\mathbf{r}_0$. Note that low frequencies have long delay times and high

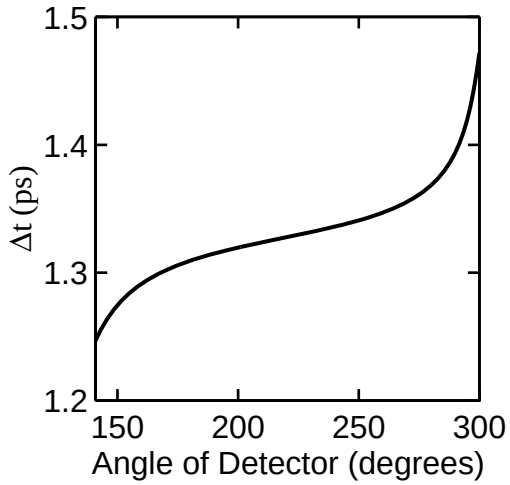

Figure 3.21: Pulse delay time from $\mathbf{r}_0$ to $\mathbf{r}$ as a function of detector orientation, $\hat{\eta}$, for the system illustrated in Fig. 3.18. Angle is measured from the horizontal x-axis.

frequencies have short delay times. As mentioned before, the normalized spectral distribution depends on the choice of $\hat{\eta}$. Figure 3.20(b) plots $\rho(\mathbf{r},\omega)$ for the three cases where $\hat{\eta}$ is oriented at 160° (dashed), 220° (solid), and 280° (dotted) measured from the positive x-axis. Notice that the high frequency components are detected more efficiently at low angles, and low frequency components become more important at high angles. As usual, the delay time for the pulse is calculated via (3.1). Figure 3.21 plots this delay time as the sensor is rotated (i.e., $\hat{\eta}$ is varied) at $\mathbf{r}$. The delay time increases as the detector rotates counterclockwise and becomes more sensitive to low frequencies and less sensitive to the high frequencies. In generating this plot, we have considered the detector to be sensitive on only one side so that contributions to the integrals in (3.2) with positive dot product were ignored. This effect is not important when the detector is oriented roughly towards the grating.

While the sensor angle plays a role in determining the delay time associated with traversing $\Delta\mathbf{r}$, the result is not influenced by the state of the pulse's chirp. This stems from the fact that the Poynting vector in (3.2) is insensitive to the phases of the individual

spectral field components. Therefore, the propagation time for the pulse to traverse $\Delta\mathbf{r}$ cannot recognize the presence of chirp within the context of (3.1). Whether the pulse begins relatively compressed and then incurs chirp, begins with a negative chirp which compresses during propagation, or begins with a positive chirp which becomes more pronounced during propagation, the delay time is the same. (In our example, the pulse starts unchirped and incur positive chirp as it propagates.) This indicates that the direction of the Poynting vector evolves in time in such a way as to counteract asymmetries in the chirping process so that propagation time as noted by the sensors at $\mathbf{r}$ and $\mathbf{r}_0$ is independent of the state of chirp. For this to be true, it is important that the orientation of the two sensors match since this was assumed in deriving (2.43).

3.3.2 Diffraction Gratings and Group Delay

In addition to providing an example of how detector orientation can affect delay times, diffraction gratings provide an interesting illustration[26] of the superposition principle discussed in section 2.6. In order to appreciate this illustration, we first present some background about the parallel grating pair system. In the original work considering the grating pair system, Treacy[27] studied the frequency dependent phase delay experienced by a pulse as it propagates through the system. He first computed the phase delay as $\mathbf{k}\cdot\Delta\mathbf{r} = \omega l(\omega)/c$, were $l(\omega)$ is the length of the path traced by a ray (representing the frequency ω) as it traverses the system. However, he then showed that the derivative of the phase delay must be given by $\partial\mathbf{k}\cdot\Delta\mathbf{r}(\omega)/\partial\omega = l(\omega)/c$. Finally, he argued that a phase matching term should be appended to the original phase delay in order to arrive at the correct result.

The argument for the phase matching term is subtle and connected with the specific geometry of the gratings. This prompted Brorson and Haus[28] to reexamine the setup in terms of an energy transport argument. They first showed that the diffraction grating law

(3.7) is derivable using variational methods. They then stated that since energy transport must occur at velocity c (assuming vacuum between gratings) along the path predicted by variational methods, the group delay function $\partial\mathbf{k}(\omega)\cdot\Delta\mathbf{r}\big/\partial\omega$ must be equal to $l(\omega)/c$, where $l(\omega)$ is the frequency-dependent path length used by Treacy. In this manner they were able to obtain Treacy's result without the need for the phase matching term introduced by Treacy. The argument of Brorson and Haus implies linear superposition principle for group delays, although this fact was not emphasized in the paper. (It is appropriate to associate the group delay with energy transport in this situation since no energy is absorbed in the system.) Equation (2.44) explicitly demonstrates the linear superposition principle of group delay that is implicit in the Brorson and Haus argument.

3.4 Group Delay and Precursors

One of the failings of the traditional group velocity description is its inability to describe precursor fields. In simple terms, a precursor field is what is left over after a near-resonance pulse has propagated a large distance in an absorbing medium. This type of propagation field was first analyzed by Sommerfeld and Brillouin,[4] and their original analysis has since been refined and extended by others.[29] To illustrate the issues involved in this type of problem, we first consider a typical situation where precursors are observed. Then we compare and contrast the traditional method used to analyze the problem with a method suggested by the new group delay context.

3.4.1 Typical Precursor Problem

In this section we illustrate a scenario where precursor fields are observed. The medium in this example is given by single resonance Lorentz oscillator with parameters $\omega_0 = 50/7\gamma$, $\omega_p = 25\sqrt{5}/7\gamma$, and $f = 1$. (These parameters are the same as those used by Brillouin, and

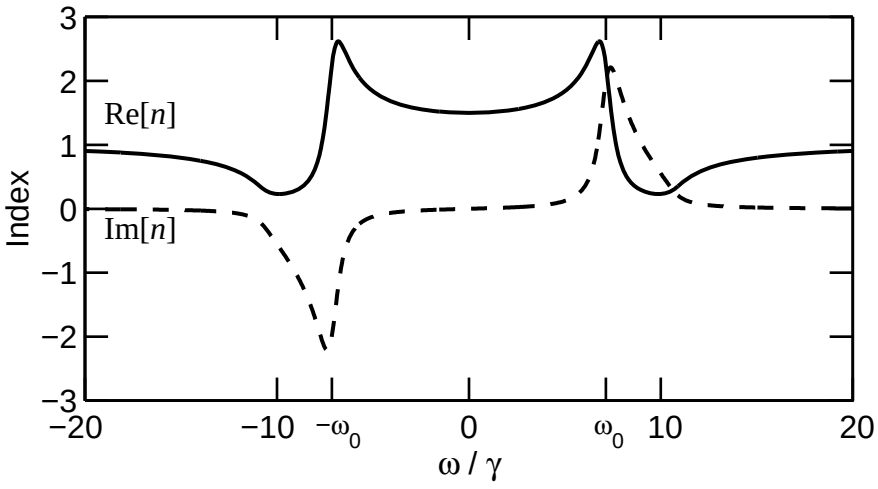

Figure 3.22: Real (solid) and imaginary (dashed) parts of the index of refraction.

are frequently used when analyzing precursors.) Figure 3.22 plots the real and imaginary parts of the index of refraction for this medium. (Note that the zero on this plot is $\omega = 0$ not the resonance frequency ω_0.)

The group delay function is plotted in Fig. 3.23 for a propagation distance of $\Delta\mathbf{r} = 15c/\gamma\,\hat{z}$. Notice that the group delay function is not symmetric about ω_0, as is roughly the case in the previous examples that we have discussed. This asymmetry is a general property of the Lorentz oscillator which becomes less pronounced when $\omega_0 \gg \gamma$. If we ignore the frequencies near ω_0 (which will be absorbed after propagating a significant distance), Fig. 3.23 shows that frequency components which are lower (i.e., closer to $\omega = 0$) have longer delay times than the higher frequency components. This suggests that after a pulse has propagated for a while, it will be chirped such that the high frequency components arrive at a point before the low frequency components.

To illustrate, we choose an initially Gaussian pulse, as in (3.4), with $\tau = 5/\gamma$ and $\bar{\omega} = 10\gamma$. This results in a pulse whose spectrum is broad compared to the resonance, and is centered slightly above ω_0. In this situation the traditional method of expansion utterly fails, as discussed in section 2.2. However, the new group delay context is still applicable,

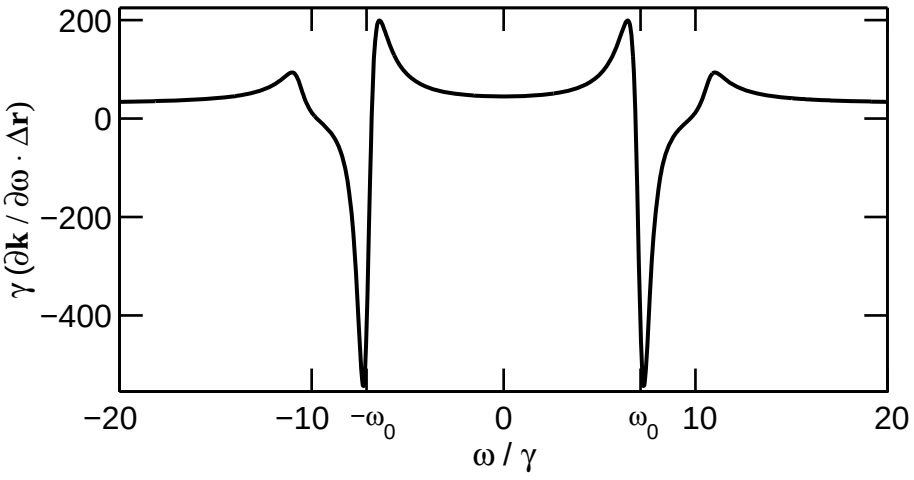

Figure 3.23: Group delay function.

and can be used to predict the delay time for this pulse. In Fig. 3.24(a) we plot the initial (dashed) and final (solid) distributions $\rho(\mathbf{r}_0,\omega)$ and $\rho(\mathbf{r},\omega)$ for this pulse. Figure 3.24(b) plots the initial temporal profile of the pulse, and Fig. 3.24(c) plots the final temporal profile of the pulse. (In contrast to the other examples discussed in this work, we plot the actual oscillation of the field rather than the envelope over these oscillations. This allows us to observe the chirp of the final pulse.) Since the initial pulse is symmetric in time, the overall delay of the pulse is calculated using (3.1) as $\Delta t = 24.74/\gamma$. Because the spectral components near ω_0 have been removed from the pulse by the time it reaches $\mathbf{r}$, the large negative delay times for the near-resonance components do not play a role in the overall delay. Notice that the pulse is chirped so that the high frequency components arrive at $\mathbf{r}$ before the low frequency components, as predicted by the group delay function.

This example clearly illustrates why the traditional group delay derived in section 2.2 fails for a broadband pulse whose spectrum is centered near resonance. The traditional approach predicts the delay time based on the group delay function evaluated at the central frequency in the *initial* pulse. However, in this example none of the energy associated with spectral components near $\bar{\omega}$ survives propagation to influence the arrival

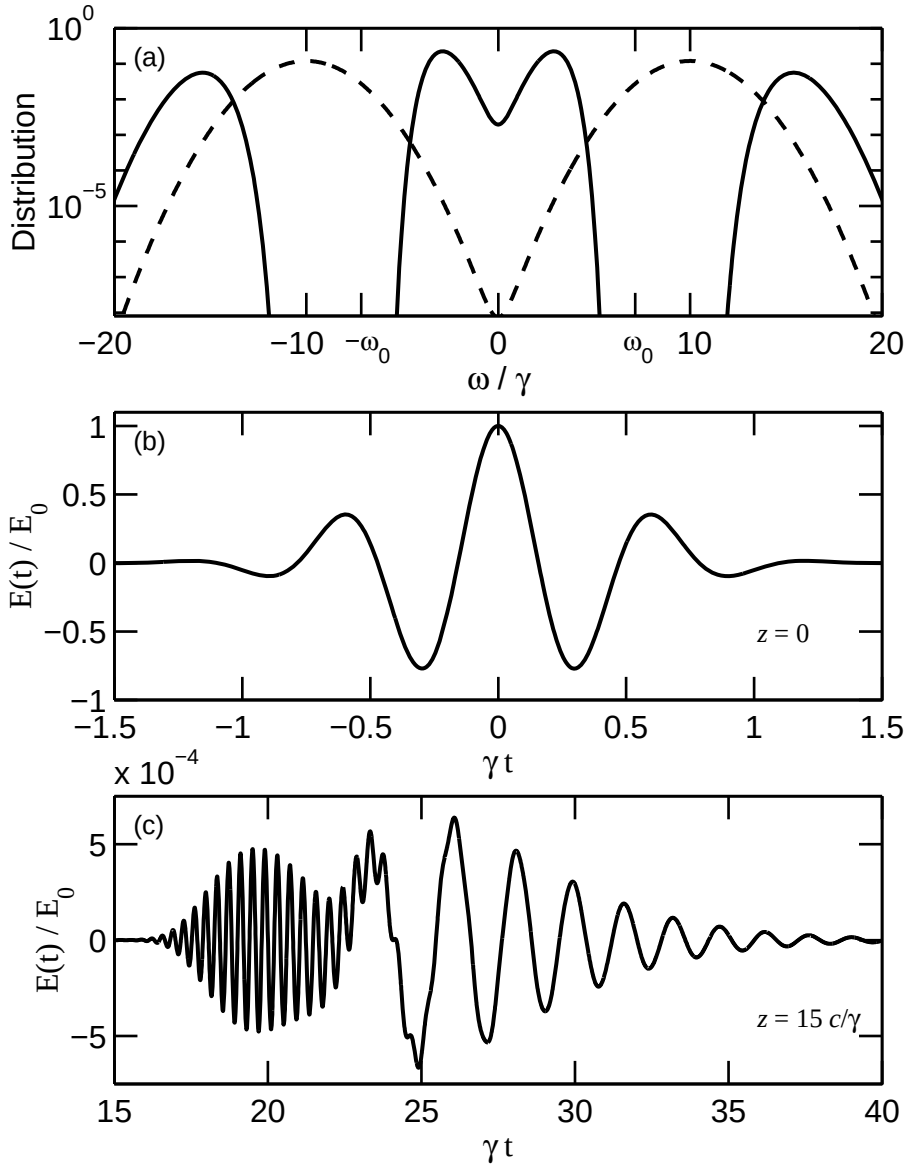

Figure 3.24: (a) Normalized spectral distributions at the initial (dashed) and final (solid) points. (b) Temporal profile at the initial point. (c) Temporal profile at the final point.

at the observation point. This shows why the prediction of propagation delay must be made using the spectrum that survives propagation, as is done in the new context of group delay.

3.4.2 Traditional Description of Precursors

The field plotted in Fig. 3.24(c) is a specific example of a precursor field. This type of field occurs in the 'mature' dispersion regime, where pulse dynamics (such as propagation velocity) settle into a stable situation. Absorption is minimal in this regime since the spectral components which experience significant attenuation are absorbed before the pulse reaches the mature region. Notice that for the parameters that we have chosen, the precursor field separates nicely into an early high frequency bump and a later low frequency bump. Although we were able to track the center of mass for the propagation field using group delay, the traditional method of describing precursor fields in the mature dispersion regime allows the tracking of the two bumps individually.

The traditional method[10] of analyzing precursor field begins with the standard integral solution to Maxwell's equations, with propagation considered in only one direction (the $\hat{z}$ direction). This solution can be written as

$$\mathbf{E}(z,t) = \frac{1}{\sqrt{2\pi}} \int_{-\infty}^{\infty} \mathbf{E}(z=0,\omega)\, e^{\phi(\omega,t)}\, \mathrm{d}\omega \tag{3.11}$$

where

$$\phi(\omega,t) = i\,[k(\omega)\,z - \omega t]\,. \tag{3.12}$$

A single resonance Lorentz oscillator is used to obtain an explicit form for $k(\omega)$. If one then assumes that $z \to \infty$ (i.e., the mature dispersion regime), it is possible to obtain an asymptotic solution to (3.11) using the method of steepest descents.[17] In this method the integral is performed using contour integration. In the asymptotic limit where z is arbitrarily large, the contour integral depends only on the saddle points of $\phi(\omega)$ (i.e., the

frequencies in the complex ω plane where $\mathrm{d}\phi/\mathrm{d}\omega = 0$). The solution (3.11) can then be written as

$$\mathbf{E}(z,t) = \mathbf{E}_S(z,t) + \mathbf{E}_B(z,t). \tag{3.13}$$

The term $\mathbf{E}_S$ is known as the Sommerfeld precursor, and $\mathbf{E}_B$ is the Brillouin precursor. Each precursor term is composed of an amplitude function multiplying an oscillatory function. Both the amplitude and the phase of the oscillation are written as functions of the various saddle point frequencies of $\phi(\omega, t)$. As time progresses the locations of the saddle points shift, and the time evolution of the pulse is found by tracking the trajectories of these saddle points in the complex plane. After performing this analysis, it is seen that the Sommerfeld precursor describes the high frequency portion of the pulse, and the Brillouin precursor describes the low frequency portion. In the example shown in Fig. 3.24 these two fields can both be distinctly observed in the final pulse.

The concept of group delay can be used to describe the behavior of the solution obtained using these methods. Since both precursor fields are known as a function of time (once the trajectories of the saddle points are known), the delay for each individual precursor field can be calculated in the same manner as the delay for the total field. Of course the asymptotic nature of the solutions requires that delay times be calculated between two points which both have large z.

3.4.3 Alternative Description of Precursor Fields

Although the traditional method for describing precursor fields works quite well if z is sufficiently large, the process of tracking the location of saddle points can be complicated. In this section we illustrate a different approach which allows one to track the center of mass for each of the separate precursor fields individually without having to resort to the asymptotic solution. While this method does not give all of the detail provided by the

traditional approach, it provides a much simpler way to predict when the two precursor fields will arrive at a given point.

Because the Fourier transform is a linear operation, we can separate the spectrum of a pulse propagating in a single resonance absorber (with resonance frequency ω_0) into two pieces as follows:

$$\mathbf{E}(\mathbf{r},\omega) = \mathbf{E}_S(\mathbf{r},\omega) + \mathbf{E}_B(\mathbf{r},\omega) \tag{3.14}$$

where

$$\mathbf{E}_B(\mathbf{r},\omega) = \begin{cases} \mathbf{E}(\mathbf{r},\omega) & , \quad |\omega| \le \omega_0 \\ 0 & , \quad |\omega| > \omega_0 \end{cases} \tag{3.15}$$

$$\mathbf{E}_S(\mathbf{r},\omega) = \begin{cases} 0 & , \quad |\omega| \le \omega_0 \\ \mathbf{E}(\mathbf{r},\omega) & , \quad |\omega| > \omega_0 \end{cases} . \tag{3.16}$$

The temporal profile of the pulse then is given by

$$\mathbf{E}(z,t) = \mathbf{E}_S(z,t) + \mathbf{E}_B(z,t), \tag{3.17}$$

where the two terms in (3.17) are the inverse Fourier transforms of (3.15) and (3.16). The term $\mathbf{E}_S(\mathbf{r},t)$ is then the 'above resonance' portion of the pulse, and $\mathbf{E}_B(\mathbf{r},t)$ is the 'below resonance' portion.

If a pulse's initial spectrum $\mathbf{E}(\mathbf{r}_0,\omega)$ has significant on-resonance amplitude, then $\mathbf{E}_S(\mathbf{r}_0,\omega)$ and $\mathbf{E}_B(\mathbf{r}_0,\omega)$ will have a significant discontinuity at ω_0. Because an abrupt discontinuity in frequency requires a broad temporal profile, $\mathbf{E}_S(\mathbf{r}_0,t)$ and $\mathbf{E}_B(\mathbf{r}_0,t)$ will be poorly localized. In this case the two terms have little significance individually except that when added together they produce the temporal profile of the total field. However, as the pulse propagates the on-resonance amplitude of $\mathbf{E}(\mathbf{r},\omega)$ decreases and the discontinuity becomes less important. Eventually the discontinuity becomes insignificant, and $\mathbf{E}_S(\mathbf{r},t)$ and $\mathbf{E}_B(\mathbf{r},t)$ represent two independent pulses. These pulses can be tracked using the new group delay context.

We illustrate this procedure using the pulse and medium in section 3.4.1. Figure 3.25 illustrates the low frequency component $\mathbf{E}_B$. We calculate the initial spectrum $\mathbf{E}_B(\mathbf{r}_0,\omega)$ at a point displaced by one absorption depth z_d from the original reference point (in section 3.4.1) where the total pulse is Gaussian. (An absorption depth is the distance over which the on-resonance components are reduced by e^{-1}. In this example $z_d \approx 0.2c/\gamma$.) The final spectrum is calculated at the same point as in Fig. 3.24. Figure 3.25(a) shows the initial and final distributions, Fig. 3.25(b) plots the initial temporal profile, and Fig. 3.25(c) plots the final temporal profile. The delay time for $\mathbf{E}_B$ between these two points is calculated using (2.43) as $\Delta t = 25.54/\gamma$, and the arrival time at $\mathbf{r}_0$ is $\langle t\rangle_{\mathbf{r}_0} = 0.82/\gamma$. Thus, the group delay predicts that the low frequency portion of the pulse arrives to $\mathbf{r}$ at $\langle t\rangle_{\mathbf{r}} = 26.36/\gamma$, which can be roughly verified by eye in the figure.

Figure 3.26 repeats this process for the high frequency component $\mathbf{E}_S$. In this case, the delay time calculated with (2.43) is $\Delta t = 19.75/\gamma$ and the arrival time at $\mathbf{r}_0$ is $\langle t\rangle_{\mathbf{r}_0} = 0.37/\gamma$. This predicts that the high frequency portion arrives to $\mathbf{r}$ at $\langle t\rangle_{\mathbf{r}} = 20.12/\gamma$. The reshaping delay is small for both the high and low frequency components cases (about a 2% correction to Δt_G in both cases). As with the traditional approach described above, this alternative approach gets progressively better as $\mathbf{r}_0$ and $\mathbf{r}$ are moved deeper into the medium.

In the example considered here, the high and low frequency components separate into distinct bumps in the final pulse. However, this is not always the case. The arrival time of each component is easily predicted using the new group delay context when using the approach illustrated here. In addition to calculating the separation of the precursor fields, the new group delay context can be used to analyze the chirping of the precursors. The arrival time of a frequency in the final pulse can be predicted by noting that each frequency is delayed according to its group delay.

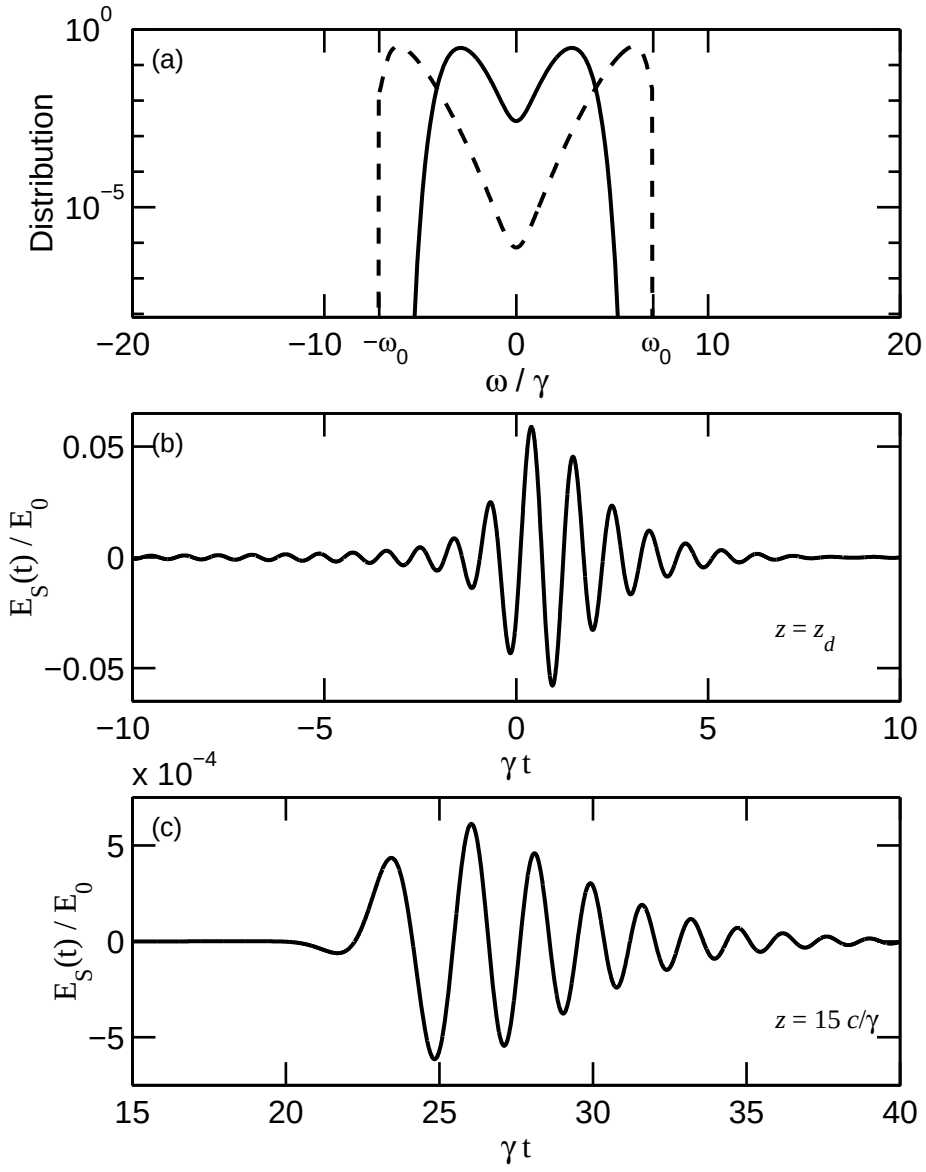

Figure 3.25: (a) Normalized spectral distributions at the initial (dashed) and final (solid) points for $\mathbf{E}_B$. (b) Temporal profile at the initial point. (c) Temporal profile at the final point.

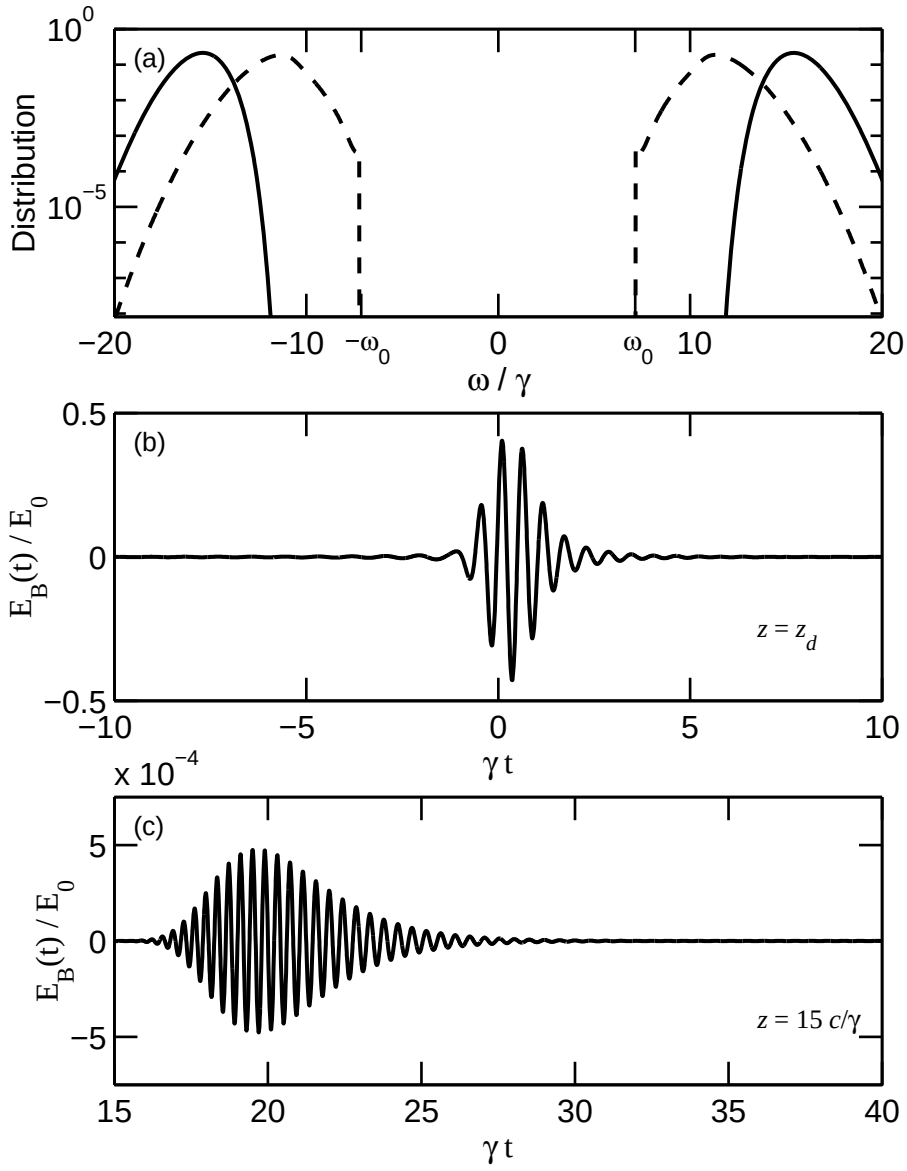

Figure 3.26: (a) Normalized spectral distributions at the initial (dashed) and final (solid) points for $\mathbf{E}_S$. (b) Temporal profile at the initial point. (c) Temporal profile at the final point.

3.4.4 Comparison of Approaches

The alternative approach described here has some drawbacks when compared to the traditional asymptotic approach. First, the temporal representation of the fields must still be found by performing an integral. The asymptotic approach gives an analytic form for the temporal profile. Second, it is difficult to obtain information about the chirping of a pulse from the integral representation. In the asymptotic solution, the phase of oscillation is known as a function of time (i.e., in terms of the saddle point locations), so that the chirping behavior of a pulse is explicit. In addition to these two drawbacks, there are some other features of propagation that are more subject to analysis using the asymptotic solution than with the integral representation.

Despite these drawbacks, there are significant advantages to the alternative approach. First, this approach is independent of the model used to describe the medium. All that is required is that the resonance frequency be known. Second, this method is easily generalizable to describe precursor fields in multiple resonance media. (For example, in a two resonance medium there are three precursor fields describing different spectral regions: one below the lower resonance, one above the higher resonance, and one between the two resonances.) The traditional method can be expanded to describe multiple resonance Lorentz oscillators, but the extension quickly becomes complex as more resonances are added.

Perhaps the biggest advantage of the approach used in section 3.4.3 is its conceptual clarity. In the traditional approach, the solution is buried in so much detail that it is difficult to see what is being described by a precursor field. In the alternative approach it is clear that we are simply analyzing and comparing the behavior different spectral regions of a pulse after it has propagated a large distance.

Chapter 4

Energy Transport in Dispersive Media

In chapter 3 we presented several examples in which the locus of a pulse's field energy travels at speeds greater than c. It is important to note that one is tracking the presence of only the electromagnetic field energy when these superluminal observations are made. Of course in a dielectric medium, field energy is only part of the energy picture. Energy is also stored in the medium; the pulse continually exchanges energy with the medium as it propagates. Thus, the overly rapid appearance of electromagnetic energy at one point and its simultaneous disappearance at another does not require superluminal *transport* of energy, but merely an exchange between energy forms at individual locations.

In this chapter we examine the actual transport of energy and how energy is exchanged between the pulse field and the medium. We briefly review Poynting's theorem and show how it leads to the traditional concept of energy transport velocity. We demonstrate that the global energy transport velocity (i.e., the average velocity of the *total* energy) is strictly bounded by c. We then show that there is no such limit on the velocity tracking the average position of only the field energy, even though the velocity at which field energy is transported from one point to another is strictly bounded by c. Finally, we discuss how energy is exchanged between the field of a pulse and a dielectric medium.[30,31] We

demonstrate that the asymmetric energy exchange which leads to superluminal and highly subluminal behaviors is a direct and natural consequence of causality, independent of any specific model.

4.1 Poynting's Theorem

Poynting's theorem is a direct consequence of Maxwell's equations. To obtain this theorem, we take the dot product of (2.4) from Maxwell's equations with the electric field vector:

$$\mathbf{E}\cdot\nabla\times\mathbf{B}=\mu_0\mathbf{E}\cdot\frac{\partial}{\partial t}\left(\epsilon_0\mathbf{E}+\mathbf{P}\right). \tag{4.1}$$

Then we use the vector identity $\nabla\cdot(\mathbf{E}\times\mathbf{B})=\mathbf{B}\cdot(\nabla\times\mathbf{E})-\mathbf{E}\cdot(\nabla\times\mathbf{B})$ to rewrite (4.1) as

$$\nabla\cdot(\mathbf{E}\times\mathbf{B})-\mathbf{B}\cdot\nabla\times\mathbf{E}+\mu_0\mathbf{E}\cdot\frac{\partial}{\partial t}\left(\epsilon_0\mathbf{E}+\mathbf{P}\right)=0. \tag{4.2}$$

We then substitute (2.3) from Maxwell's equations into expression (4.2) to obtain

$$\nabla\cdot(\mathbf{E}\times\mathbf{B})+\mathbf{B}\cdot\frac{\partial\mathbf{B}}{\partial t}+\mu_0\mathbf{E}\cdot\frac{\partial}{\partial t}\left(\epsilon_0\mathbf{E}+\mathbf{P}\right)=0. \tag{4.3}$$

Finally, we rearrange (4.3) to arrive at

$$\nabla\cdot\left(\mathbf{E}\times\frac{\mathbf{B}}{\mu_0}\right)+\frac{\partial}{\partial t}\left(\frac{\mathbf{B}\cdot\mathbf{B}}{2\mu_0}+\epsilon_0\frac{\mathbf{E}\cdot\mathbf{E}}{2}+\int_{-\infty}^{t}\mathbf{E}\cdot\frac{\partial\mathbf{P}}{\partial t}\,\mathrm{d}t\right)=0, \tag{4.4}$$

where we have assumed that the fields are zero at $t=-\infty$.

Equation (4.4) is recognized as the familiar form of Poynting's theorem:

$$\nabla\cdot\mathbf{S}\left(\mathbf{r},t\right)+\frac{\partial u\left(\mathbf{r},t\right)}{\partial t}=0, \tag{4.5}$$

where the Poynting vector is

$$\mathbf{S}\left(\mathbf{r},t\right)\equiv\mathbf{E}\left(\mathbf{r},t\right)\times\frac{\mathbf{B}\left(\mathbf{r},t\right)}{\mu_0} \tag{4.6}$$

and the total energy density is given by

$$u(\mathbf{r},t) = u_{\text{field}}(\mathbf{r},t) + u_{\text{exchange}}(\mathbf{r},t) + u(\mathbf{r},-\infty). \tag{4.7}$$

This expression for the energy density includes all relevant forms of energy, including a non-zero integration constant $u(\mathbf{r},-\infty)$, which corresponds to energy stored in the medium before the arrival of any pulse. The electromagnetic field energy density is

$$u_{\text{field}}(\mathbf{r},t) \equiv \frac{B^2(\mathbf{r},t)}{2\mu_0} + \frac{\epsilon_0 E^2(\mathbf{r},t)}{2}. \tag{4.8}$$

The time-dependent accumulation of energy density transferred into the medium from the field is given by

$$u_{\text{exchange}}(\mathbf{r},t) \equiv \int_{-\infty}^{t} \mathbf{E}\left(\mathbf{r},t'\right) \cdot \frac{\partial \mathbf{P}\left(\mathbf{r},t'\right)}{\partial t'} \mathrm{d}t'. \tag{4.9}$$

As u_{exchange} increases, the energy in the medium increases. Conversely, as u_{exchange} decreases, the medium surrenders energy to the electromagnetic field. While it is possible for u_{exchange} to become negative, the combination $u_{\text{exchange}} + u(-\infty)$ (i.e., the net energy in the medium) cannot go negative since a material cannot surrender more energy than it has to begin with. Both u_{field} and u_{exchange} are zero before the arrival of the pulse (i.e. at $t = -\infty$). In addition, the field energy density returns to zero after the pulse has passed (i.e. at $t = +\infty$).

4.2 Energy Transport Velocity

Poynting's theorem has the form of a continuity equation which, when integrated spatially over a small volume V, yields

$$\int_A \mathbf{S}(\mathbf{r},t) \cdot \mathrm{d}\mathbf{a} = -\frac{\partial}{\partial t} \int_V u(\mathbf{r},t)\, \mathrm{d}^3 r, \tag{4.10}$$

where the left-hand side has been transformed into an area integral representing the power leaving the volume. Let the volume V be small enough to take $\mathbf{S}$ to be uniform

throughout. The energy transport velocity (directed along **S**) is then defined to be the effective speed at which the energy contained in the volume (i.e. the result of the 3-D integral) would need to travel in order to achieve the power transmitted through one side of the volume (e.g., the power transmitted through one end of a tiny cylinder aligned with **S**). The energy transport velocity as traditionally written[4] is then

$$\mathbf{v}_E(\mathbf{r},t) \equiv \frac{\mathbf{S}(\mathbf{r},t)}{u(\mathbf{r},t)}. \tag{4.11}$$

It is not essential to time-average **S** and u over rapid oscillations, although this average is often made.[32] (One may choose to add the curl of an arbitrary vector function to **S**. However, this possibility should not be injected into (4.11) since it cannot contribute to the integral in (4.10).)

When the total energy density u is used in computing (4.11), the energy transport velocity is *fictitious* in its nature; it is not the actual velocity of the total energy (since the energy stored in the medium is stationary), but rather the effective velocity necessary to achieve the same energy transport that the electromagnetic flux alone delivers. There is no behind the scenes flow of mechanical energy. Moreover, if only u_{field} is used in evaluating (4.11), we have

$$\begin{aligned} \mathbf{v}_{E_{\text{field}}} &= \frac{2\mathbf{E}\times\mathbf{B}}{\epsilon_0\mu_0\mathbf{E}\cdot\mathbf{E}+\mathbf{B}\cdot\mathbf{B}} \\ &= c\frac{2\mathbf{E}\times c\mathbf{B}}{E^2+(cB)^2}. \end{aligned} \tag{4.12}$$

The Cauchy-Schwartz inequality, $\alpha^2+\beta^2 \geq 2\alpha\beta$, then ensures that $\mathbf{v}_{E_{\text{field}}}$ is strictly bounded by the speed of light in vacuum c. Equation (4.12) thus demonstrates that no field energy is *transported* between points in the medium at speeds greater than c. We insist that the total energy density $u(\mathbf{r},t)$ should be at least as great as the field energy density, which maintains the strict luminality of $\mathbf{v}_E$. In this we differ from previous usage of the energy transport velocity in connection with amplifying media[1,8,13] where the constant

of integration $u(-\infty)$ was left at zero (apparently by default), resulting in the viewpoint of superluminal and negative (opposite to the direction of $\mathbf{S}$) energy transport velocities.

4.3 Average Energy Transport Velocity

Since the point-wise energy transport velocity defined by (4.11) is strictly luminal, it follows that the global energy transport velocity (the average speed of *all relevant energy*) is also bounded by c. This has been discussed for pulses propagating in vacuum.[33] The analysis given here includes also the effects of a linear medium. To obtain the global properties of energy transport, we begin with a weighted average of the energy transport velocity at each point in space. A suitable weighting parameter is the energy density at each position. The global energy transport velocity is then

$$\langle \mathbf{v}_E \rangle \equiv \frac{\int \mathbf{v}_E(\mathbf{r},t)\, u(\mathbf{r},t)\, \mathrm{d}^3 r}{\int u(\mathbf{r},t)\, \mathrm{d}^3 r} = \frac{\int \mathbf{S}(\mathbf{r},t)\, \mathrm{d}^3 r}{\int u(\mathbf{r},t)\, \mathrm{d}^3 r} \tag{4.13}$$

where we have inserted the definition (4.11), and the integral is taken over all relevant space. Integration by parts leads to

$$\langle \mathbf{v}_E \rangle = \frac{\int \mathbf{r} \nabla \cdot \mathbf{S}(\mathbf{r},t)\, \mathrm{d}^3 r}{\int u(\mathbf{r},t)\, \mathrm{d}^3 r} = \frac{\int \mathbf{r} \frac{\partial}{\partial t} u(\mathbf{r},t)\, \mathrm{d}^3 r}{\int u(\mathbf{r},t)\, \mathrm{d}^3 r}, \tag{4.14}$$

where we have assumed that the volume for the integration encloses all energy in the system and that the field near the edges of this volume is zero. We have also made a substitution from (4.5).

Because the continuity relation (4.5) is written with no explicit source terms (i.e. zero on the right-hand side), the total energy in the system is conserved and is equal to the denominator of (4.14). This allows the time derivative in (4.14) to be brought out in front of the entire expression, giving

$$\langle \mathbf{v}_E \rangle = \frac{\partial \langle \mathbf{r} \rangle}{\partial t}, \tag{4.15}$$

where

$$\langle \mathbf{r} \rangle \equiv \int \mathbf{r} u(\mathbf{r}, t)\, \mathrm{d}^3 r \Big/ \int u(\mathbf{r}, t)\, \mathrm{d}^3 r\,. \tag{4.16}$$

Equation (4.16) represents the spatial 'center of mass' or centroid of the total energy in the system.[30] Because $\langle \mathbf{v}_E \rangle$ luminal, (4.15) guarantees that the centroid of the *total* energy moves at a velocity less than c.

4.4 Group Velocity and Field Energy

The precise relationship (4.15) requires the total energy density $u(\mathbf{r}, t)$. If only the field energy density u_{field} is used in defining the energy transport velocity, as in (4.12), the time derivative could not be brought out in front of the entire expression as in (4.15) since the integral in the denominator would retain time dependence. Mathematically, we have

$$\langle \frac{\mathbf{S}}{u_{\text{field}}} \rangle \neq \frac{\partial}{\partial t} \frac{\int \mathbf{r} u_{\text{field}}(\mathbf{r}, t)\, \mathrm{d}^3 r}{\int u_{\text{field}}(\mathbf{r}, t)\, \mathrm{d}^3 r}. \tag{4.17}$$

While the left-hand side of (4.17) is strictly luminal, the right hand side can easily exceed c as the medium exchanges energy with the field. In this section, we demonstrate that the right-hand side of (4.17) is connected to an average over group velocities rather than an average energy transport velocity.

In chapter 2 we considered the time difference between the arrival of pulse energy at two points in space in order to make the connection between the presence of field energy and the concept of group delay. In the present context, it is enlightening to examine the converse scenario, namely the displacement of the field energy's spatial centroid at two points in time. We use the centroid of field energy appearing in the right-hand side of (4.17) to define the pulse's position (according to an 'observer' who sees only field energy):

$$\langle \mathbf{r}_{\text{field}} \rangle_t \equiv \int \mathbf{r} u_{\text{field}}(\mathbf{r}, t)\ \mathrm{d}^3 r \Big/ \int u_{\text{field}}(\mathbf{r}, t)\ \mathrm{d}^3 r\,. \tag{4.18}$$

As a pulse evolves from an initial time t_0 to time $t_0 + \Delta t$, the difference in the average position of the field energy is given by

$$\Delta \mathbf{r} \equiv \langle \mathbf{r}_{\text{field}} \rangle_{t_0+\Delta t} - \langle \mathbf{r}_{\text{field}} \rangle_{t_0}. \tag{4.19}$$

In Appendix A we show how (4.19) can be rewritten (using techniques similar to those presented in section 2.4) as the sum of two terms with intuitive interpretations:

$$\Delta \mathbf{r} = \Delta \mathbf{r}_G + \Delta \mathbf{r}_R. \tag{4.20}$$

Note the similarity between (4.20) and (2.43).

In most situation, the net group displacement $\Delta \mathbf{r}_G$ is the dominant contributor to the total displacement. It is defined by

$$\Delta \mathbf{r}_G \equiv \Delta t \int \left[\nabla_{\mathbf{k}} \operatorname{Re} \omega(\mathbf{k})\right] \rho(\mathbf{k}, t)\ \mathrm{d}^3 k, \tag{4.21}$$

where $\rho(\mathbf{k}, t)$ is a normalized k-space distribution of field energy density (see (A.11)) at the final time $t \equiv t_0 + \Delta t$:

$$\rho(\mathbf{k}, t) \equiv u_{\text{field}}(\mathbf{k}, t) \Big/ \int u_{\text{field}}(\mathbf{k}, t)\ \mathrm{d}^3 k\,. \tag{4.22}$$

Equation (4.21) explicitly demonstrates how the group velocity function $\nabla_{\mathbf{k}} \operatorname{Re} \omega(\mathbf{k})$ is connected to the presence of field energy. The velocity of the centroid of field energy is predicted by an average of the group velocity function weighted by the k-space distribution of field energy in the *final* pulse (i.e. the pulse at $t = t_0 + \Delta t$). The distribution $\rho(\mathbf{k}, t)$ defines the fraction of the pulse's field energy that can be associated with a given range of wave vectors, and the group velocity function gives the velocity at which energy associated with a given wave vector appears downstream. (Again, the fact that energy *appears* downstream does not necessarily require that the energy was *transported* downstream.) Since the group velocity function can be superluminal or negative, the displacement per time $\Delta \mathbf{r}_G / \Delta t$ can take on virtually any value.

The term $\Delta\mathbf{r}_R$ in (4.20) represents a displacement which arises solely from a reshaping of the pulse through absorption or amplification (without considering the dispersion introduced by propagation). This reshaping displacement is the difference between the pulse position at the *initial time* t_0 evaluated without and with the spatial frequency amplitude that is lost during propagation (speaking as though the medium is absorptive). For the explicit form for $\Delta\mathbf{r}_R$, see (A.14). The reshaping displacement is zero if the pulse does not experience absorption or amplification. The reshaping displacement is also negligible if the pulse is unchirped before propagation. In addition, it goes to zero in the narrowband limit even if pulses experience strong absorption or amplification. (In the narrowband limit, $\Delta\mathbf{r}_G$ reduces to $\nabla_{\mathbf{k}}\,\mathrm{Re}\,\omega\left(\bar{\mathbf{k}}\right)$, where $\bar{\mathbf{k}}$ is the central wave-vector in the pulse. This recovers the standard group velocity obtained using expansion techniques.)

Because $\Delta\mathbf{r}_R$ is usually small, the presence of field energy is generally tracked by group velocity, as shown in (4.21). Thus, while the velocity of the centroid of total energy is strictly bounded by c (as demonstrated in (4.15)), the centroid of field energy can move with any speed. This is not very mysterious when one recalls that we have made no mention of where the field energy comes from when deriving (4.20). For example, in an amplifying medium that exhibits superluminal behavior the rapid appearance of a pulse downstream is merely an artifact of not recognizing the energy already present in the medium until it converts to the form of field energy.[1,13]

Note that in (4.21) we use real wave-vectors associated with complex frequencies. Also, in writing (4.21) we made the restrictive assumption that $\omega(\mathbf{k})$ is single-valued. Although this assumption is quite limiting, it is not uncommon to use it. (For instance, see Ref. [15] pp. 324–325.) The group delay context discussed in chapter 2 avoids this issue altogether. For details on these issues, see appendix A.

4.5 Exchange of Energy in Dielectrics

In this section, we turn our attention to the exchange of energy between the field and the medium, which is responsible for the seemingly exotic behavior of superluminal and highly subluminal pulses. For this purpose it is enlightening to consider $u_{\text{exhchange}}$ given in (4.9) within a frequency context. Here we return to the convention of real frequencies ω as used in (2.6) and (2.7). We assume a linear, isotropic (but not necessarily homogeneous) medium so that the polarization is connected to the electric field in the frequency domain via

$$\mathbf{P}(\mathbf{r},\omega) = \epsilon_0 \chi(\mathbf{r},\omega)\,\mathbf{E}(\mathbf{r},\omega). \tag{4.23}$$

The susceptibility $\chi(\mathbf{r},-\omega)$ retains the symmetry

$$\chi(\mathbf{r},-\omega) \quad = \quad \chi^*(\mathbf{r},\omega) \tag{4.24}$$

as in the homogeneous case (2.13).

We can immediately rewrite the exchange energy density (4.9) as

$$\begin{aligned} u_{\text{exchange}}(\mathbf{r},t) \quad = \quad & \int_{-\infty}^{t} \left[\frac{1}{\sqrt{2\pi}} \int_{-\infty}^{\infty} \mathbf{E}\left(\mathbf{r},\omega'\right) e^{-i\omega' t'}\, \mathrm{d}\omega' \right] \\ & \cdot \left[\frac{-i\epsilon_0}{\sqrt{2\pi}} \int_{-\infty}^{\infty} \omega \chi(\mathbf{r},\omega)\,\mathbf{E}(\mathbf{r},\omega)\, e^{-i\omega t'}\, \mathrm{d}\omega \right] \mathrm{d}t' \end{aligned} \tag{4.25}$$

using the Fourier transform (2.6). With a rearrangement of integration order, the expression (4.25) becomes

$$u_{\text{exchange}}(\mathbf{r},t) = -i\epsilon_0 \int_{-\infty}^{\infty} \mathrm{d}\omega\omega\chi(\mathbf{r},\omega)\,\mathbf{E}(\mathbf{r},\omega) \cdot \int_{-\infty}^{\infty} \mathrm{d}\omega' \mathbf{E}(\mathbf{r},\omega) \frac{1}{2\pi} \int_{-\infty}^{t} e^{-i(\omega+\omega')t'} \mathrm{d}t'. \tag{4.26}$$

The final integral in (4.26) becomes the delta function when t goes to $+\infty$. In this case, the middle integral can also be performed. Therefore, after the point $\mathbf{r}$ has experienced the entire pulse, the total amount of energy density that the medium has exchanged with the field is

$$u_{\text{exchange}}(\mathbf{r},+\infty) = -i\epsilon_0 \int_{-\infty}^{\infty} \omega\chi(\mathbf{r},\omega)\,\mathbf{E}(\mathbf{r},\omega) \cdot \mathbf{E}(\mathbf{r},-\omega)\,\mathrm{d}\omega. \tag{4.27}$$

Finally, we use the symmetries (2.10) and (4.24) to obtain

$$u_{\text{exchange}}(\mathbf{r}, +\infty) = \epsilon_0 \int_{-\infty}^{\infty} \omega \operatorname{Im} \chi(\mathbf{r}, \omega) |\mathbf{E}(\mathbf{r}, \omega)|^2 \, \mathrm{d}\omega. \tag{4.28}$$

Equation (4.28) is well known and appears in a textbook by Landau and Lifshitz.[34] It describes the net exchange of energy density after all interaction between the pulse and the medium has ceased at the point $\mathbf{r}$. We can modify this formula in a simple and intuitive way so that it describes the exchange energy density for any time during the pulse. This requires no approximations; the slowly-varying envelope approximation need not be made. The principle of causality guides us in considering how the medium perceives the electric field for any time.

Since the medium is unable to anticipate the spectrum of the entire pulse before experiencing it, the material must respond to the pulse according to the history of the field up to each instant. In particular, the material at all times must be prepared for the possibility of an abrupt cessation of the pulse, in which case all exchange of energy with the medium ceases. If the pulse were in fact to abruptly terminate at a given moment, then obviously (4.28) would immediately apply since the pulse would be over; it would not be necessary to integrate the Fourier transform (2.6) beyond the termination time t for which all contributions are zero. Causality requires that the medium be indifferent to whether the pulse actually ceases at a given instant before that instant arrives. Therefore, (4.28) in fact applies at all times where the spectrum (2.6) is evaluated over that portion of the field previously experienced by the medium.

The following is then an exact representation for the exchange energy density defined in (4.9):

$$u_{\text{exchange}}(\mathbf{r}, t) = \epsilon_0 \int_{-\infty}^{\infty} \omega \operatorname{Im} \chi(\mathbf{r}, \omega) |\mathbf{E}_t(\mathbf{r}, \omega)|^2 \, \mathrm{d}\omega, \tag{4.29}$$

where

$$\mathbf{E}_t(\mathbf{r}, \omega) \equiv \frac{1}{\sqrt{2\pi}} \int_{-\infty}^{t} \mathbf{E}\left(\mathbf{r}, t'\right) e^{i\omega t'} \, \mathrm{d}t'. \tag{4.30}$$

The time dependence enters only through $|\mathbf{E}_t(\mathbf{r},\omega)|^2$, the *instantaneous power spectrum*, which has been used to describe the response of driven electronic circuits,[35] the acoustical response of materials to sound waves,[36] and the behavior of photon counters.[37]

The causality argument presented above comprises a sufficient proof of (4.29) and (4.30). It is essentially the same argument as that used to justify that the susceptibility $\chi(\mathbf{r},\omega)$ has no poles in upper half of the complex ω plane, which leads to the Kramers-Kronig relations.[15] However, in section 4.6 we provide a formal proof starting from the more familiar Kramers-Kronig relations.[30,31] This section may be skipped without a loss of continuity.

4.6 Derivation of the Instantaneous Spectrum

The goal in this section is to obtain the form (4.29) from (4.9). This theorem was first derived by S. Glasgow.[30] Using (2.6), (2.7), and (4.23), the polarization at a point in the medium can be written as

$$\mathbf{P}(t) = \int_{-\infty}^{\infty} \mathbf{E}\left(t'\right) G\left(t-t'\right)\, \mathrm{d}t', \tag{4.31}$$

where

$$G(t) \equiv \frac{\epsilon_0}{2\pi} \int_{-\infty}^{\infty} \chi(\omega)\, e^{-i\omega t}\, \mathrm{d}\omega. \tag{4.32}$$

The Green's function $G(t)$ can be written as the sum of two parts, the first being associated with the real part of the susceptibility and the second being associated with the imaginary part:

$$G(t) = G_{\mathrm{Re}}(t) + G_{\mathrm{Im}}(t) \tag{4.33}$$

where

$$G_{\mathrm{Re}}(t) \equiv \frac{\epsilon_0}{2\pi} \int_{-\infty}^{\infty} \mathrm{Re}\left[\chi(\omega)\right] e^{-i\omega t}\, \mathrm{d}\omega \tag{4.34}$$

and

$$G_{\mathrm{Im}}(t) \equiv i\frac{\epsilon_0}{2\pi}\int_{-\infty}^{\infty} \mathrm{Im}\left[\chi(\omega)\right] e^{-i\omega t}\ \mathrm{d}\omega. \tag{4.35}$$

We now show that G_{Re} and G_{Im} are equal for $t>0$ and equal but opposite for $t<0$. To do this we invoke the Kramers-Kronig relation[15]

$$\mathrm{Re}\,\chi(\omega) = \frac{1}{\pi}P\int_{-\infty}^{\infty}\frac{\mathrm{Im}\,\chi\left(\omega'\right)}{\omega'-\omega}\ \mathrm{d}\omega'. \tag{4.36}$$

(The letter P in front of the integral indicates the principle part.) Substitution of this relation, which embodies the principle of causality, into the expression for $G_{\mathrm{Re}}(t)$ yields

$$G_{\mathrm{Re}}(t) = \frac{\epsilon_0}{2\pi^2}\int_{-\infty}^{\infty}\mathrm{d}\omega'\,\mathrm{Im}\,\chi\left(\omega'\right)P\int_{-\infty}^{\infty}\frac{e^{-i\omega t}}{\omega'-\omega}\ \mathrm{d}\omega \tag{4.37}$$

where the ordering of integration has been reversed. The final integral in (4.37) can be performed analytically,[17] and it yields

$$P\int_{-\infty}^{\infty}\frac{e^{-i\omega t}}{\omega-\omega'}\ \mathrm{d}\omega = \begin{cases} i\pi e^{-i\omega' t} & , \quad t>0 \\ -i\pi e^{-i\omega' t} & , \quad t<0 \end{cases}. \tag{4.38}$$

Equation (4.37) then becomes

$$G_{\mathrm{Re}}(t) = \begin{cases} G_{\mathrm{Im}}(t) & , \quad t>0 \\ -G_{\mathrm{Im}}(t) & , \quad t<0 \end{cases}. \tag{4.39}$$

We are now able to express the polarization $\mathbf{P}(t)$ in terms of the electric field and only the imaginary part of $\chi(\omega)$. Then (4.31) becomes

$$\begin{aligned} \mathbf{P}(t) &= \int_{-\infty}^{\infty}\mathbf{E}\left(t'\right)2G_{\mathrm{Im}}\left(t-t'\right)\ \mathrm{d}t' \\ &= \frac{i\epsilon_0}{\pi}\int_{-\infty}^{\infty}\mathrm{d}\omega\,\mathrm{Im}\left[\chi(\omega)\right]e^{-i\omega t}\int_{-\infty}^{t}\mathrm{d}t'\mathbf{E}\left(t'\right)e^{i\omega t'}, \end{aligned} \tag{4.40}$$

where again we have changed the order of integration. Note that the upper limit of integration has also been changed to t since (4.32) is zero for negative time arguments.

To evaluate (4.9) we require the time derivative of (4.40):

$$\frac{\partial \mathbf{P}(t)}{\partial t} = \frac{\epsilon_0}{\pi}\int_{-\infty}^{\infty} \mathrm{d}\omega\omega \,\mathrm{Im}\left[\chi(\omega)\right] e^{-i\omega t}\int_{-\infty}^{t} \mathrm{d}t'\mathbf{E}\left(t'\right)e^{i\omega t'} + \frac{\epsilon_0\mathbf{E}(t)}{\pi}\int_{-\infty}^{\infty}\mathrm{d}\omega\,\mathrm{Im}\,\chi(\omega). \tag{4.41}$$

The final term vanishes since $\mathrm{Im}\,\chi(\omega)$ is an odd function of frequency (given that $\mathbf{E}(t)$ and $\mathbf{P}(t)$ are both real). In addition, the truncated Fourier transform in (4.41) can be replaced by the definition (4.30). Then the exchange energy density given by (4.9) becomes

$$u_{\text{exchange}}(t) = 2\epsilon_0\int_{-\infty}^{\infty}\mathrm{d}\omega\omega\,\mathrm{Im}\,\chi(\omega)\int_{-\infty}^{t}\frac{1}{\sqrt{2\pi}}e^{-i\omega t'}\mathbf{E}\left(t'\right)\cdot\mathbf{E}_{t'}(\omega)\,\mathrm{d}t', \tag{4.42}$$

where the order of integration was again changed.

While noting that $e^{-i\omega t}\mathbf{E}(t)/\sqrt{2\pi}$ is the time derivative of the complex conjugate of (4.30), the exchange energy density can be re-written as

$$u_{\text{exchange}}(t) = 2\epsilon_0\int_{-\infty}^{\infty}\mathrm{d}\omega\omega\,\mathrm{Im}\,\chi(\omega)\int_{-\infty}^{t}\frac{\partial\mathbf{E}^*_{t'}}{\partial t'}\cdot\mathbf{E}_{t'}(\omega)\,\mathrm{d}t' \tag{4.43}$$

Since u_{exchange} is a real quantity, it costs nothing to add its complex conjugate and divide by 2. The exchange energy density then becomes

$$\begin{aligned} u_{\text{exchange}}(t) &= \epsilon_0\int_{-\infty}^{\infty}\mathrm{d}\omega\omega\,\mathrm{Im}\,\chi(\omega)\int_{-\infty}^{t}\left[\frac{\partial\mathbf{E}^*_{t'}}{\partial t'}\cdot\mathbf{E}_{t'}(\omega)+\frac{\partial\mathbf{E}_{t'}}{\partial t'}\cdot\mathbf{E}^*_{t'}(\omega)\right]\mathrm{d}t' \\ &= \epsilon_0\int_{-\infty}^{\infty}\mathrm{d}\omega\omega\,\mathrm{Im}\,\chi(\omega)\int_{-\infty}^{t}\frac{\partial|\mathbf{E}_{t'}(\omega)|^2}{\partial t'}\mathrm{d}t' \\ &= \epsilon_0\int_{-\infty}^{\infty}\omega\,\mathrm{Im}\,\chi(\omega)\,|\mathbf{E}_t(\omega)|^2\,\mathrm{d}\omega \end{aligned} \tag{4.44}$$

and (4.29) is verified.

4.7 Discussion of the Instantaneous Spectrum

The expression (4.29) reveals physical insights into the manner in which causal dielectric materials exchange energy with different parts of an electromagnetic pulse. In chapter 5

we discuss several specific examples where the instantaneous spectrum can be used to understand the behavior of a pulse. Here we discuss some of the general properties of (4.29).

4.7.1 Interaction with Resonances not in a Pulse's Spectrum

The instantaneous spectrum formulation of u_{exchange} provides an analytical description of how pulses interact with near-by resonances in linear causal media even when the spectral content of the pulse seems insufficient to permit the interaction. This provides analytical support for the qualitative arguments made by Chiao and coworkers regarding superluminal pulse propagation in an amplifying medium. Their simulations and analysis of the Lorentz model showed that the leading portion of a pulse can 'borrow' energy from an amplifying medium which is then returned to the medium from the later portions of the pulse.[1,8,13] Thus, the superluminal behavior is understood to be a pulse reshaping effect caused by an exchange of energy with the medium.

To see how this interaction is possible, note that the magnitude of u_{exchange} in (4.29) is controlled by the amount of overlap that the instantaneous spectrum has with the resonances in the medium (described by $\text{Im}\,\chi(\mathbf{r},\omega)$). Since the function $\mathbf{E}_t(\mathbf{r},\omega)$ is the Fourier transform of the pulse truncated at the current time and set to zero thereafter, it can include frequency components that are not present in the pulse taken in its entirety. Thus a pulse may interact with resonances at frequencies that are not present in the spectrum of the entire pulse. This also explains why the medium responds differently to the front of a pulse versus the back. The instantaneous spectrum perceived by the medium during early portions of the pulse is generally wider than the spectrum of the entire pulse, and can momentarily overlap nearby resonances. The medium cannot anticipate the future of the pulse, and so it amplifies or attenuates according to this perceived spectrum. During the trailing portion of the pulse, the instantaneous spectrum

generally narrows and the medium adjusts accordingly. In doing this, the material is always prepared for the possibility of an abrupt termination of the field, in which case there is no further exchange of energy.

4.7.2 All Media can both Amplify and Absorb

The actual value of u_{exchange} is usually not as interesting as how the value changes in time. As discussed in section 4.1, when u_{exchange} increases the medium absorbs energy from the pulse and when u_{exchange} decreases the medium surrenders energy to the pulse (i.e., it amplifies the pulse). The value of u_{exchange} does not increase (or decrease) monotonically, but depends upon the history of the pulse up until the current time t. This time dependence enters only through the square magnitude of $\mathbf{E}_t(\omega)$. If, for example, the amount of overlap between $\mathbf{E}_t(\omega)$ and an absorbing resonance is increasing during the leading portion of a pulse then u_{exchange} will increase during this portion of the pulse (i.e., the leading edge experiences absorption). If the instantaneous spectrum later withdraws from this absorbing resonance, the medium returns energy to the trailing portion of the pulse. Thus a point in the medium may absorb energy from the pulse at one instant while amplifying it at another, depending on the behavior of the instantaneous spectrum. This gives a physical explanation for the phenomenon of pulse reshaping.

The explanation of the asymmetric absorption using the instantaneous spectrum is consistent with the explanation given by Crisp.[6] He explained this effect in terms of the time dependence of the polarization in the Lorentz model, and described a kind of delayed response by the oscillator to the stimulus of the pulse field.

4.7.3 Model Independence

The expression (4.29) is independent of the model used to describe pulse/medium interaction. We may apply it to any medium where the linear constitutive relation (4.23) applies and where the function $\chi(\omega)$ obeys the Kramers-Kronig relations.[15] Only the imaginary part of $\chi(\omega)$ is needed since it directly controls absorption and is therefore responsible for the energy exchange. (Although the real part of $\chi(\omega)$ is not formally present in (4.29), it is of course connected to the imaginary part via the Kramers-Kronig relations.) For a strictly absorptive medium we have $\omega \operatorname{Im}\chi(\omega) \geq 0$, since fields are taken to be real in the time domain. Thus u_{exchange} is seen to be positive-definite in this case, so that the total energy density is always greater than u_{field} (with $u(-\infty)$ appropriately set to zero). In an active medium we have $\omega \operatorname{Im}\chi(\omega) \leq 0$, and the integrand in (4.29) goes negative as energy is pulled from the medium and given to the field. In this case, $u(-\infty)$ is chosen sufficiently large to avoid removing (even if momentarily) energy from the medium that is not there to begin with. In either case, strict luminality of the energy transport velocity is maintained with $u(\mathbf{r}, t) \geq u_{\text{field}}(\mathbf{r}, t)$.

4.7.4 Sommerfeld-Brillouin Result

Finally, we note that the expressions (4.29) and (4.30) manifestly contain the Sommerfeld-Brillouin result[14,32] that a sharply defined signal edge cannot propagate faster than c. If a signal edge begins abruptly at time t_0, the instantaneous spectrum $\mathbf{E}_t(\omega)$ clearly remains identically zero until that time. In other words, no energy may be exchanged with a material until the field energy from the pulse arrives. Since, as was pointed out in connection with (4.11), the Cauchy-Schwartz inequality prevents the field energy from traveling faster than c, at no point in the medium can a sharp signal front exceed c.

Chapter 5

Energy Exchange and Pulse Propagation

The instantaneous spectrum description of the exchange energy derived in the chapter 4 provides analytical insight into the behavior of optical pulse in dielectric media. The explanations for many of the superluminal or highly subluminal propagation effects have previously been understood in qualitative and model-dependent contexts. The instantaneous spectrum description gives a model independent, analytic explanation for these superluminal effects. In this chapter we explore several examples illustrating how the instantaneous spectrum can be used to understand both superluminal and highly subluminal behavior.

5.1 Energy Exchange in an Absorbing Medium

In this sections we explore two situations where pulses propagate in a single resonance absorbing medium. As usual, we employ the Lorentz model to describe the medium, even though the the theory we are illustrating is independent of the model. The linear susceptibility in this model is given by

$$\chi(\omega) = \frac{f{\omega_p}^2}{{\omega_0}^2 - \omega^2 - i\gamma\omega}. \tag{5.1}$$

The medium parameters for these two examples are: $\omega_0 = 100\gamma$, $f{\omega_p}^2 = 100\gamma$ (i.e., the same absorbing medium discussed in section 3.1). The pulses are Gaussian as in (3.4).

5.1.1 Subluminal Propagation in an Absorber

For our first example, we consider the common situation where a pulse propagates at a subluminal speed in this medium. Figure 5.1(a) plots the imaginary part of $\chi(\omega)$ for the medium described above. The pulse parameters are chosen as follows: $\bar{\omega} = \omega_0 - 10\gamma$ and $\tau = 1/\gamma$. Figure 5.1(b) plots the temporal profile of this pulse. The overall spectrum of this pulse is broad compared to the resonance, and is centered slightly below the resonance frequency.

The subluminal behavior exhibited by this type of pulse is easily understood in terms of the instantaneous spectrum description. Figure 5.1(c) plots the instantaneous spectrum at various times during the pulse. The line style of each instantaneous spectrum corresponds to the times at which it is evaluated. These times are indicated by the vertical lines of the same style in Fig. 5.1(b). During the early portion of the pulse, the instantaneous spectrum is broad, and its overlap with the absorbing resonance is increasing. Thus the material absorbs energy from the field during this portion of the pulse. During the trailing portion of the pulse, the overlap decreases, whereupon the medium surrenders stored energy to the pulse. The overall effect is that the pulse is slowed down by this reshaping.

In Fig. 5.1(d), u_{exchange} is plotted as a function of time. The decrease in u_{exchange} at the end of the pulse indicates that the medium returns energy to the field in the latter portion of the pulse as the instantaneous spectrum withdraws from the resonance. The gray curve in Fig. 5.1(d) depicts the rapid oscillations of u_{exchange} (approximately 100—not resolved in the figure), while the black curve is time-averaged.

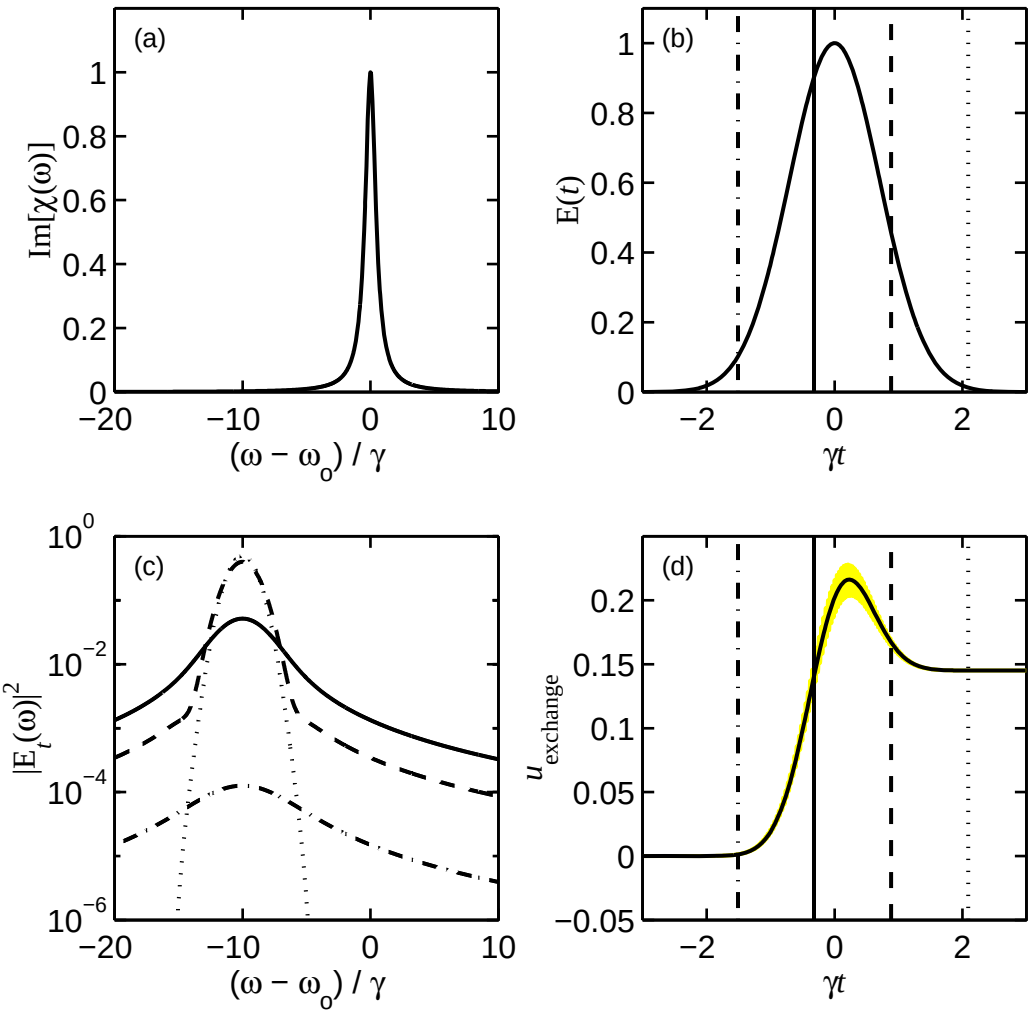

Figure 5.1: (a) Imaginary part of $\chi(\omega)$ for an absorbing medium. (b) Initial pulse temporal profile. (c) Instantaneous spectrum at the times indicated in (b) with vertical lines. (d) Exchange energy density as a function of time.

5.1.2 Superluminal Propagation in and Absorber

For our second example, we illustrate a situation where the pulse exhibits superluminal behavior. As noted before in connection with group delay, this behavior occurs when the pulse spectrum has a narrow bandwidth and is centered on the absorption resonance. To illustrate this effect, we consider a pulse with the following parameters: $\tau = 10/\gamma$ and $\bar{\omega} = \omega_0$. Thus, the pulse bandwidth is narrow compared to the resonance and centered on the resonance frequency. Figure 5.2(b) shows the temporal profile of this pulse.

Figure 5.2(c) plots the instantaneous power spectrum evaluated at various times during the pulse, with the line style again corresponding to the times at which it is evaluated. In this case, the instantaneous spectrum during the early portions of the pulse extends away from the absorption peak, and the on-resonance peak of the instantaneous spectrum grows slowly. During the trailing portion of the pulse, its instantaneous spectrum narrows and the on-resonance peak grows quickly.

Figure 5.2(d) shows u_{exchange} as a function of time. The dot in the center of Fig. 5.2(d) corresponds to the exchange energy at time $t = 0$ (i.e. the midpoint in time of the Gaussian field profile). The plot shows that significantly less than half of the final exchanged energy has been absorbed by this time. Thus the early part of the field envelope is less attenuated than the rear portion (recall Fig. 3.4). The net result is an advancement of the pulse center of mass at a speed greater than c. This provides a theoretical explanation for the asymmetric absorption of the pulse which results in the superluminal effect seen in section 3.1.

5.2 Energy Exchange in an Amplifying Medium

The description of energy exchange in amplifying media is similar to that given above for absorbing media. In an amplifying medium, an increase in the overlap between

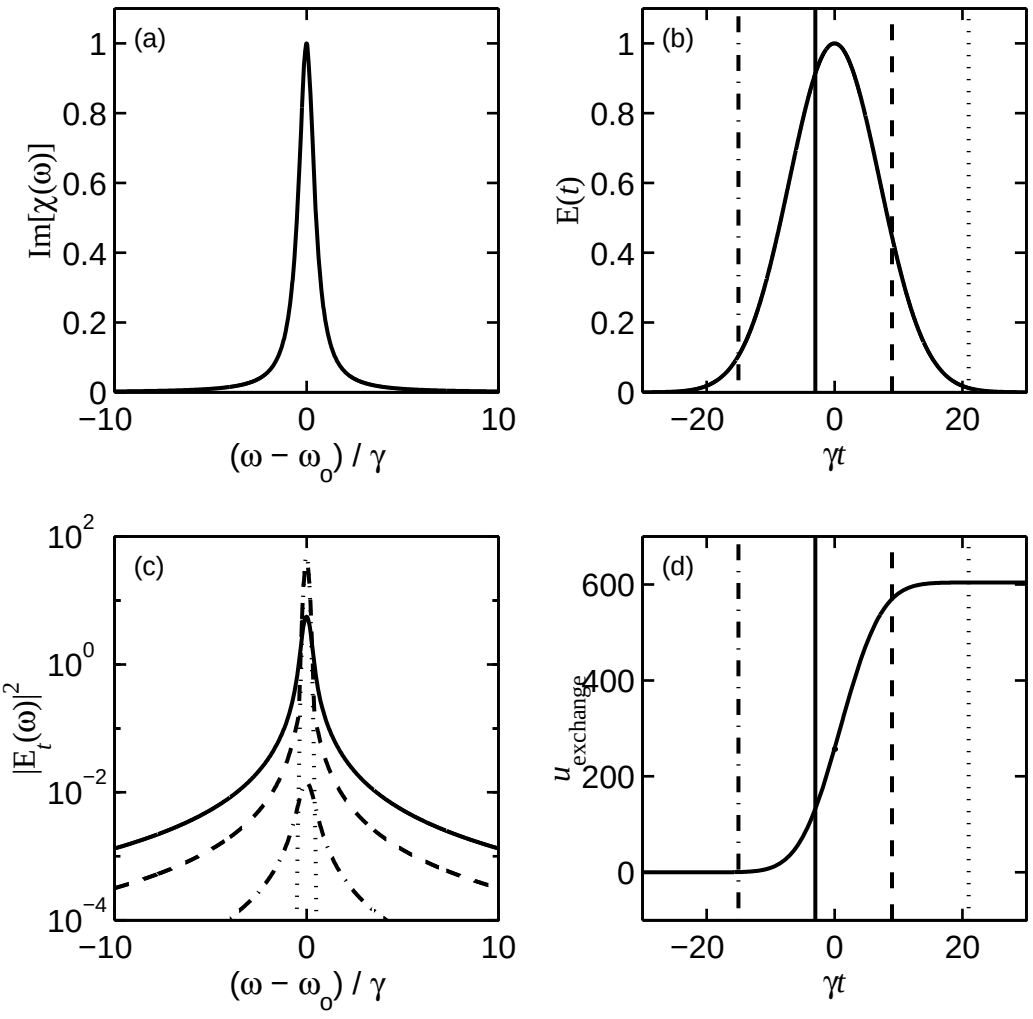

Figure 5.2: (a) Imaginary part of $\chi(\omega)$ for an absorbing medium. (b) Initial pulse temporal profile. (c) Instantaneous spectrum at the times indicated in (b) with vertical lines. (d) Exchange energy density as a function of time.

$\mathbf{E}_t(\omega)$ and resonance frequency corresponds to amplification and a decrease in overlap corresponds to absorption. In this section we consider two examples where pulses propagate superluminally in an amplifier. We then demonstrate how the instantaneous spectrum description can be used to give an estimate of how much a pulse will be advanced.

5.2.1 Superluminal Propagation in an Amplifier, Example 1

As a first illustration we choose the medium parameters with the same values as given in section 5.1 except we change the oscillator strength to $f = -1$ so that we have an amplifying medium. The pulse is the same as the pulse in Fig. 5.1 with $\tau = 1/\gamma$ and the carrier frequency centered below resonance at $\bar{\omega} = \omega_0 - 10\gamma$. Figure 5.3 repeats the figures of section 5.1 for this case. During the early part of the pulse, the overlap of the instantaneous spectrum with the resonance peak increases, and the leading portion is amplified (i.e., u_{exchange} decreases). During the trailing portion, the instantaneous spectrum withdraws from the peak and the medium absorbs energy from the field of this portion of the pulse. The net effect moves the pulse peak forward faster than c. This effect is not only consistent with the principle of causality (as has been previously demonstrated via the Lorentz model[1,8,13]), but it is in fact a direct and general consequence of causality as demonstrated by (4.29) and (4.30).

The prediction that this relatively broadband pulse will travel faster than c is a little surprising when we recall the discussion of section 3.1. The explanation for this apparent difference lies in the fact that we have examined the instantaneous spectrum for this pulse at only the initial point in the medium without considering propagation. At this point, the instantaneous spectrum withdraws from the resonance for large t. However, at points farther in the medium (after the pulse has experienced modification), the spectrum of the pulse taken in its entirety is quite different. As the pulse is amplified, it acquires

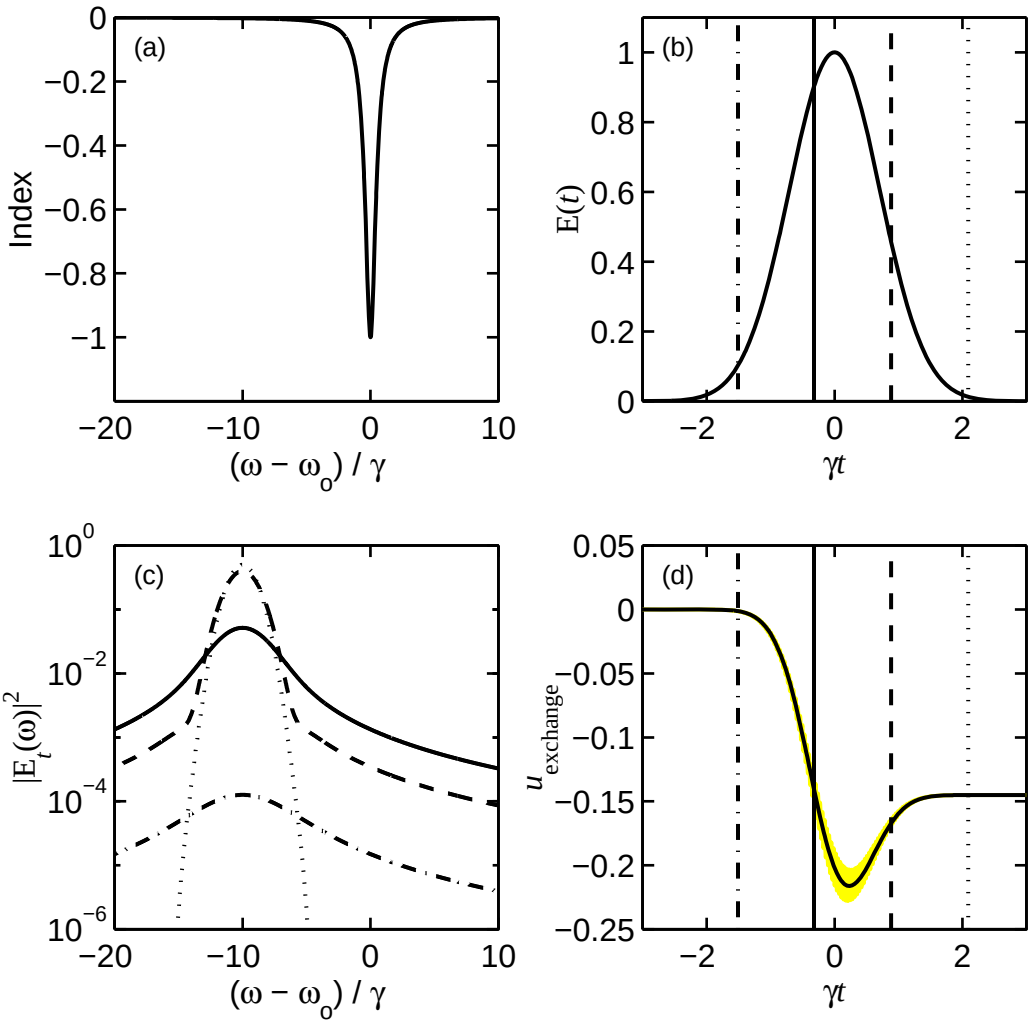

Figure 5.3: (a) Imaginary part of $\chi(\omega)$. (b) Initial pulse temporal profile. (c) Instantaneous spectrum at the times indicated in (b) with vertical lines. (d) Exchange energy density as a function of time.

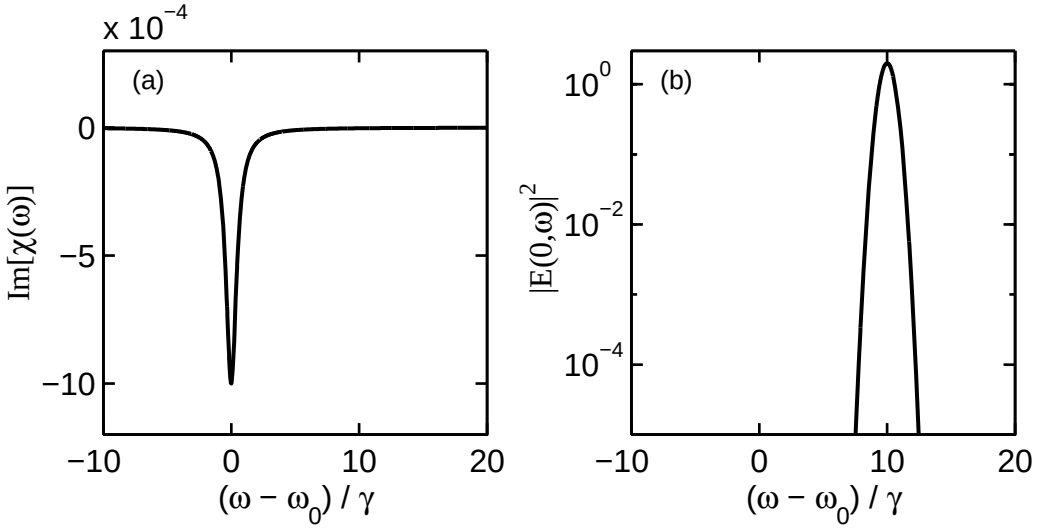

Figure 5.4: (a) Imaginary part of $\chi(\omega)$. (b) Initial pulse spectrum.

significant on-resonance spectral components, which manifest themselves primarily in the trailing portion of the pulse. Because the overlap of the instantaneous spectrum with the resonance increases during the trailing portion of the downstream pulse, the trailing portion of the pulse tends to be amplified to a greater extent than the leading portion. This provides another explanation (in addition to the arguments of section 3.2) for why superluminal propagation does not occur over indefinite lengths in an amplifying medium.

5.2.2 Superluminal Propagation in an Amplifier, Example 2

The superluminal effect in section 5.2.1 is relatively modest and will not persist as propagation distance is increased. To see a more dramatic example, we choose the medium parameter values as follows: $\omega_0 = 1 \times 10^5 \gamma$, $f{\omega_p}^2 = -100\gamma$. Figure 5.4(a) shows the imaginary parts of $\chi(\omega)$ for these parameters. The electric field of the initial pulse is Gaussian with the following parameters: $\tau = 2/\gamma$ and $\bar{\omega} = \omega_0 + 10\gamma$. Thus, the carrier frequency is a modest distance above the resonance structure, and there is little spectral overlap

between the spectrum of the entire pulse and the resonance structure. Figure 5.4(b) shows the total spectrum of the initial pulse.

It is informative to consider a spatial plot of the various energy densities in (4.7) as this pulse propagates. The left column in Fig. 5.5 shows a time sequence of the energy densities associated with the pulse as it propagates through the medium. The rectangle in the middle represents the medium of thickness $1.9c/\gamma$, with vacuum on either side. The solid line indicates the field energy density. The dashed line in the medium represents the combination $u_{\text{exchange}} + u(-\infty)$ (the energy density in the medium). We have assigned $u(-\infty)$ to be the same value at each point in the medium, chosen such that the energy density in the medium never becomes negative at any point. For reference, the dotted line represents the field energy density of a pulse that propagates exactly at c (i.e. as if the medium were not there). The actual pulse exiting the medium is ahead of this pulse, indicating that the centroid of field energy moved superluminally through the medium.

The right column in Fig. 5.5 shows the instantaneous spectrum for the first point in the medium. As in the previous example, during leading portion of the pulse the amount of overlap of the instantaneous spectrum with the resonance (at ω_0) increases and the medium surrenders energy to the leading portion of the pulse. As this point experiences the entire pulse, the instantaneous spectrum withdraws from the resonance, and energy is returned to the medium from the trailing portion of the pulse (notice that the energy in the medium rebounds slightly at the end of the pulse).

5.2.3 Energy Exchange Description of Pulse Advancement

Superluminal propagation in an amplifying medium was realized experimentally by Wang.[9] In his experiment the pulse spectrum is centered between two amplifying peaks, so that the broad instantaneous spectrum in the early portion of the pulse accesses the resonances on both sides and then withdraws in the later portions. In their report of this

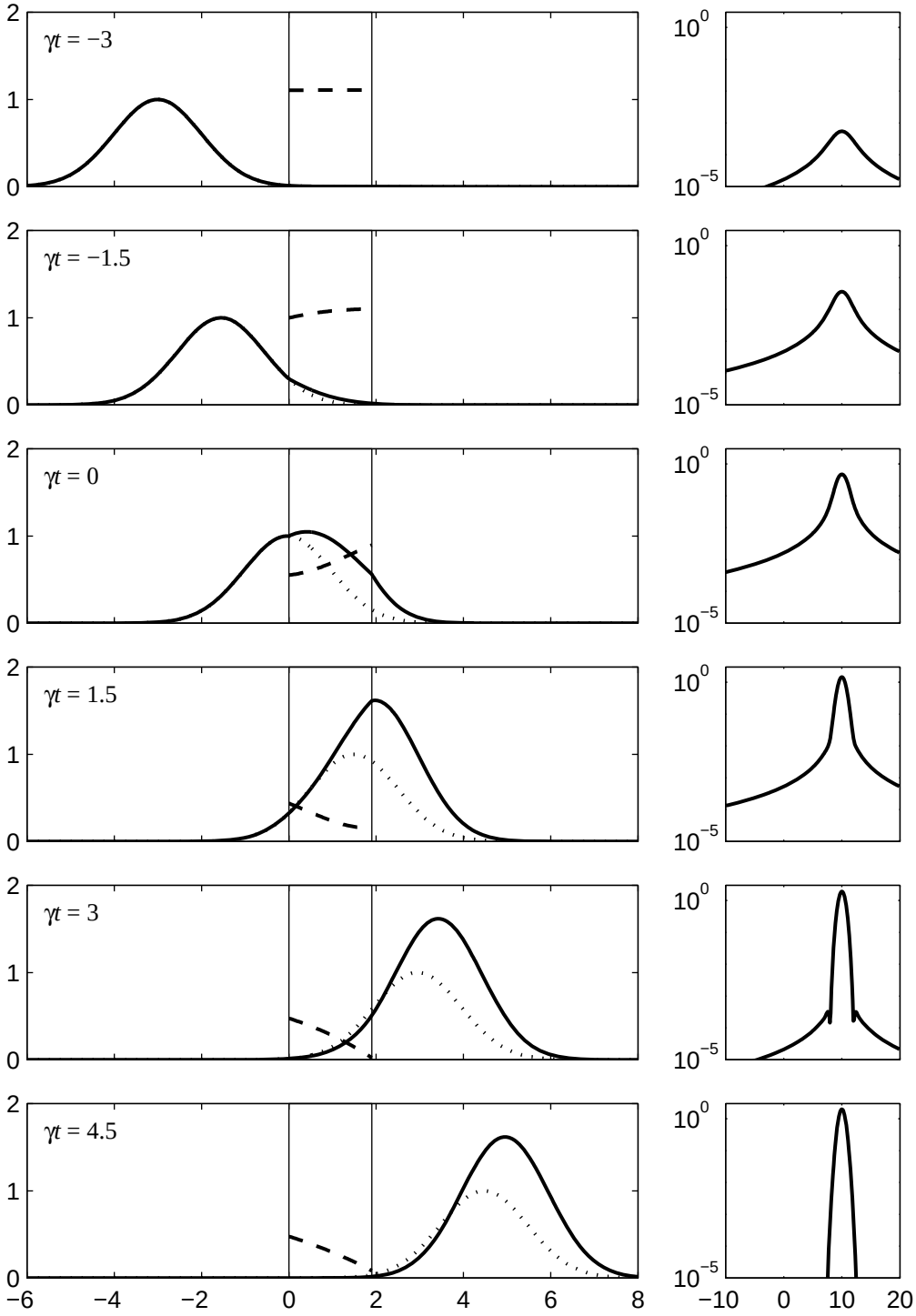

Figure 5.5: Time sequence of a Gaussian pulse traversing an amplifying medium.

experiment the authors specifically deny that the superluminal effect was associated with amplification of the front edge of the pulse since the pulse taken in its entirety contained essentially no spectral components resonant with the nearby gain lines. However, the instantaneous spectrum reveals how the leading portion of the pulse may be amplified even in this circumstance. In this section we illustrate how the instantaneous spectrum description can be used to predict the results obtained by Wang.

In the Wang experiment, the time required for a 4μs pulse to traverse a $\Delta r = 6$cm amplifying medium was $\Delta t \approx -63$ns. This means that the pulse moved forward in time by about 1% of its width. The strength of the wings in the instantaneous spectrum can be approximated as $E_t(\omega) \sim E(t)/(\omega - \bar{\omega})$, where $\bar{\omega}$ represents a carrier frequency and $E(t)$ is the strength of the field at the moment the pulse is truncated. The imaginary part of the susceptibility in a low-density vapor is approximately $\mathrm{Im}\,\chi(\omega) \approx cg/\omega$, where g is the frequency dependent gain coefficient (in the Wang experiment, $g \approx 0.1\mathrm{cm}^{-1}$ at a spectral shift of $\delta\omega \equiv \omega - \bar{\omega} \approx 2\pi(2\mathrm{MHz})$). A crude approximation to the integral (4.29) renders $u_{\mathrm{exchange}} = \epsilon_0 E^2(t)\, cg/\delta\omega$. This suggests that in the case of the Wang experiment the front of the pulse extracts an energy density of about $250 \times \epsilon_0 E^2(t)$ from the medium (i.e. 250 times the energy density in the electromagnetic field of the pulse). This energy density (extracted from the 6cm vapor cell) is distributed over about a kilometer, corresponding to the duration of the front half of the pulse. Thus, the electromagnetic field energy on the forward part of the pulse is enhanced by several percent and similarly the field energy diminishes on the trailing edge. This is consistent with the data presented in the paper.

Although this analysis properly describes the experimental result, the group delay analysis is a more convenient way to predict the transit time of the pulse. The utility of (4.29) lies in its interpretation of how the pulse and the medium interact. Neither analysis substitutes for the full solution to Maxwell's equations, but rather indicates some features of the solution.

5.3 Highly Subluminal Propagation

Subluminal propagation is the most common behavior for pulses in dielectric media, and occurs in both amplifying and absorbing media. Recently, research groups[38] have tried to enhance this effect to the point where delay times correspond to highly subluminal propagation speed (e.g., walking speed). In most situation, subluminal propagation is accompanied by an overall absorption or amplification of the pulse. When studying highly subluminal propagation, it is more fashionable to create a situation in which the overall pulse is neither amplified nor attenuated so that the entering and exiting pulses may be more easily compared. In this section we illustrate how this may be done, and show how the instantaneous spectrum description explains the subluminal behavior.

We employ a double resonance Lorentz oscillator to model the medium in this section, so that the linear susceptibility is

$$\chi(\omega) = \frac{f_1 {\omega_p}^2}{{\omega_0}^2 - \omega^2 - i\gamma_1\omega} + \frac{f_2 {\omega_p}^2}{{\omega_0}^2 - \omega^2 - i\gamma_2\omega}. \tag{5.2}$$

One of the resonances is amplifying, while the other is absorbing. Both resonances are centered at $\omega_0 = 100\gamma_1$, and the other parameters are given by: $\gamma_2 = 4.14\gamma_1$, $f_1\omega_p^2 = -400\gamma_1^2$, and $f_2\omega_p^2 = 100\gamma_1^2$. The structure of the imaginary part of $\chi(\omega)$ is plotted in Fig. 5.6(a). Figs. 5.6(b) and 5.6(d) show the field envelope and the exchange energy for a pulse with duration $\tau = 10/\gamma_1$ which has a narrow spectrum centered at $\bar{\omega} = \omega_0$.

The combined effect of the amplifying and absorbing resonances is such that there is no net energy exchange after the passage of the entire pulse. Thus, the exiting pulse does not experience overall attenuation or amplification. Nevertheless, as is evident in Fig. 5.6(d), there is a strong transfer of energy from the early portion of the pulse to the medium which is offset nearly completely as the energy returns to the rear of the pulse. The effect is pronounced since the instantaneous spectrum accesses the absorptive spectral regions on both sides of center and finally narrows to the region of transmission[38]

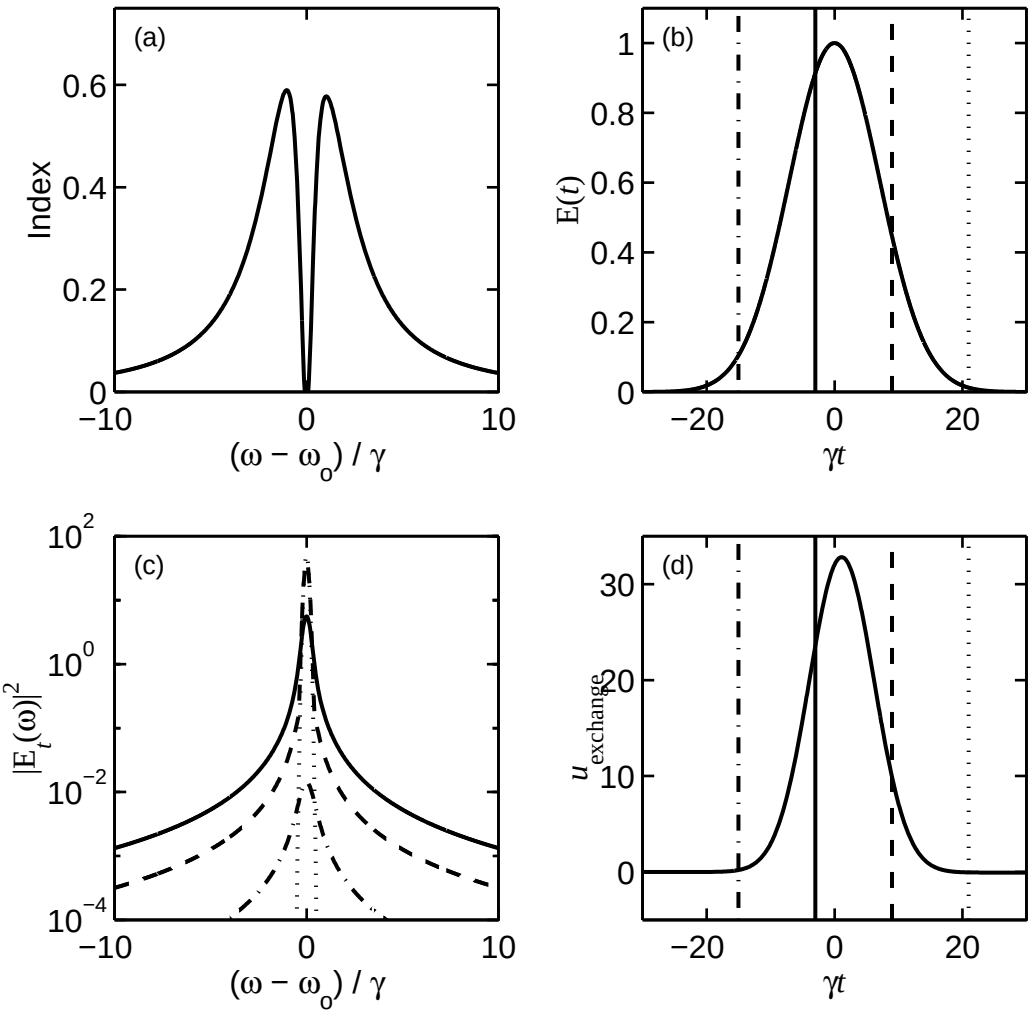

Figure 5.6: (a) Imaginary part of $\chi(\omega)$. (b) Initial pulse temporal profile. (c) Instantaneous spectrum at the times indicated in (b) with vertical lines. (d) Exchange energy density as a function of time.

where the absorption and amplifying resonances offset each other. Although this example corresponds to strongly subluminal propagation, the experiments demonstrating this effect depend on much narrower resonance structures than those used in this example.

5.4 Superluminal Propagation and Causality

In this section we illustrate the Sommerfeld-Brillouin result that a sharp signal edge travels exactly at c. For this example, we construct the medium with a narrow absorbing resonance superimposed on a wide amplifying resonance (both still centered at the same frequency). This is basically the inverse of the medium constructed in section 5.3. As with the medium in section 5.3, a relatively narrowband pulse whose spectrum is centered on-resonance can be sent through this medium with relatively little spectral modification. However, there is a strong transfer of energy to the pulse in the early portion, which is offset be a transfer of energy back to the medium in the trailing portion. This results in highly superluminal propagation of the pulse peak.

We choose the medium parameter values as follows: $\omega_0 = 1 \times 10^5 \gamma_1$, $\omega_p = 10\gamma_1$, $f_1 = 0.02$, $f_2 = -0.1$, and $\gamma_2 = 5\gamma_1$. Figure 5.7(a) illustrates the imaginary part of $\chi(\omega)$ for these parameters. The pulse is Gaussian as before, with parameters as follows: $\tau = 70/\gamma_1$ and $\bar{\omega} = \omega_0$. Figure 5.7(b) shows the spectrum of the initial pulse taken in its entirety.

Figure 5.8 is a time sequence of the energy densities associated with this pulse as it traverses a medium of thickness $30c/\gamma_1$. Again, the solid line represents the field energy density, the dashed line in the medium represents the combination $u_{\text{exchange}} + u(-\infty)$, and the dotted line represents the pulse as it would have propagated in vacuum. In this case, the enhancement of the leading portion and the absorption of the trailing portion causes the exiting pulse to emerge from the medium before the incoming pulse enters.

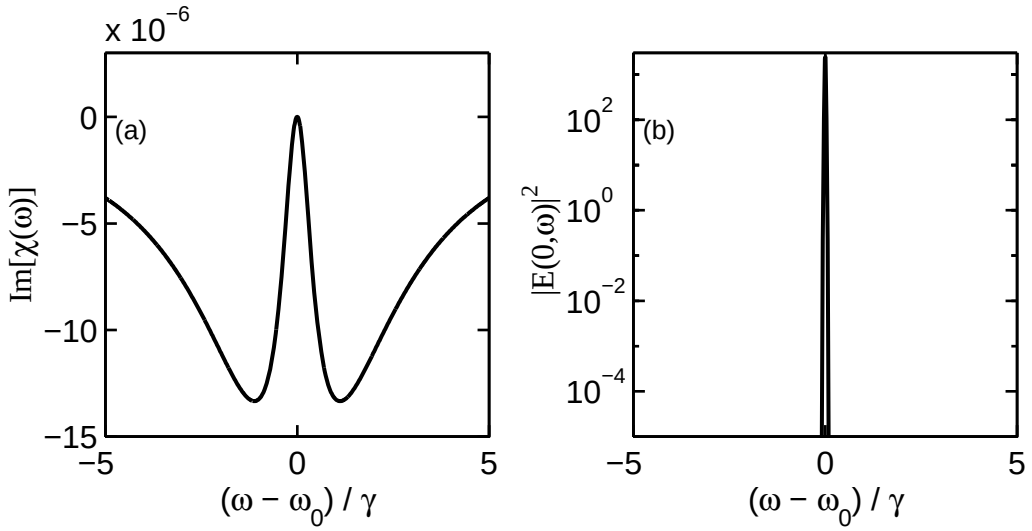

Figure 5.7: (a) Imaginary part of $\chi(\omega)$. (b) Initial pulse spectrum.

5.4.1 Sharp Signal Edge

When a Gaussian pulse is used to study superluminal effects, the wings of the temporal profile extend infinitely in both directions. Thus, the peak of the pulse exiting a medium may be shifted arbitrarily far into the leading edge without violating causality. However, if the leading edge is set to zero for times before the pulse is 'switched on' this is not the case; no pulse energy can be shifted beyond the signal edge propagated forward at c. Explanations for this effect are given in terms of the group delay context in section 3.1.3 and in terms of the instantaneous spectrum description in section 4.7.4.

Figure 5.9 illustrates this principle for a pulse whose leading edge has been set to zero, with the trailing edge given by the same Gaussian as in Fig. 5.8. Figure 5.10) repeats Fig. 5.9 on a logarithmic scale. The dashed pulse represents the behavior of the full Gaussian, as shown in Fig. 5.8, and the star indicates the truncation point propagated forward at exactly c. The pulse experiences extreme amplification since its entire spectrum overlaps the amplification peaks. However, none of this energy moves beyond the truncation point propagated forward at c.

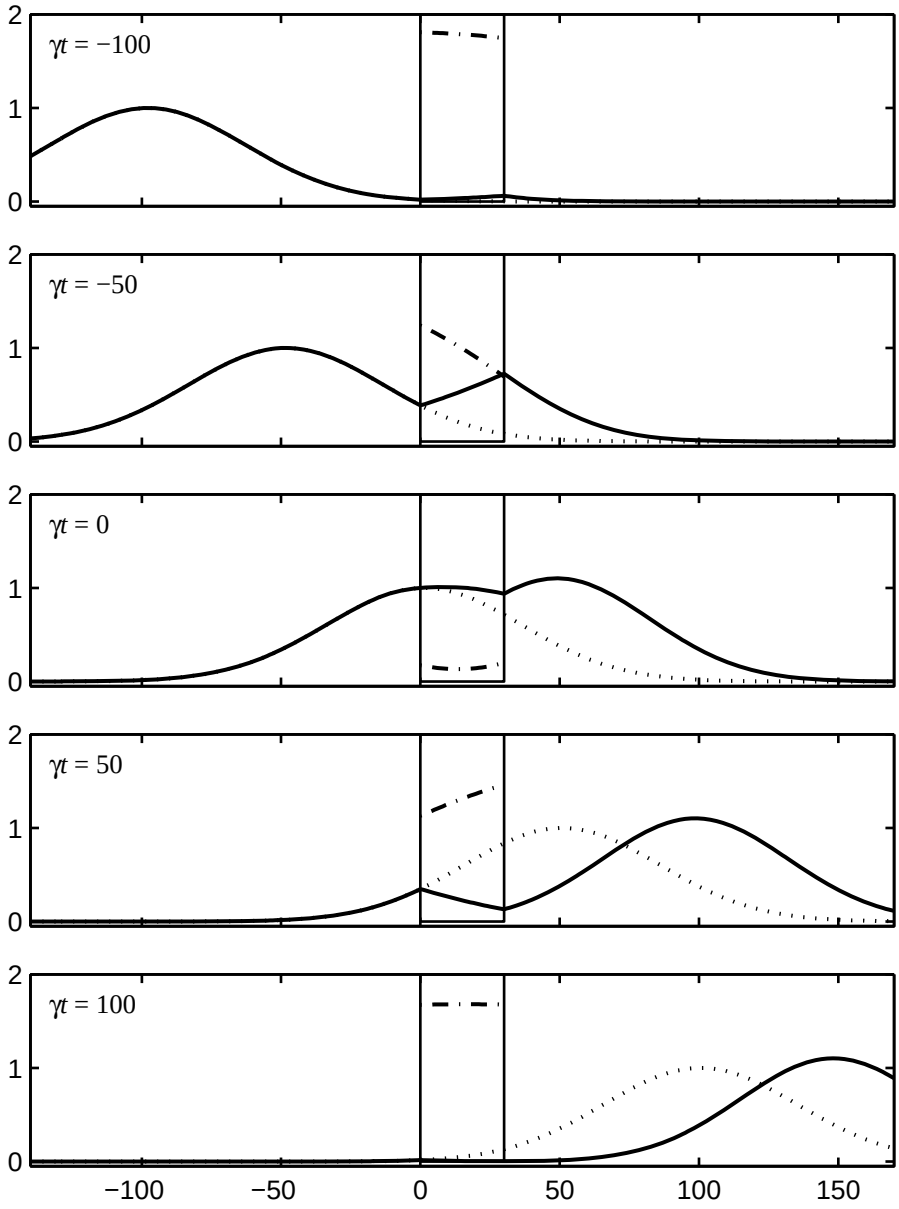

Figure 5.8: Time sequence of energy densities for the Gaussian pulse traversing the medium (distances are in units of c/γ and energy densities are in units of E_0^2/ϵ_0).

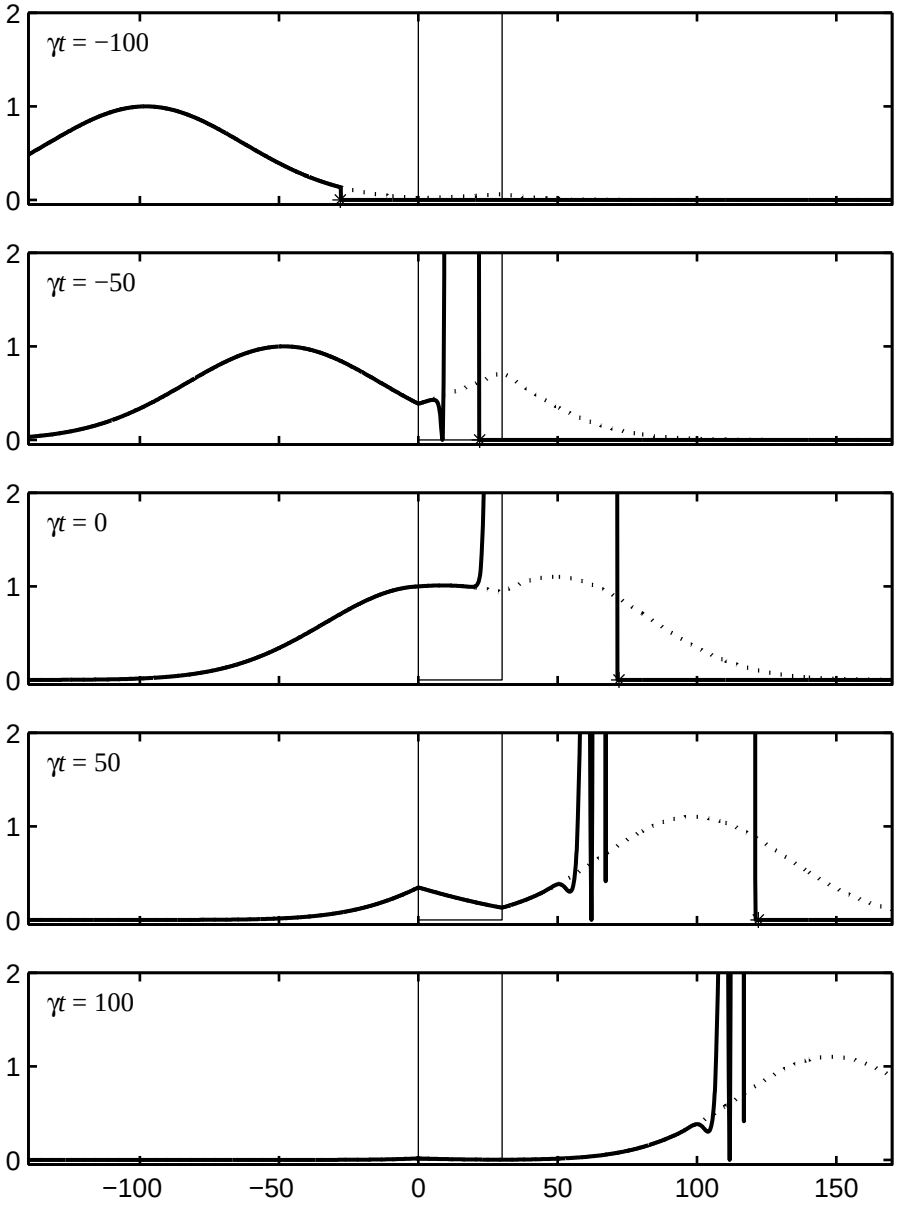

Figure 5.9: Animation of energy densities for a pulse whose trailing edge is the same as the Gaussian pulse in Fig. 5.8, and whose leading edge has been truncated. The medium is the same as in Fig. 5.8.

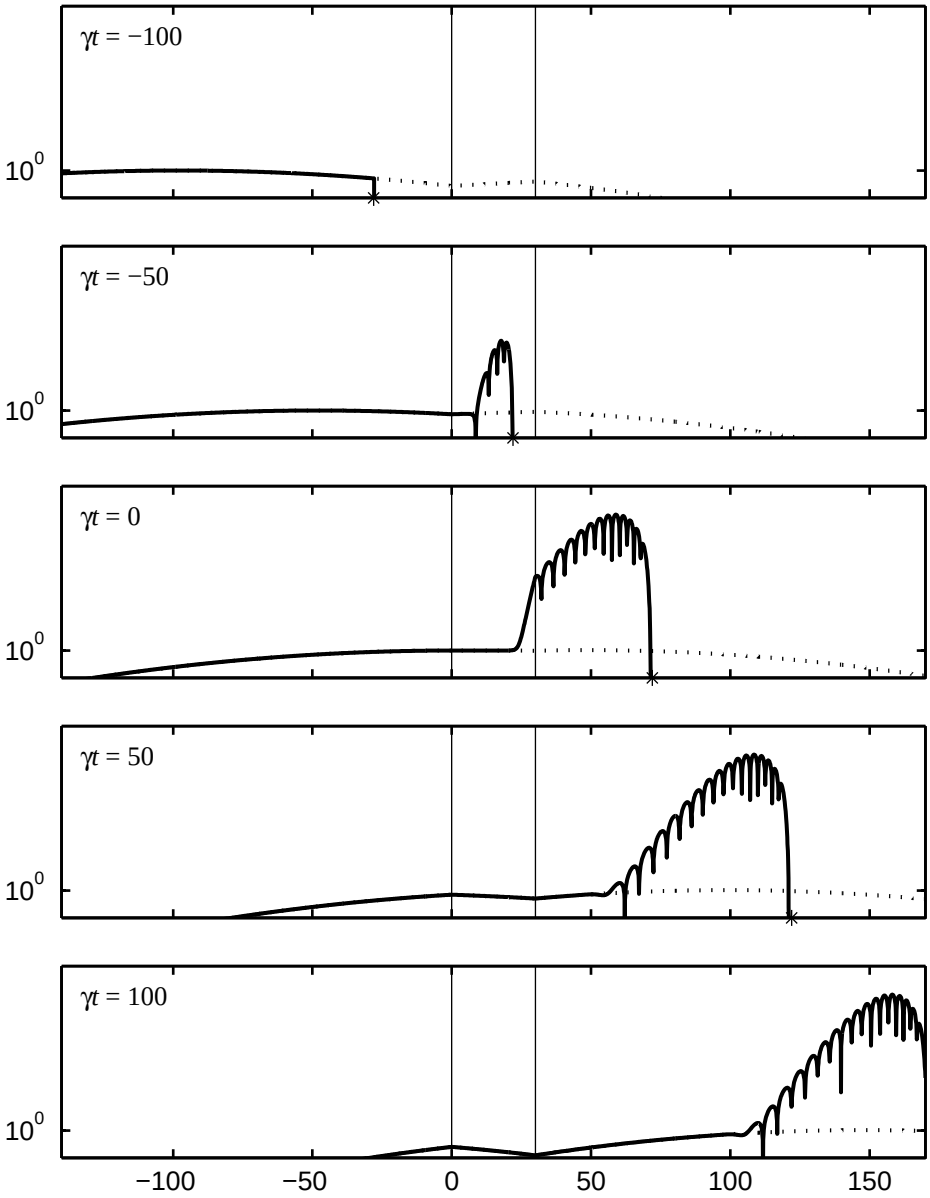

Figure 5.10: Same as Fig. 5.9, but on a logarithmic scale.

5.4.2 Leading Portion of a Pulse

There has been some discussion about whether the pulse exiting the medium in superluminal situations arises solely from the leading portion of the incoming pulse. This issue is clear in light of expression (4.29). Since the energy exchanged between the pulse and the medium can only depend on the portion of the pulse that a given point has already experienced, later portions of the pulse can have no influence on forward portion.

To illustrate this effect, in Fig. 5.11 we repeat the time sequence of Fig. 5.8 for a pulse whose leading edge is identical to the original pulse and is truncated at the peak of the Gaussian profile. (Figure 5.12 plots the this time sequence on a logarithmic scale). The field energy density of the truncated pulse is plotted with a solid line. The dashed line shows the untruncated pulse of Fig. 5.8. Because the truncated pulse taken in its entirety contains a large amount overlap with the amplification resonance it experiences a great deal of amplification in the trailing portion. It is clear from the plots that the leading portions of both pulses are identical as causality demands. The entering peak and the exiting peak are not causally connected.[39] The Gaussian appearance of the exiting peak is connected only to the Gaussian leading edge, and not with the shape of the latter portion of the incoming pulse.

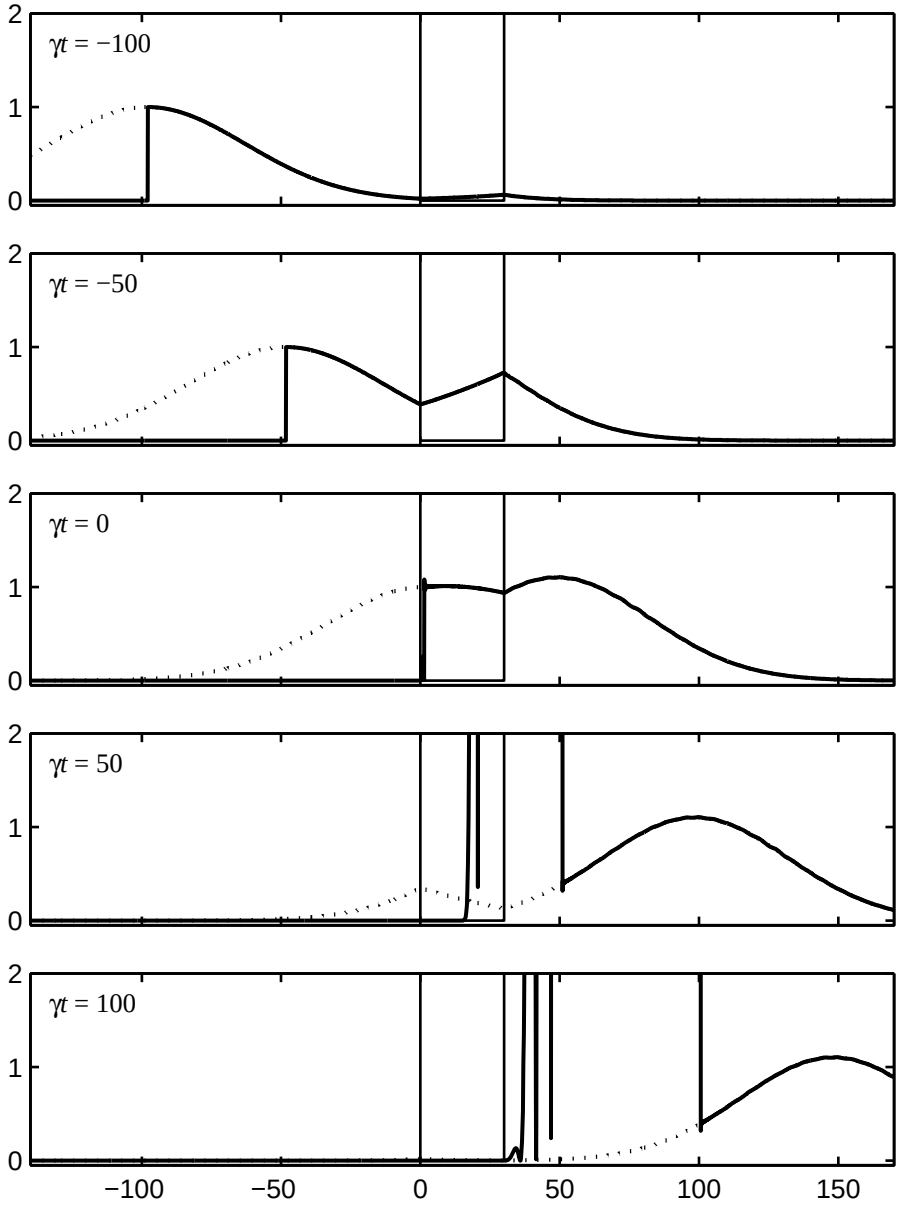

Figure 5.11: Animation of energy densities for a pulse whose leading edge is the same as the Gaussian pulse in Fig. 5.8, and whose trailing edge has been truncated. The medium is the same as in Fig. 5.8.

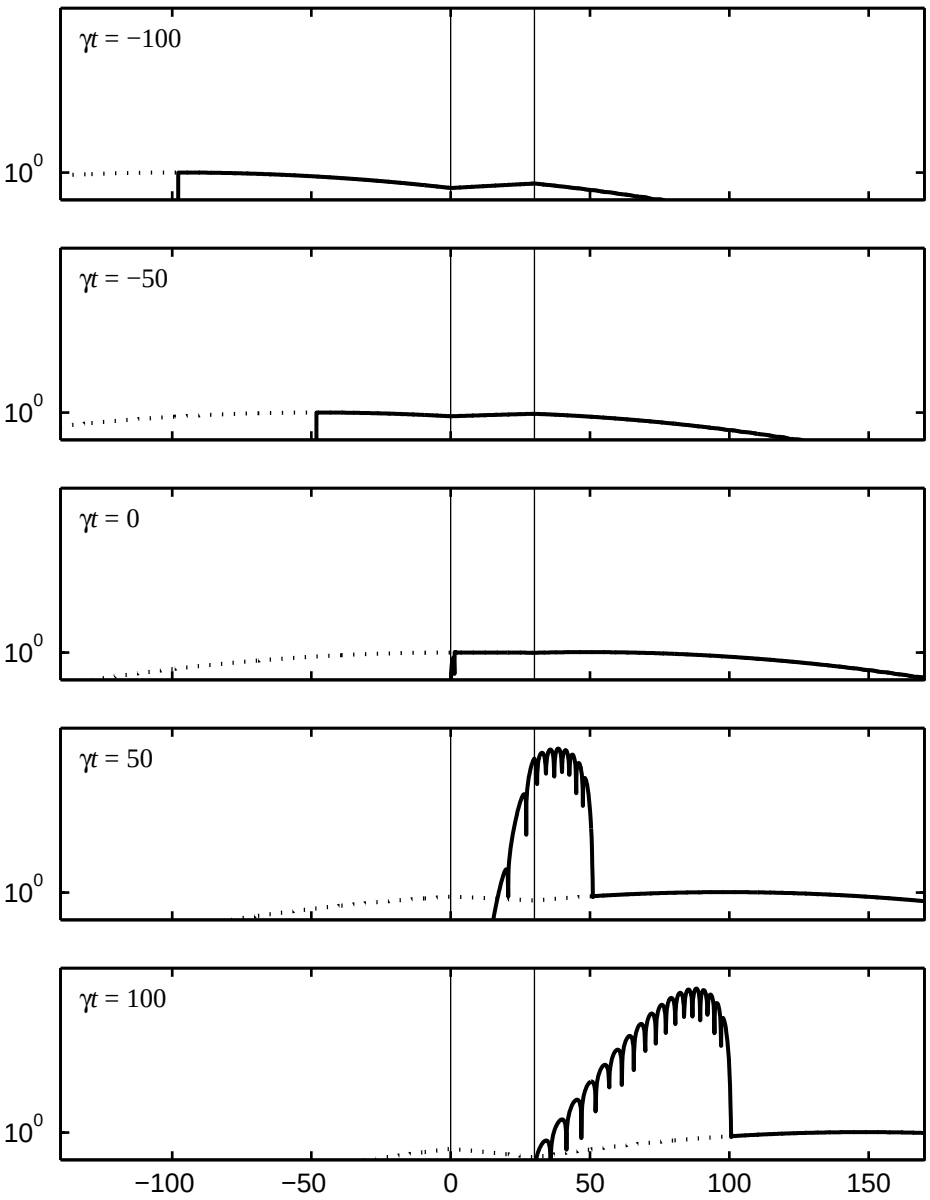

Figure 5.12: Same as Fig. 5.11, but on a logarithmic scale.

Chapter 6

Conclusion

In this chapter we briefly summarize the results obtained in this work. We then use the perspective gained from these results to compare and contrast the new group delay context with an energy velocity description that is often used. Finally, we discuss the superluminal effects illustrated in the work, and show why it is improbable that they will have practical uses in communication.

6.1 Summary

In this work we have discussed several techniques which are used to describe the behavior of the solutions of Maxwell's equations. We began by introducing the concept of group delay. We illustrated why the traditional formulation of the concept fails for a broadband pulse with its spectrum near resonance. We then introduced a new context for group delay wherein the group delay function always retains meaning in a uniform linear medium. The results apply to pulses of arbitrary bandwidth and temporal complexity, even in the presence of anomalous dispersion where the pulse shape can evolve dramatically during propagation.

The formalism distinguishes the roles of group velocity and spectral reshaping in determining total delay time. The net group delay is averaged over the final spectrum after the propagation takes place. The reshaping delay measures the effect of eliminating from (or adding to) the original pulse the spectral amplitude that is lost (or gained) during propagation when the pulse is initially chirped. This formalism does not attempt to identify a specific velocity as being representative of the overall pulse propagation as can be done for narrowband pulses. Rather it shows that a linear superposition of the group delays is necessary to determine total delay time. Since the formalism tracks the temporal 'center of mass' of the arrival of a pulse's *electromagnetic field energy* only, superluminal delay times do not represent a problem for causality.

We have also discussed energy transport in dielectric media. We examined the centroid of total energy and found that its velocity of transport is strictly luminal. We also pointed out that the velocity at which field energy *transported* from one point to another is strictly bound by c. However, the average *location* of the field energy density can move at any speed, as predicted by group velocity. The overly rapid motion of the centroid of field energy occurs when the medium exchanges energy asymmetrically with the leading and trailing portions of the pulse. The principle of causality requires this asymmetric energy exchange as governed by the instantaneous power spectrum used in (4.29). The instantaneous spectrum description of energy exchange provides an intuitive understanding of superluminal and highly subluminal phenomena in the vicinity of absorbing and amplifying resonances. This intuition is distinct from but complementary to the perspective gained through an understanding of group delay.

6.2 Energy Velocity Versus Group Velocity

In section 1.2 we mentioned that there has not been a clear consensus on the usefulness of group velocity. In large measure this was because of the failings of the group velocity description when applied to broadband pulses near resonance. The new context detailed in this work demonstrates how the concept of group delay can always be applied to propagation, regardless of a pulse's bandwidth and the proximity of resonance structures in the medium. We also mentioned in the introduction that Oughstun had observed[11] that traditional group velocity becomes less accurate with greater propagation distance, while the energy velocity description becomes more accurate with increasing propagation distance. At this point we are prepared to discuss and compare the two different descriptions in terms of the material presented in this work.

The decreasing accuracy of the traditional group velocity description for large propagation distances is due to the fact that in the expansion context velocity is predicted using the *initial* spectrum. Since components of the initial spectrum may be absorbed (or amplified) before they arrive at the observation point this can lead to erroneous predictions. It is therefore essential that the delay time be predicted using the spectral components that survive propagation, as is done in the new context. When this is done, the group delay description is equally valid for all propagation distances.

Since the group delay description is valid for all displacements, it is interesting to investigate how it relates to the energy velocity description, which becomes valid after large propagation distances. In order to compare the two descriptions, we briefly summarize the approach to energy velocity used by Oughstun,[29] which is slightly different from the description presented in chapter 4. In this approach, one considers a monochromatic wave with frequency ω. The energy transport velocity for this frequency is then defined as

$$v_E(\omega) \equiv \frac{\langle |S(\omega)| \rangle}{\langle u_{tot}(\omega) \rangle}, \tag{6.1}$$

where the brackets indicate the time average of the quantity enclosed. $S(\omega)$ is the time representation of the Poynting vector for the frequency ω, not the frequency domain representation constructed from the fourier transforms of the fields. The energy density $\langle u_{tot}(\omega)\rangle$ is defined by

$$\langle u_{tot}(\omega)\rangle \equiv \langle u_{field}(\omega)\rangle + \langle u_{osc}(\omega)\rangle . \tag{6.2}$$

The field energy density u_{field} is the same as in (4.8), and u_{osc} is the energy density stored in the oscillations of the medium. (In order to calculate u_{osc} a model must be assumed for the medium. The usual choice is a Lorentz medium.) Again, the argument ω reminds us that we are looking at a harmonic wave. In the limit where absorption becomes negligible, (6.1) can be shown to reduce to the classical group velocity, evaluated at the frequency ω.

The connection between (6.1) and pulse propagation comes when considering the asymptotic solution to Maxwell's equations. (The method used to obtain this solution is sketched in section 3.4.2.) This solution is valid after a pulse has propagated a large distance in an absorbing medium. The asymptotic solution is comprised of an amplitude function which multiplies an oscillatory function. The frequency of the oscillation varies in time, so that it is possible to define an instantaneous frequency of oscillation for the pulse. Sherman and Oughstun stated the connection between this instantaneous frequency of the pulse and the energy propagation velocity defined in (6.1) as follows:

> The field is dominated by a single real frequency at each space-time point. That frequency ... is the frequcny of the time-harmonic wave with the least attenuation that has energy velocity equal to z/t.[40]

This description of how the energy velocity predicts pulse behavior sounds very similar to the group delay description developed in this work. In the group delay context, we can state the meaning of the mathematical expression (2.43) in words as follows:

> The electromagnetic flux associated with a given frequency will be delayed according to the group delay function. When a pulse has been chirped by propagated a large distance, the field at a point **r** will be dominated by the frequency component with the least attenuation that has a group delay equal to t (assuming that the initial pulse was unchirped and arrived at $\mathbf{r}_0$ at $t = 0$).

Since the energy velocity (6.1) and the group velocity are known to predict different values for delay times in many cases, it may not be clear at first how both the Sherman statement and the group delay statement can be correct.

The resolution to this situation comes by recalling that the energy velocity (6.1) reduces to the group velocity when absorption is small. The only spectral components that survive to the 'mature' dispersion regime are those that do not experience much absorption. Thus, the qualification that the observed frequency component is the one which experiences "the least attenuation" assures that the two descriptions will agree in the limit of large propagation distances.

If we are only interested in predicting when different frequency components would appear after long propagation distances, we can get the correct answer using either energy velocity or group velocity. However, since the group delay description (as introduced in this work) is valid for all propagation distances, while the energy velocity description given by (6.1) is valid only for large distances, we see no advantage to using the energy velocity.

6.3 Can Superluminal Effects be Useful?

In many of the example in this work we have studied situations where the field energy of a pulse has superluminal delay times between various points in the system. It is abundantly clear that no information can ever be transmitted faster than c. However,

in most situations where we use light to transmit information (e.g., fiber optics) the transmission rate is well below the speed of light. Some have wondered if superluminal effects could somehow be employed to bring the speed of information transfer closer to c. In this section we use the perspective gained in this work to discuss the implausibility of using the current class of superluminal effects to achieve this goal.

6.3.1 Geometric Superluminal Effects

There are many situations in which superluminal delay times are observed simply due to geometry. For example, if a spotlight is scanned across a mountain side, the spot on the mountain can move arbitrarily fast depending on the rate at which the light source turns and its distance from the mountainside. However, the delay between the arrival of the spot at various points on the mountain side does not indicate that anything was transmitted between the points. We define a geometric superluminal effect as one in which the energy arriving at one point is unaffiliated with the energy arriving at another (i.e., the 'signal' could still reach the second point even if you prevent the energy from arriving at the first point). While the geometric nature of the superluminal delay times is obvious for the spotlight example, there are other situations where it is more subtle (for instance, the effect in Ref. [41] is purely geometric although the authors never discuss this). All geometric superluminal effects are useless for information transfer.

6.3.2 Superluminal Delays in Absorbers

We have noted several times in this work that the peak of an on-resonance narrowband pulse moves faster than c in an absorbing medium. Since we often associate the peak of the pulse with a signal, one might consider using this effect to 'hurry up' information transfer. However, there is really nothing to be gained by shifting the peak forward in this

manner. The exiting peak is always below the envelope of the original pulse propagated forward at c. Any detector sensitive enough to 'click' at the peak of the absorbed pulse would click earlier simply by letting the full pulse through and triggering at the lower intensity on the rising edge of the full pulse. In addition, this setup absorbs signal while leaving noise, and requires signals that are long in (i.e., narrow bandwidth). Neither of these qualities is desirable when trying to enhance the speed of information transfer. Thus, there seems to be no advantage to using this type of setup.

6.3.3 Superluminal Delays in Amplifiers.

Superluminal effects in amplifying media present the only situation where a signal might be better off for having travelled through the system. In these systems, the leading edge of the signal is amplified while the trailing edge is attenuated. Thus, the exiting signal could be detected sooner than would be the case if the original signal were simply allowed to propagate through vacuum. However, as the pulse is advanced in this manner it acquires on-resonance frequency components. These components manifest themselves in the trailing edge of the pulse (very far behind the signal pulse). If propagation distance in the medium becomes too great, these components become the dominant signal, and cause the peak to emerge with a very slow velocity. (This problem can be alleviated somewhat by using more complicated resonance structures than those discussed in this work.)

In addition to the trailing edge problem, it is also clear that the advancement of a pulse cannot affect the *rate* of information transfer. Information is generally sent as a series of pulses. While the first peak in a pulse train can get through the amplifier quickly, the inter-peak distance remains the same. Thus, once the first peak arrives at the detector, the rate of information transfer is unaffected by the advancement. Since the phenomenon requires extremely narrowband pulses, a train of the pulses must be spaced far apart in order to maintain distinct peaks. This reduces information transfer rates.

Since information transfer rates cannot be affected by the advancement of a pulse, one might try using this system to advance a single signal pulse. However, the requirement that the advanced pulse be narrowband makes this unattractive. To see why this is so, imagine that we decide to send a signal at some instant of time. At that instant, we begin to send the long leading edge (which is required for a narrowband pulse) of the signal through the amplifier. Eventually the peak arrives at the amplifier, and is advanced by some fraction of the pulse width. If we instead began a broadband pulse at the instant when we decide to send a signal, its peak would be somewhere in the rising edge of the narrowband signal. Even if this broadband pulse travels slower than c, it can usually be arranged for the broadband peak to arrive at a detector before the peak of the advanced narrowband pulse. Thus, there is little advantage to be gained by the advancement of a narrowband pulse.

In summary, we see no probability that the current class of superluminal effects will be able to enhance communication speed. These effects are of interest primarily because of the insights which they give to the study of light propagation and the nature of pulse/medium interaction, and not because they hold great promise for enhancing information transfer.

Bibliography

[1] E. L. Bolda, J. C. Garrison, and R. Y. Chiao, "Optical pulse propagation at negative group velocities due to a nearby gain line," Phys. Rev. A **49,** 2938–2947 (1994).

[2] G. Galilei, *Two New Sciences Pertaining to Mechanics and Local Motions* (Leyden, 1638).

[3] T. H. Havelock, *The Propagation of Disturbances in Dispersive Media* (Cambridge University Press, 1914).

[4] L. Brillouin, *Wave Propagation and Group Velocity* (Academic Press, New York, 1960).

[5] C. G. B. Garrett and D. E. McCumber, "Propagation of a Gaussian Light Pulse through an Anomalous Dispersion Medium," Phys. Rev. A **1,** 305–313 (1970).

[6] M. D. Crisp, "Concept of Group Velocity in Resonant Pulse Propagation," Phys. Rev. A **4,** 2104–2108 (1971).

[7] S. Chu and S. Wong, "Linear Pulse Propagation in an Absorbing Medium," Phys. Rev. Lett. **48,** 738–741 (1982).

[8] R. Y. Chiao, "Superluminal (but causal) propagation of wave packets in transparent media with inverted atomic populations," Phys. Rev. A **48,** R34–R37 (1993).

[9] L. J. Wang, A. Kuzmmich, and A. Dogariu, "Gain-Assisted Superluminal Light Propagation," Nature **406,** 277–279 (2000).

[10] K. E. Oughstun and C. M. Balictsis, "Gaussian Pulse Propagation in a Dispersive, Absorbing Dielectric," Phys. Rev. Lett. **77,** 2210–2213 (1996).

[11] K. E. Oughstun and H. Xiao, "Failure of the Quasimonochromatic Approximation for Ultrashort Pulse Propagation in a Dispersive, Attenuative Medium," Phys. Rev. Lett. **78,** 642–645 (1997).

[12] H. Xiao and K. E. Oughstun, "Failure of the group-velocity description for ultrawideband pulse propagation in a causally dispersive, absorptive dielectric," J. Opt. Soc. Am. B **16,** 1773–1785 (1999).

[13] R. Y. Chiao and A. M. Steinberg, "Tunneling Times and Superluminality," Progress in Optics **37,** 347–406 (Emil Wolf ed., Elsevier, Amsterdam, 1997).

[14] M. Born and E. Wolf, *Principles of Optics*, sixth ed. (Pergamon, Oxford, 1980).

[15] J. D. Jackson, *Classical Electrodynamics*, 3rd ed. (Wiley, New York, 1998).

[16] O. E. Martinez, "Grating and Prism Compressors in the Case of Finite Beam Size," J. Opt. Soc. of Am. B **3,** 929–934 (1986).

[17] G. B. Arfken and H. J. Weber, *Mathematical Methods for Physicists*, fourth ed. (Academic Press, San Diego, 1995).

[18] R. L. Smith, "The Velocities of Light," Am. J. Phys. **38,** 978–984 (1970).

[19] J. Peatross, S. A. Glasgow, and M. Ware, "Average Energy Flow of Optical Pulses in Dispersive Media," Phys. Rev. Lett. **84,** 2370–2373 (2000).

[20] M. Ware, S. A. Glasgow, and J. Peatross, "The Role of Group Velocity in Tracking Field Energy in Linear Dielectrics," Opt. Express (2001).

[21] M. Ware, W. E. Dibble, S. A. Glasgow, and J. Peatross, "Energy Flow in Angularly Dispersive Optical Systems," J. Opt. Soc. Am. B **18,** 839–845 (2001).

[22] M. A. I. Talukder, Y. Amagishi, and M. Tomita, "Superluminal to Subluminal Transition in the Pulse Propagation in a Resonantly Absorbing Medium," Phys. Rev. Lett. **86,** 3546–3549 (2001).

[23] M. Pessot, P. Maine, and G. Mourou, "1000 Times Expansion/Compression of Optical Pulses for Chirped Pulse Amplification," Opt. Comm. **62,** 419–421 (1987).

[24] D. N. Fittinghoff, B. C. Walker, J. A. Squier, C. S. Toth, C. Rose-Petruck, and C. P. J. Barty, "Dispersion Considerations in Ultrafast CPA Systems," IEEE J. Sel. Top. Quant. Electron. **4,** 430 (1998).

[25] C. G. D. III, S. Backus, M. M. Murnane, and H. C. Kapteyn, "Design and Implementation of a TW-Class High-Average Power Laser System," IEEE J. Sel. Top. Quant. Electron. **4,** 395–405 (1998).

[26] M. J. Ware, *Phase Delay and Energy Flow in Angularly Dispersive Optical Systems* (Senior Thesis, Brigham Young University, 1999).

[27] E. B. Treacy, "Optical Pulse Compression With Diffraction Gratings," IEEE J. of Quant. Electron. **QE-5,** 454–458 (1969).

[28] S. D. Brorson and H. A. Haus, "Diffraction gratings and geometric optics," J. Opt. Soc. Am. B **5,** 247–248 (1988).

[29] K. E. Oughstun and G. C. Sherman, *Electromagnetic Pulse Propagation in Causal Dielectrics* (Springer-Verlag, New York, 1994).

[30] S. A. Glasgow, M. Ware, and J. Peatross, "Poynting's Theorem and Luminal Energy Transport Velocity in Causal Dielectrics," Phys. Rev. E **64,** 046610–1–046610–14 (2001).

[31] J. Peatross, M. Ware, and S. A. Glasgow, "The Role of the Instantaneous Spectrum in Pulse Propagation in Causal Linear Dielectrics," J. Opt. Soc. Am. A **18,** 1719–1725 (2001).

[32] R. Loudon, "The propagation of electromagnetic energy through an absorbing dielectric," J. Phys. A **3,** 233–245 (1970).

[33] K. R. Bownstein, "Some Time Evolution Properties of an Electromagnetic Wave," Am. J. Phys. **65,** 510–515 (1997).

[34] L. D. Landau, E. M. Lifshitz, and L. P. Pitaevskii, *Electrodynamics of Continuous Media*, 2nd ed. (Pergamon, Oxford, 1982).

[35] C. H. Page, "Instantaneous Power Spectra," J. Appl. Phys. **23,** 103–106 (1952).

[36] M. B. Priestley, "Power Spectral Analysis of Non-Stationary Random Processes," J. Sound Vib. **6,** 86–97 (1967).

[37] J. H. Eberly and K. Wodkiewicz, "The Time-Dependent Physical Spectrum of Light," J. Opt. Soc. Am. **67,** 1252–1260 (1977).

[38] L. V. Hau, S. E. Haris, Z. Dutton, and C. H. Behroozi, "Light Speed Reduction to 17 Metres per Second in an Ultracold Atomic Gas," Nature **397,** 594–598 (1999).

[39] G. Diener, "Superluminal group velocities and information transfer," Phys. Lett. A **223,** 327–331 (1996).

[40] G. C. Sherman and K. E. Oughstun, "Description of Pulse Dynamics in Lorentz Media in Terms of the Energy Veleocity and Attenuation of Time-Harmonic Waves," Phys. Rev. Lett. **47,** 1451–1454 (1981).

[41] R. R. D. Mugnai, A. Ranfagni, "Observation of Superluminal Behaviors in Wave Propagation," Phys. Rev. Lett. **84,** 4830–4833 (2000).

Appendix A

The Spatial Centroid of Field Energy

In this appendix we sketch the derivation of expression (4.20) which connects group velocity with the presence of field energy. To accomplish this, we solve Maxwell's equations by selecting an instant in time and considering the spatial distribution of the pulse at that instant. This is in contrast to the more common method in which one chooses a point in space and considers the time behavior of the fields at that point. Since the spatial method of obtaining solutions is less common (owing to the fact that the material polarization **P** enters into Maxwell's equations through a time derivative as opposed to a spatial derivative) we take a moment to review how the solutions are obtained.

The k-space and spatial distributions of the electric field at an instant t are related by

$$\mathbf{E}(\mathbf{k}, t) = \frac{1}{(2\pi)^{3/2}} \int e^{-i\mathbf{k}\cdot\mathbf{r}} \mathbf{E}(\mathbf{r}, t)\ \mathrm{d}^3 r, \tag{A.1}$$

$$\mathbf{E}(\mathbf{r}, t) = \frac{1}{(2\pi)^{3/2}} \int e^{i\mathbf{k}\cdot\mathbf{r}} \mathbf{E}(\mathbf{k}, t)\ \mathrm{d}^3 k. \tag{A.2}$$

Analogous expressions for **B** and **P** give the k-space representation for the magnetic and polarization fields. We take $\mathbf{E}(\mathbf{r}, t)$, $\mathbf{B}(\mathbf{r}, t)$, and $\mathbf{P}(\mathbf{r}, t)$ to be real functions, so that the following symmetry holds for their k-space representations:

$$\mathbf{E}(-\mathbf{k}, t) = \mathbf{E}^*(\mathbf{k}, t) \tag{A.3}$$

with analogous expressions for $\mathbf{B}(\mathbf{k}, t)$, and $\mathbf{P}(\mathbf{k}, t)$. In a homogeneous, isotropic medium, Maxwell's equations have as a solution

$$\mathbf{E}(\mathbf{k}, t_0 + \Delta t) = \sum_m \mathbf{E}_m(\mathbf{k}, t_0)\, e^{-i\omega_m(k)\Delta t}. \tag{A.4}$$

The initial pulse form $\mathbf{E}(\mathbf{k}, t_0)$ is chosen at the instant t_0 for each frequency associated with the wave number $\mathbf{k}$. The solution renders the pulse form $\mathbf{E}(\mathbf{k}, t_0 + \Delta t)$ (in terms of the initial pulse form) after an arbitrary time interval Δt. The magnetic field is connected to the electric field via

$$\mathbf{B}(\mathbf{k}, t) = \sum_m \mathbf{k} \times \mathbf{E}_m(\mathbf{k}, t) \big/ \omega_m(k)\,, \tag{A.5}$$

and the spatial profile of the pulse at the later time is obtained using (A.2).

The connection between the frequency ω_m and wave number k is:

$$\frac{\omega_m^2}{c^2}\left[1 + \chi(\omega_m)\right] = k^2. \tag{A.6}$$

We choose real values for k and solve Eq. (A.6) for ω_m. The subscript m and the summations in (A.4) and (A.5) reflect the fact that the solution to (A.6) is in general multi-valued. We take this degeneracy to be countable and therefore use a summation rather than an integral. (For example, a single Lorentz oscillator is four-fold degenerate with two distinct frequencies for a given $\mathbf{k}$ which can each propagate forwards or backwards.) This degeneracy reflects the physical reality that in the presence of a complex linear susceptibility $\chi(\omega)$, different frequencies can correspond to the same wavelength. As mentioned in the text, we make the simplifying assumption that only a single frequency ω is associated with each $\mathbf{k}$, so that we can write the solution to Maxwell's equations as:

$$\mathbf{E}(\mathbf{k}, t_0 + \Delta t) = \mathbf{E}_0(\mathbf{k}, t_0)\, e^{-i\omega(k)\Delta t}. \tag{A.7}$$

If this assumption is not made one can still derive expressions with the same interpretation as those obtained here. However, the sums involved make the expressions more complicated.

The viewpoint of real $\mathbf{k}$ leads to the use of complex frequencies ω. The meaning of complex frequencies is clear. The susceptibility of a complex frequency is determined by the medium's response to an oscillatory field whose amplitude either decays or builds exponentially in time. If the susceptibility $\chi(\omega)$ is known (measured) only for real values of ω, its behavior for complex frequencies can be inferred through a Fourier transform followed by an inverse Fourier transform with complex frequency arguments. Given the real $\mathbf{k}$ vectors, the complex frequencies correspond to uniform plane waves that decay or build everywhere in space as a function of time. (This is in contrast with the time picture where the pulse is comprised of waves that are steady in time but which decayed or build as a function of position.)

We now consider the average position of field energy at an instant and consider the displacement at a later time. As mentioned in the text, we use the centroid of field energy to define the pulse's position (see (4.18)):

$$\langle \mathbf{r}_{\text{field}} \rangle_t \equiv \int \mathbf{r} u_{\text{field}}(\mathbf{r}, t)\ \mathrm{d}^3 r \Big/ \int u_{\text{field}}(\mathbf{r}, t)\ \mathrm{d}^3 r\,. \tag{A.8}$$

Motivated by a desire to make a connection with group velocity, we rewrite (A.8) in terms of the k-space representation of the fields:

$$\langle \mathbf{r}_{\text{field}} \rangle_t = \mathbf{R}[\mathbf{E}(\mathbf{k}, t)]\,, \tag{A.9}$$

where

$$\mathbf{R}[\mathbf{E}(\mathbf{k}, t)] \equiv i \frac{\int \mathrm{d}^3 k \sum\limits_{j=x,y,z} \left[\frac{\epsilon_0}{2} E_j^*(\mathbf{k}, t) \cdot \nabla_k E_j(\mathbf{k}, t) + \frac{1}{2\mu_0} B_j^*(\mathbf{k}, t) \cdot \nabla_k B_j(\mathbf{k}, t) \right]}{\int u_{\text{field}}(\mathbf{r}, t)\ \mathrm{d}^3 r}. \tag{A.10}$$

The k-space representation of the energy density is

$$u_{\text{field}}(\mathbf{k}, t) = \frac{\epsilon_0 \mathbf{E}(\mathbf{k}, t) \cdot \mathbf{E}^*(\mathbf{k}, t)}{2} + \frac{\mathbf{B}(\mathbf{k}, t) \cdot \mathbf{B}^*(\mathbf{k}, t)}{2\mu_0}. \tag{A.11}$$

We have included only the electric field in the argument of the displacement $\mathbf{R}$ since the magnetic field can be obtained through (A.5).

The expression (A.10) is not very useful in itself. Its usefulness comes when applied to the difference in the pulse's average position at two different instants in time. Consider a pulse as it evolves from an initial time t_0 to time $t_0 + \Delta t$. The difference in the average position at these two times is

$$\Delta \mathbf{r} \equiv \langle \mathbf{r}_{\text{field}} \rangle_{t_0+\Delta t} - \langle \mathbf{r}_{\text{field}} \rangle_{t_0} = \mathbf{R}\left[\mathbf{E}\left(\mathbf{k}, t_0 + \Delta t\right)\right] - \mathbf{R}\left[\mathbf{E}\left(\mathbf{k}, t_0\right)\right] \tag{A.12}$$

Using the solution (A.7), the displacement can be written as the sum of two intuitive terms (see (4.20)):

$$\Delta \mathbf{r} = \Delta \mathbf{r}_G\left(t\right) + \Delta \mathbf{r}_R\left(t_0\right). \tag{A.13}$$

The first term in (A.13), the net group displacement, is given in (4.21) and discussed in the text. The second term in (4.20), the reshaping displacement, is given by

$$\Delta \mathbf{r}_R\left(t_0\right) \equiv \mathbf{R}\left[e^{\text{Im}\,\omega(\mathbf{k})\Delta t}\mathbf{E}\left(\mathbf{k}, t_0\right)\right] - \mathbf{R}\left[\mathbf{E}\left(\mathbf{k}, t_0\right)\right]. \tag{A.14}$$

The reshaping displacement is the difference between the pulse position *at the initial time* t_0 evaluated without and with the spatial frequency amplitude that is lost during propagation. Dispersion effects due to propagation are not included since $\mathbf{E}\left(\mathbf{k}, t_0\right)$ is used in both terms of (A.14).